

**Processing of Open-cell Structures
by Additive Manufacturing
Technique of Metal and Salt
Mixtures**

By Ge ZHAO, BEng

Thesis submitted to the University of
Nottingham for the award of Master of
Philosophy

Department of Mechanical, Materials and
Manufacturing Engineering
November, 2020 (Revised)

Abstract

A novel type of metallic feedstock material for powder-bed additive manufacturing (AM) processes is proposed that enables the manufacture of cellular structures without the time consuming and computationally intensive step of digitally representing the internal geometry of a part. The feedstock is a blend of metal and salt particles and investigation started with Selective Laser Melting (SLM) processing, to better understand the effect of feedstock and processing parameters so that the salt is dissolved to leave a metallic, cellular structure after fabrication.

The conditions for successfully processing the feedstock are first demonstrated, followed by an investigation into how the feedstock composition can be used to control the relative density of the cellular material. Mechanical testing reveals that the strength and stiffness of the cellular structures can be tuned through control of feedstock composition, and hence, relative density.

Followed by the technique proposed above, a novel method for functionally graded cellular structures fabrication is investigated by using the same metal and salt blend. The graded density is controlled by adjusting processing parameters. The method is further investigated about how the processing parameters can be used to control the relative density of the cellular material. Mechanical testing indicates that the relative density and compressive properties can be processing parameters.

This presents an enhancement to the state-of-the-art for manufacturing processes of Functionally Graded Materials (FGMs), since graded cellular structures can be created by parameters set-up without explicitly defining or analysing the unit cell geometry.

Acknowledgements

This course is an arduous journey full of challenges for me. Apart from self-motivation and patience, I cannot arrive at the destination without the support and guidance from people who are around me.

I would like to thank my dearest father, who was suffering from disease but encouraging and supporting me during my study no matter what difficulties I have met. Although he passed away on 7th December, 2018, I never think that he leaves me. I would like to thank my husband, You LI as well. He gave me much encouragement and advice during my study, which has made this journey to be possible and achievable. I would like to thank my little angel, Willow Xinuo LI, who was born on 13th April, 2019. Without her, I could not start a new life after my father's leave.

Finally, I am grateful for the guidance from my supervisors Prof. Ian Ashcroft Prof. Adam Clare and Prof. Richard Hague, who help to improve my knowledge and understanding of Additive Manufacturing. I also wish to thank our esteemed lab technicians Mark Hardy and Mark East, who's experience working in AM and running the lab like clockwork is highly valued by us all.

Publications

Journal Papers

G. Zhao, I.A. Ashcroft, R. J. M. Hague, A.R. Kennedy, A.T. Clare, “*Salt-metal feedstocks for the creation of stochastic cellular structures with controlled relative density by powder bed fabrication*”, *Materials & Design* 149, April 2018.

N. T. Aboulkhair, G. Zhao, R. J. M. Hague, A.R. Kennedy, I. A. Ashcroft, A.T. Clare, “*Generation of graded porous structures by control of process parameters in the selective laser melting of a fixed ratio salt-metal feedstock*”, *Journal of Manufacturing Processes*, Volume 55, Pages 249-253, July 2020.

Conference presented

Industrial Laser Applications Symposium (ILAS) 2017, Grantham, 22-23rd March, 2017: Salt-metal feedstocks for the creation of stochastic cellular structures with controlled relative density by powder bed fabrication.

Table of Contents

1 Introduction	1
1.1 Background -----	1
1.2 Aim and Objectives of the Research-----	4
1.3 Singnificance and Novelty of the Research-----	4
1.4 Research Methodology -----	5
1.5 Thesis Layout-----	6
2. Literature Review	9
2.1 Additive Manufacturing-----	9
2.1.1 Directed energy deposition-----	13
2.1.2 Powder bed fusion-----	15
2.1.3 Summary-----	19
2.2 Titanium Foam and Manufacturing Methods-----	20
2.2.1 Titanium and its alloys-----	20
2.2.2 Cellular structures -----	21
2.2.3 Reactive sintering-----	22
2.2.4 Loose powder sintering and hollow sphere sintering -----	24
2.2.5 Space holder technique -----	25
2.2.6 Additive Manufacturing of titanium alloys -----	30
2.2.6.1 Directed energy deposition for titanium foam-----	31
2.2.6.2 Powder bed fusion for titanium foam-----	26
2.2.7 Summary-----	38
2.3 Functionally Graded Material-----	39
2.3.1 Conventional Methods for Functionally Graded Materials (FGMs)-----	40
2.3.2 Additive Manufacturing (AM) for Functionally Graded Materials (FGMs) ---	43

2.3.3 Summay-----	44
2.4 Summary of Literature and Identified Gaps in the Literature -----	45
3. Experimental Methods and Materials	47
3.1 Experimental Apparatus-----	48
3.1.1 Realizer SLM 50 -----	48
3.1.2 Techniques for characterisation of meso and microstructure-----	50
3.2 Experimental Materials-----	51
3.2.1 Materials morphology in the research -----	51
3.2.2 Thermal properties of materials -----	52
3.2.3 Powder Mixing-----	53
3.2.4 Flowability Test-----	55
3.3 Types of Samples -----	56
3.3.1 SLM samples with various NaCl content-----	56
3.3.2 An investigation of relationship between densities of SLM samples and processing parameters-----	57
3.3.3 SLM vertical graded samples-----	57
3.3.4 SLM horizontal graded samples-----	58
3.3.5 Graded overhang structure -----	59
3.4 Salt Dissolution-----	60
3.5 Mechanical Testing -----	60
3.6 Heat Treatment-----	61
4. Composition Modulation for Ti-6Al-4V Cellular Structures with Various NaCl Content	62

4.1 Flowability Test -----	62
4.2 Thin Walls Built by SLM Process with Ti-6Al-4V and Salt Mixture-----	63
4.3 Optimisation of Processing Parameters -----	67
4.4 Salt Dissolution -----	68
4.5 Characterisation of the Cellular Structure-----	70
4.6 Characterisation of Microstructure-----	72
4.7 Relationship between Feedstock Composition and Relative Density-----	74
4.8 Mechanical Testing-----	76
4.9 Summary-----	81
5. Modulation for Functionally Graded Structures	82
5.1 Effect of Laser Processing Parameters on Relative Density-----	82
5.2 Compressive Properties of the Structure-----	84
5.3 Compressive Properties for Heat Samples -----	85
5.3.1 Compressive properties for treated samples without NaCl -----	85
5.3.2 Compressive properties for treated samples with 50% NaCl by various parameters -----	86
5.4 Graded Structure in Vertical Direction-----	88
5.4.1 Relative density of the structure -----	88
5.4.2 Compressive properties of the structure -----	90
5.5 Graded Structure in Horizontal Direction -----	91
5.6 Graded Structure in Vertical Direction -----	91
5.7 Summary-----	93
6. Discussion	94
7. Conclusions and Future Work	97
7.1 Conclusions -----	97

7.2 Future Work-----	98
References	101

List of Figures

1.1	Framework for the research to determine the effect of NaCl on the structural properties-----	6
2.1	Basic layout for a LENS system [22]-----	13
2.2	Schematic drawing of the DED process [23]-----	15
2.3	Schematic of the SLS process [31] -----	16
2.4	Schematic drawing of the EBM process [2]-----	18
2.5	A titanium diamond lattice structure manufactured by EBM [52]-----	19
2.6	Ti-6Al-4V phase diagram showing α , β and $\alpha+\beta$ phase change by temperature and the addition of vanadium [60] -----	21
2.7	A schematic of combustion reaction to produce foam structure[64]-----	23
2.8	The porosity is increased with the addition of various content of Ti+B ₄ C [64] -----	23
2.9	Hollow spheres (left) sintered to an open-cell foam (right) [4]-----	25
2.10	An example of flow sheet for making open cell titanium foam [11]-----	26
2.11	Production of an open cell aluminium foam by sintering metal and salt powders [2] -----	27
2.12	Ti-Co foam manufactured by the space holder sintering process [70] -----	28
2.13	Schematic of designed graded structures with (a) three layers of various porosities and cell sizes, (b) differing interior porosity and cell size [71]--	30
2.14	Ti-6Al-4V lattice structures fabricated by SLM process [72]-----	31
2.15	A schematic of LasformSM system [74]-----	32
2.16	(a) LENSTM processed titanium cylindrical rods with porosity of 25% vol. (b) SEM image showing the porous surface of the produced samples [78]---	34
2.17	Microstructure of fabricated Ti-6Al-4V parts with (a) pore due to trapped gas and (b) pre due to insufficient heating [22]-----	35
2.18	Ti-6Al-4V scaffold manufactured by SLM with (a) top view; (b) bottom view; (c) SEM observation with 150 \times magnification and (d) SEM observation with 100 \times magnification after chemical etching [88] -----	38

2.19	FGMs made of material A and B showing (a) stepwise graded FGMs and (b) continuous graded FGMs-----	40
2.20	Flow chart diagram to produce FGMs by PM technique-----	41
2.21	Figure 2.21. shows pore size grading in a structure [92]-----	42
2.22	Optical micrographs of (a) uniform lattice structure and (b) graded lattice structure [96]-----	44
3.1	A schematic shows the ReaLizer SLM 50 with: 1, building platform; 2, feed container; 3, deposition unit; 4, power source; 5, argon flow nozzle [99]-	48
3.2	Schematic of the double scan strategy showing that each layer N is scanned both in x and y direction-----	50
3.3	Morphology and particle size of (a). Ti-6Al-4V particles; (b). NaCl powders -----	52
3.4	Exemplar blend of 50% mixture by volume. Salt and metal constituents can be clearly observed -----	55
3.5	Schematic draw of the hall flow test measuring the time needed for 50g mixtures of powders to flow through -----	56
3.6	A 9 mm sample in three various process parameters with each one of 3 mm -----	58
3.7	Simple assembly of structures and assignment of localised ‘build’ parameters (see Table 3.6) allows location specific density to be created -	58
3.8	Letter ‘A’ is fully encased in a dissimilar porosity matrix demonstrating the effect of distinct process parameters on resulting porosity -----	59
4.1	Hall flow test results as a function of salt content in the mixed powder feedstock-----	63
4.2	Single slice built with various processing parameters using Ti-6Al-4V and NaCl mixture with 40 vol.% salt-----	64
4.3	Single slice built without NaCl by energy density of (a) 92.6 J/mm ³ ; (b) 49.3 J/mm ³ and (c) 25.9 J/mm ³ -----	65
4.4	Element mapping by SEM of the as-built single slice with (a): as-built slice with un-melted metal powders and cracked NaCl powders; and mapping of element (b) Ti, (c) Cl and (d) Na. -----	65
4.5	SEM of (a) as-built slice and (b) after dissolving in water for NaCl removal -----	66
4.6	Schematic of the process creating cellular structures. a) The powder bed consists of both Ti6Al4V powder and larger NaCl particles. b) Following laser consolidation metal flows around the salt inclusion but connectivity is retained for a successful parameter set c) A leaching procedure removes the salt and a porous structure results. Noting full removal will only take place with sufficiently high connectivity between NaCl particles-----	67

4.7	Processing map of mixtures with various NaCl content-----	68
4.8	Salt dissolution as measure by the change in specimen mass with time----	70
4.9	Optical micrograph sections in the x-y plane showing the pore distribution within cubes with varying volume fraction of NaCl at (a) 10%; (b) 20%; (c) 30%; (d) 40%; (e) 50%; (f) 60%.-----	72
4.10	Metallurgy comparison between (a) cube without NaCl and (b) cube with 30 vol. % NaCl-----	73
4.11	The contribution of Na and Cl to the elemental composition of the porous structure is minimal. b) shows an elemental EDX map of the micrograph shown in a). c) and the inset table show the distribution of Na within the solid as minimal. Cl was not detected here.-----	74
4.12	The experimentally obtained relative density showing the uniform error across salt content within the feedstock. Equation for the linear region is given by $\rho_r = -1.2016X + 1.2245$ where X is the NaCl volume fraction. XCT was used to calculate the relative density here-----	76
4.13	Effect of salt content on mechanical properties in compression demonstrated by the characteristic stress-strain relationships-----	77
4.14	Specimens failed under loading: (a), (b), (c) failed with 30 vol.% NaCl and (d), (e), (f) failed with 60 vol.% NaCl-----	78
4.15	Relationship between cube relative density and compressive properties. Error bars result from the standard deviation of 5 compression test and three density measurements per specimen. a) Shows specimen relative compressive yield strength and b) shows relative compressive modulus normalised by compressive modulus of 100% Ti6Al4V built using parameters optimised for salt inclusion (see Section 4.3)-----	80
5.1	Sections in the x-y plane showing the pore distribution within cubes with 50 vol.% NaCl varying processing parameters at (a) 30W, 200mm/s; (b) 40W, 200 mm/s; (3) 50W, 200 mm/s-----	83
5.2	Laser power against structure relative density which shows that the relative density increases with laser power-----	84
5.3	Effect of laser power on mechanical properties in compression-----	85
5.4	Compressive properties of as-built and heat treated pure Ti-6Al-4V cubes-----	86
5.5	Microstructure and phase distribution in pure Ti-6Al-4V cubes with (a) as-built samples and (b) heat treated samples -----	86
5.6	Compressive properties of heat treated cubes in several processing parameters: (a) 30W, 200 mm/s; (b) 30W, 300 mm/s; (c) 30W, 400 mm/s-----	87

5.7	Graduation in density can also be achieved through modulation of layer-wise build parameters resulting in this case in three distinct regions. Sections of the graduation (b), (c) and (d) confirm the apparent variation.-----89
5.8	EDS maps at a pore showing NaCl on the pore boundary -----90
5.9	Graded specimen shows the compression behaviour of several stages at (I) beginning; (II) first collapse; (III) plateau region; (IV): further fracture----- -----91
5.10	Simple assembly of structures and assignment of localised ‘build’ parameters (see Table 3.6) allows location specific density to be created, where (a) is the CAD design model and (b) is the cross section scanned by XCT-----92
5.11	Letter ‘A’ is fully encased in a dissimilar porosity matrix demonstrating the effect of distinct process parameters on resulting porosity, where (a) is the CAD model; (b) and (c) shows XCT scanning result of XY and XZ plane respectively -----93

List of Tables

2.1	Commercially AM systems for metallic products fabrication [22] -----	12
2.2	Mechanical properties of Ti-6Al-4V fabricated by LENS process [22]-----	33
2.3	Tensile properties of Ti-6Al-4V parts fabricated by various techniques [22]--	37
3.1	Technical specifications of the ReaLizer SLM50 in this study-----	49
3.2	Composition of the Ti-6Al-4V as supplied by LPW-----	52
3.3	Thermal properties of Ti-6Al-4V and NaCl after Nagasaka et al. [17] and Boiveneau et al. [18] -----	53
3.4	Weights of two powders in various NaCl volume fraction-----	54
3.5	Processing parameters set-up for SLM samples with various NaCl-----	57
3.6	Volume specific parameters used to create the nested cylinder-----	59
4.1	Weight change with time of cube with 10 vol.% NaCl after placing in water-	69
5.1	The density of regions demonstrating functional graduation in the z-axis-----	72

Abbreviations

FGM	Functionally Graded Material
PVD	Physical Vapour Deposition
CVD	Chemical Vapour Deposition
AM	Additive Manufacturing
SLM	Selective Laser Melting
DMD	Directed Metal Deposition
ASTM	American Society for Testing and Materials
CNC	Computer Numerical Control
CAD	Computer-Aided Design
SLA	Stereolithography
STL	Stereolithography
UV	Ultraviolet
SLS	Selective Laser Sintering
DOD	Drop on Demand
DED	Directed Energy Deposition
PBF	Powder Bed Fusion
LENS	Laser Engineered Net Shape
Nd: YAG	Neodymium-doped Yttrium Aluminium Garnet
DMLS	Direct Metal Laser Sintering
HCP	Hexagonal Closely Packed
BCC	Body-Centred Cubic
HIPing	Hot Isostatic Pressing
CP	Commercial Pure
PVA	Polyvinylalcohol
EBM	Electron Beam Melting

PM	Powder Metallurgy
XCT	X-Ray Computed Tomography
EDX	Energy-dispersive X-ray Spectroscopy
SEM	Scanning Electron Microscope

Nomenclature

E	Energy density [J/mm ³]
P	Laser power [W]
r	Spot diameter [mm]
v	Scan speed [mm/s]
h	Hatch spacing [mm]
t	Layer thickness [mm]
ρ	Density [kg/m ³]
M	Mass [kg]
V	Volume [m ³]
ρ_r	Relative density [kg/m ³]
ρ^*	Experimental density of lattice structure [kg/m ³]
ρ_s	Density of solid material [kg/m ³]
σ^*	Experimental compressive strength of lattice structure [MPa]
σ_s	Compressive strength of solid structure [MPa]
C_1	Approximately 0.3 obtained from literature
C_2	Approximately 1.0 obtained from literature
E^*	Experimental young's moduli of lattice structure [GPa]
E_s	Young's moduli of solid structure [GPa]

Chapter 1

Introduction

1.1 Background

Cellular materials are commonly found in nature in both regular and irregular (or stochastic) arrays. The advantages of such structures, including high specific strength and weight, have been exploited in engineered analogues, such as honeycomb and foamed metal structures. For example, sandwich panels with foamed or honeycomb titanium cellular cores are used as structural materials for aerospace engineering, due to their low densities, high melting temperature and excellent mechanical properties. They have also been developed as implant materials as they show good compressive properties and often exhibit excellent biocompatibility when appropriate alloys are used. Furthermore, the compressive strength and modulus of titanium foams can be adjusted through the control of pore size, strut thickness and relative density. Functionally graded cellular materials have their application in areas including aerospace and medical fields. They are a material which the composition or the structure varies gradually over the volume, leading to be graded in depth in the composition, microstructure or mechanical properties in a single part.

Cellular titanium alloys, particularly Ti-6Al-4V alloys, have been widely used for areas including aerospace, automotive and medical industries due to their excellent mechanical properties, corrosion resistance and high specific strength to density ratio. Traditional methods to fabricate cellular Ti structures include reactive sintering [4], hollow sphere sintering [5], loose powder sintering [6] and 'space holder' techniques, which require a dissolution procedure [7]. Among these powder metallurgy techniques, the 'space holder technique' has attracted significant attention. Cellular structures are manufactured by mixing and compacting metal powders with space holder material, which is removable during or after sintering by dissolving

or thermal degrading to leave pores in structures. It offers the ability to control pore size, shape and distribution [8]. Magnesium [9], carbamide [10], [11], NaCl [12], [13] and acrowax [14] have all been used as space holders in the literature. Metallic foams such as aluminium, FeAl, Ti-Co and Ti-6Al-4V foams have been manufactured in this way. However, a major drawback to the more general adoption of these materials is that current methods of Ti cellular structure manufacture present significant limitations, such as multiple process steps and the production of geometries which are limited by the mould tooling complexity. Furthermore, removal of the space-holder without surface residue and deleterious effects upon the near surface metallurgy are critical concerns when selecting materials for this purpose. The development of Additive Manufacturing (AM) enables the manufacture of complex structures without the need for sophisticated tooling or multiple processes. Additive Manufacturing (AM), used to be called rapid prototyping (RP), (also referred to as 3D printing), which is the technology of translating Computer-Aided Design (CAD) models into finished parts layer by layer, is identified as an effective method to fabricate parts with more complex geometries. AM techniques, therefore, have the potential to remove many of the limitations associated with current cellular structure fabrication, such as greater control over cell type, density and grading, incorporation into solid structures in a single step and conformance to complex external geometries.

Researchers have categorized AM processes by various perspectives. ASTM categorization, which classified AM into the following seven items, has been commonly accepted [1]. It includes material extrusion, vat photo polymerisation, powder bed fusion, material jetting, sheet lamination, directed energy deposition and binder jetting. Among these processes, powder bed fusion (PBF), which uses either a laser or electron beam to melt and fuse material powder together, are most widely used for cellular structures fabrication. Selective laser melting (SLM) is one of the powder bed fusion methods, which makes use of a scanning laser to melt metal powders layer-by-layer in an inert gas atmosphere.

At the early stage, density of titanium and its alloys manufactured by SLM was not as high as those by traditional processes [15]. With the development of knowledge on SLM, the relationship between processing parameters and final product properties were investigated. Processing of titanium and the production of titanium alloy lattice structures using SLM is well established now [16].

With further development of technology, it has been found that most pure metals cannot meet the requirements in some applications which need several properties. Therefore, functionally graded material (FGM), which the composition or the structure varies gradually over the volume, leading to be graded in depth in the composition, microstructure or mechanical properties in a single part was investigated and developed. FGMs can be produced by processes such as Plasma Spraying, Self-propagating High temperature Synthesis, Physical Vapour Deposition (PVD) and Chemical Vapour Deposition (CVD) etc. However, these methods comprise several steps, are time and materials consuming. The thickness, chemical composition and microstructure cannot be precisely controlled so that the properties are not achieved as desired. With the advent of SLM process, it enables the creation of functionally graded lattice structure with spatially varying solid volume fraction. It also has a lot of advantages including high productivity, less energy consumption, material recycling, and ability to manufacture structure without shape and size limitation. However, the manufacture of lattice and cellular type structures within SLM requires the explicit design, analysis and optimisation of complex geometries. This is extremely challenging, in terms of computational methods and computer resources.

1.2 Aim and Objectives of the Research

The overall aim of this study was to develop a new method, combining SLM with a space-holder technique to build cellular Ti-6Al-4V parts without the explicit design stage. By selection of processing parameters with various NaCl content, uniform Ti-6Al-4V cubes should be fabricated in various relative densities. This should help to further produce functionally graded Ti-6Al-4V parts by control of mixtures and processing parameters, therefore there is a basic understanding of the relationship within materials, processing parameters, microstructure and properties. This aim was achieved through the following objectives:

- Investigate the achievability of SLM processes to produce cellular Ti-6Al-4V parts
- Develop the processing map for successful fabrication of uniform Ti-6Al-4V cubes with various NaCl content in blends
- Investigate mechanical properties on the fabricated samples and compare their performance with those manufactured by other processes
- Further develop the method to fabricate FGMs by selection and control of processing parameters in one part

1.3 Significance and Novelty of the Research

The study of the product fabrication with metal and salt blend by SLM process is challenging, due to the high energy density and working temperature in the process causing evaporation of salt particles. Performing experiments to investigate the relationship between materials, processing parameters and structure properties remains difficult owing to unable to control the pore size and distribution in the structure, therefore unpredictable mechanical properties.

In this work, thin wall was investigated first to see the performance of the SLM process. This work is significant because it works out the possibility of the two processes using this metal

and salt blend. Additionally, the study has researched the relationship between salt content and structural properties, and processing parameters and properties as well, which was not available in the literature.

This work has introduced the processing map with various salt content in the blend and predicted the relationship between NaCl content and relative density of the final part, which enables investigations into controlling the porosity of the parts by this method which was not available previously. Furthermore, this work successfully provides a new method to fabricate functionally graded structures through adjusting processing parameters, laser power and scan speed in this study.

1.4 Research Methodology

Based on the research aim and objectives in Section 1.2, a proposed experiment framework is presented in Figure 1.1, which was proposed to investigate the effect of NaCl on the final structures and study the relationship between materials, parameters and properties. The figure shows the steps and links of the research in this study.

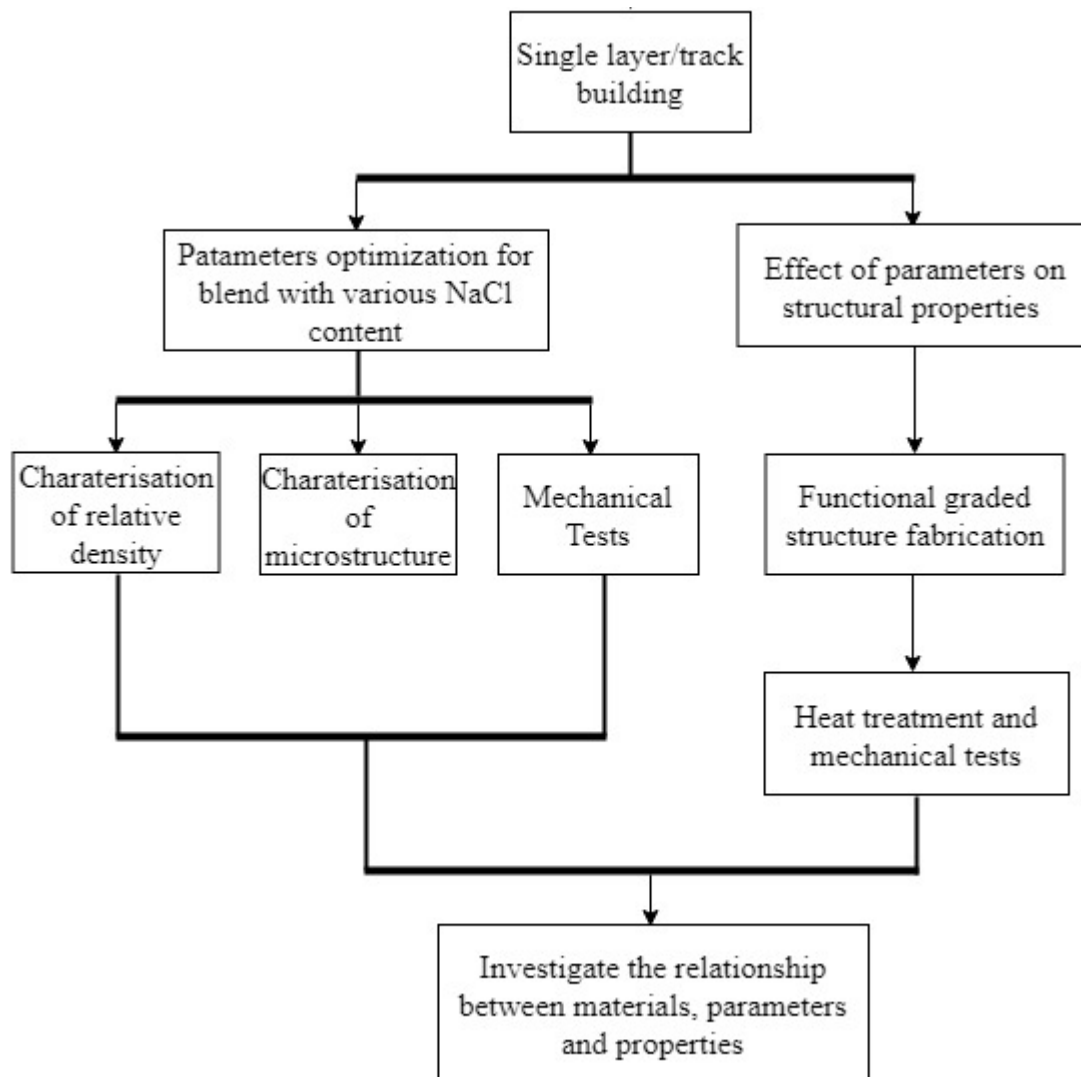


Figure 1.1. Framework for the Research to Determine the Effect of NaCl on the Structural Properties

1.5 Thesis Layout

A brief description of the content of each chapters is presented below.

Chapter 2-Literature Review

This chapter is related to three main parts. Firstly, a literature survey was performed to present researches in Additive Manufacturing. According to American Society for Testing and Materials (ASTM) categorization, seven available items of Additive Manufacturing technology

are introduced and three of them are generally reviewed, including material jetting, powder bed fusion and directed energy deposition process. In the second part, the development of titanium foam and its manufacturing methods are described. Furthermore, the limitations of current technology to fabricate titanium foam have been analysed in this section. Finally, a literature survey of functionally graded material was performed along with its current fabrication methods.

Chapter 3-Experimental Methods and Materials

In this chapter, the experimental apparatus is introduced first. The experimental setup of the SLM process has been presented. The methods to measure morphology, particle size and flowability of Ti-6Al-4V and NaCl powders are described. The thermal properties of two materials including melting temperature, boiling temperature and thermal conductivity are compared. This is followed by a table showing preparation of feedstock blend in various metal and salt ratio. A hall flow test is introduced to measure flowability of mixed powders. Finally, it describes all the types of samples designed and fabricated in this study.

Chapter 4- Composition Modulation for Ti-6Al-4V Cellular Structures with Various NaCl Content

In this chapter, a new method to fabricate cellular structure has been demonstrated. To investigate the effect of NaCl on the structure, the study starts with selective laser melting (SLM) process, it successfully builds Ti-6Al-4V foam structures with selected processing parameters. The samples after removal of NaCl are characterized by meso-and microstructure and compressive properties. The relationships between NaCl content, relative density and compressive properties have been studied and presented in this chapter.

Chapter 5- Modulation for Functionally Graded Structures

In this chapter, a novel method for functionally graded cellular structures fabrication is investigated by using the same materials as Chapter 4. It starts with investigating the effect of processing parameters on the final relative density of structures. Therefore, several types of graded structures have been built here by adjusting the processing parameters but using the same material. To enhance the compressive properties for further application, heat treatment was performed on the samples and results are compared for built and treated samples.

Chapter 6-Discussion

In this chapter, a general discussion of method proposed and results obtained from this research is proposed and compared with those in other literatures. The advantages and disadvantages of this method are analysed here and the potential application for further investigation is proposed.

Chapter 7-Conclusions and future work

In this chapter, a summary of novel and significant conclusions is listed and presented which are obtained from this study. Finally, future work has been presented on the basis of the current outcomes of this research.

Chapter 2

Literature Review

The development of Additive Manufacturing results from the improvement of various technology aspects, for example, comprehensive understanding of material and manufacturing process. AM technology has now been applied widely in many areas such as aerospace, automotive, biomedical engineering and food production. Owing to its ability to manufacture products with customised design, it has been developed to fabricate lattice and functionally graded structures in specific use. In this study, the literature review will focus on the Laser Powder Bed Fusion (LPBF) techniques and its application for manufacturing titanium foam. In comparison with AM technology, conventional sintering process to make foam structures will also be reviewed in this thesis.

2.1 Additive Manufacturing

Engineering parts created by traditional manufacturing processes, such as die casting, injection moulding and extrusion are with homogenous material and simple geometry. With the development of additive manufacturing techniques, design constraints have been reduced and more complex parts can be produced more cost effectively. Computer numerical controlled (CNC) machines allow material to be removed from a solid homogenous block to achieve the desired geometry. Compared to conventional processes, the final parts are homogeneous and predictable in quality and surface concave and convex shapes are possible [17]. However, this process cannot enable the manufacturing internal complicated cavities and structures.

Additive Manufacturing (AM), used to be called rapid prototyping (RP), (also referred to as 3D printing), which is the technology of translating Computer-Aided Design (CAD) models

into finished parts layer by layer. Charles Hull in 1986 [18] developed the AM process called stereolithography (SLA). After this, other AM techniques, such as fused deposition modelling, powder bed fusion were developed [19]. In ASTM, Additive Manufacturing is officially defined as: “A process of joining materials to make objects from 3D model data, usually layer upon layer, as opposed to subtractive manufacturing methodologies.” [20] The key to the technique is generating products by adding layers, under the control of computer aided design system (CAD). The generic processes of AM techniques are presented as [21]:

- Build CAD Model: A 3D model of desired application should be built with the help of CAD software package.
- Convert CAD Model to stereolithography (STL) File Format: STL file format is the standard format of AM industry.
- Transfer the STL File to AM Machine: The 3D model is sliced into layers, where each layer is a 2D cross section of the original model.
- Machine Setup: Build parameters like material constraints should be set up prior to the build process.
- Build: The model is built by using layer based manufacturing technique in this step.
- Removal and Post-process: The printed products and any supports are removed from the machine once the building step is finished. Additional clean up may need before they are ready to use.
- Application: Additional treatments like post-curing or painting may need to form a final application which is ready to use.

Researchers have categorised AM processes by various perspectives. For instance, according to the state of printing materials, it can be divided into liquid, solid and powder systems [22]. However, ASTM categorization, which classified AM into the following seven items, has been commonly accepted [1].

- 1) Material extrusion
- 2) Vat polymerisation
- 3) Powder bed fusion
- 4) Material jetting
- 5) Sheet Lamination
- 6) Directed energy deposition
- 7) Binder jetting

To manufacture metal parts, high working temperature is required to fuse the materials which are with relatively high melting temperatures. In these AM techniques, powder bed fusion (PBF), directed energy deposition (DED) are commercially used to fabricate metallic components. Table 2.1 lists the current commercially AM systems for metallic materials, which are classified according to the ASTM standard. Powder bed fusion (PBF), including selective laser melting (SLM), selective laser sintering (SLS), direct metal laser sintering (DMLS) and electron beam melting (EBM), and directed energy deposition (DED) including direct metal deposition (DMD) with wire or powder feed and laser engineered net shaping (LENS) are two main techniques for commercial metal fabrication. The layer thickness, laser beam diameter and energy source are also presented in Table 2.1. In this study, the work focuses on metal foam, therefore only manufacturing process for metallic parts fabrication will be reviewed here.

Table 2.1. Commercially AM System for Metallic Products Fabrication [23]

Manufacturer	System	Process	Layer thickness (μm)	Laser focus diameter (μm)	Energy source
Concept laser	M1 cusing	PBF (SLM)	20-80	50	Fiber laser 200-400 W
Sisma	MYSINT300	PBF (SLM)	20-50	100-500	Fiber laser 500 W
SLM Solutions	SLM500	PBF (SLM)	20-74	80-115	Quad fiber lasers 4 × 700W
Realizer	SLM 300i	PBF (SLM)	20-100	N/A	Fiber laser 400-1000 W
Farsoon	FS271 M	PBF (SLS)	20-80	40-100	Yb-fiber laser 200 W
EOS	M 400	PBF (DMLS)	N/A	90	Yb-fiber laser 1000 W
Arcam AB	Arcam Q20plus	PBF (EBM)	140	---	Electron beam 3000 W
Optomec	LENS Print Engine	DED (LENS)	25	---	IPG fiber laser 1- 2 kW
Sciaky	EBAM 300	DED (wire feed)	N/A	---	Electron beam
Trumpf	TruLaser Cell Series 7000	DED (powder feed)	N/A	---	CO ₂ laser 15000 W or YAG laser 6000 W
Renishaw	AM250	PBF (SLM)	20-100	70	Yb-fiber laser 200 W
Renishaw	RenAM 400	PBF (SLM)	20-100	70	Yb-fiber laser 400 W
Renishaw	RenAM 500 Series	PBF (SLM)	20-100	80	Yb-fiber laser 500-2000 W

2.1.1 Directed energy deposition

Directed energy deposition (DED) uses focused thermal energy, such as laser, electron beam and plasma arc, to fuse materials by melting as the material is being deposited. A typical DED machine consists of a nozzle mounted on a multi axis arm, which deposits melted material onto the specified surface, where it solidifies. The process is similar in principle to material extrusion, but the nozzle can move in multiple directions and is not fixed to a specific axis. The process can be used with polymers, ceramics but is typically used with metals, in the form of either powder or wire [24].

Based on the form of feedstock, DED can be divided into two categories: the first one which developed from conventional welding technique with metal wire as feedstock and second one using metal powder as feedstock named laser engineered net shaping (LENS). Figure 2.1 shows a typical LENS layout. The LENS process takes place in a building chamber filled with argon gas. A Nd:YAG laser beam focuses on the platform with a lens system. After the powder injected from the nozzle, it flows into the melt pool, fusing and solidifying quickly to form a single layer on the substrate.

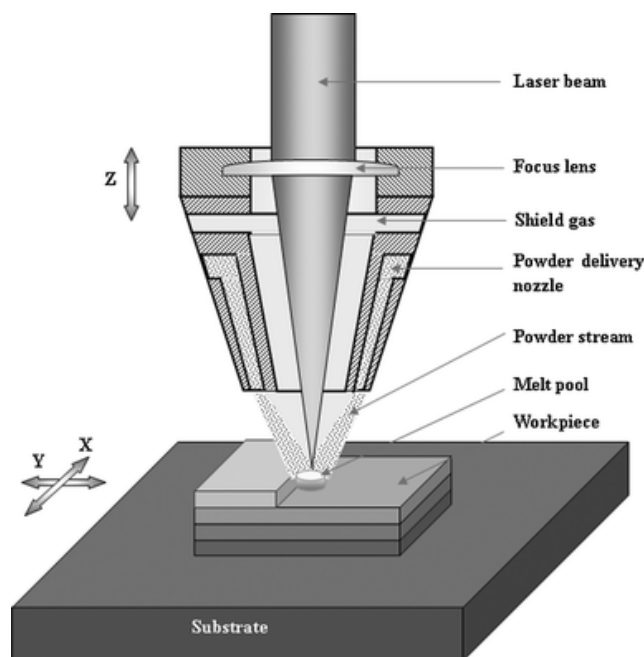


Figure 2.1. Basic Layout for a LENS System [23]

Direct energy deposition (DED) is one of the methods to fabricate metallic structures with relatively low time and machining cost. For instance, AlSi40 FGM was manufactured using an Nd: YAG laser [25]. Generally, both metallic powders and wires are used by this process. Figure 2.2 presents another concept of the DED process. The materials, one in the form of powder and the other in the form of wire, are first fed into a melt pool and fused by the laser beam. With moving of the CNC worktable, a thin layer of track is formed on the substrate. The substrate is fixed on the worktable and the laser beam is directed to the substrate. The CNC worktable is able to move in x, y and z directions under the control of the software. To prevent oxidation, the DED process may be performed in a transparent bag filled with inert gas. In order to obtain a component with desired geometry and properties, it is vital to control the processing parameters such as laser power, traverse speed, wire feed rate and powder feed rate [26]. The DED technology is mainly applied in industry to repair or build up some components [27]. In this case, titanium alloys plays a significant part, such as repairing titanium turbine blades or building up titanium rudders [28] DED has the capacity of using the solid freeform fabrication route to build titanium near-net-shape parts with the advantages of low cost, repair of complicated shape parts and high performance for the production [29]. In previous research, experiments were carried out using a 7 kW IPG fiber laser to build Ti-6Al-4V parts by the DED process. The results showed that the hardness of the DED parts was 360 ± 10 HV and higher than the forged plate. The yield and ultimate tensile strengths were 976 ± 24 MPa and 1099 ± 2 MPa respectively, superior to the cast and annealed wrought material [30]. However, the disadvantage of DED technology is its low accuracy (0.25 mm) and low surface quality [19], therefore this process is commonly used for manufacturing and repairing large components.

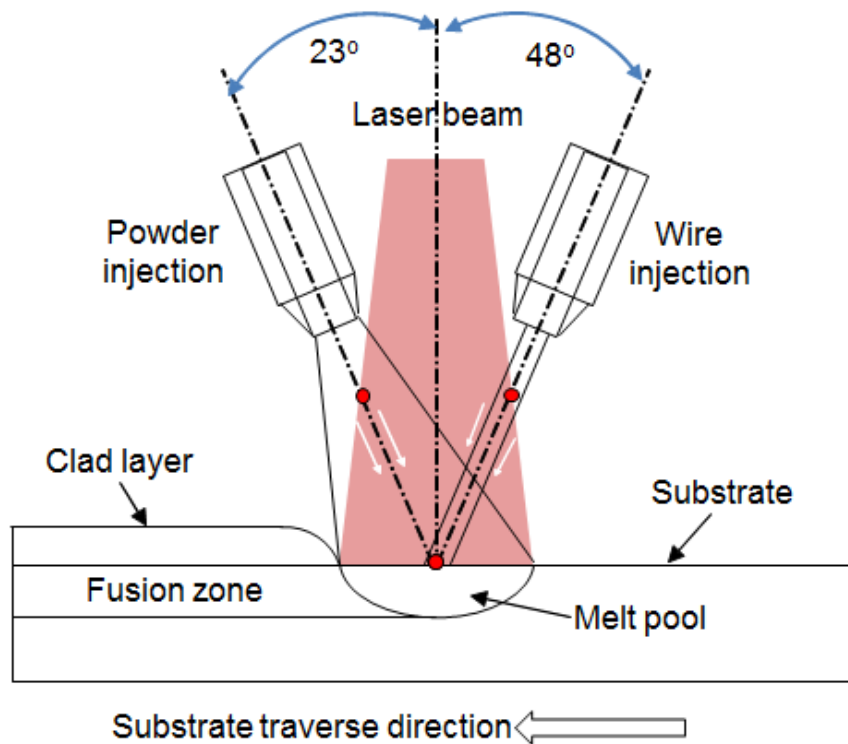


Figure 2.2. Schematic Drawing of the DED Process [24]

2.1.2 Powder bed fusion

A powder bed fusion process called selective laser sintering (SLS) was invented and patented by Deckard in 1989 [31]. This technique used laser energy to selectively fuse regions of a powder bed. The layer was scanned and fused to the previous layer. Apart from polymers, this process can also be applied to metals, such as stainless steel, titanium alloy and Inconel. Figure 2.3 shows a schematic drawing of the SLS process. It consists of a computer system to control the process, a laser, an automatic powder layering apparatus. Generally, the processing procedures of SLS include: 1) the inert gas is fed into the building chamber to lower the oxygen content to a standard value; 2) a thin layer of powder is deposited on the substrate by the layering mechanism; 3) the powder is scanned by the laser beam to form the desired profiles according to the STL files; 4) The above procedures are repeated and the components are built

layer by layer. However, metallic components fabricated by SLS process are not with good mechanical properties because powders are joined together by partial melting [32].

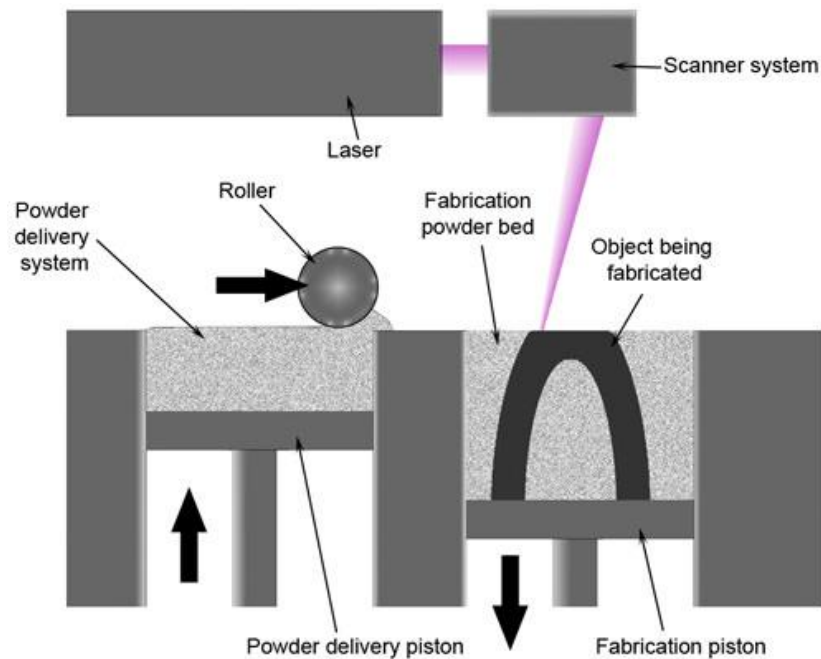


Figure 2.3. Schematic Drawing of the SLS Process [32]

Selective laser melting (SLM) development was driven by the demand to produce fully dense components with mechanical properties as good as those manufactured by conventional process [33]. The processing apparatus and procedures of laser melting and laser sintering are the same. The main difference is that laser melting involves complete melting of powders. The idea of fully melting due to improved laser processing conditions leads to improved microstructural and mechanical properties compared with SLS processed components [34]. SLM is able to process a variety of metals and alloys, such as titanium, aluminium and copper, etc. Promising areas for application of SLM include rapid tooling, functionally graded materials and satellite technology. For instance, a 316L stainless steel scaffold was built by the SLM technique, whose compressive elastic modulus and compressive yield strength were ~ 0.15 GPa and ~ 3 MPa respectively, similar to those of trabecular bone [35]. SLM allows the fabrication of parts with complex external shape and nearly fully dense structure. Therefore, it

has been investigated as a promising process for parts fabrication with various materials. Products made of aluminium alloys [36], titanium alloys [37], cobalt chromium [38], stainless steel [39] and Inconel [40] are developed to be built by the SLM technique. A lot of examples show that parts have been successfully fabricated using this process. Sun. et. al. [35] built high-density (>99%) stainless steel 316L (SS316L) parts with micro-hardness between 213 and 220 HV, much higher than that of the annealed part of ~155 HV. Yan. et. al [41] developed a biocompatible Ti-15Ta-10.5Zr alloy fabricated by SLM as a viable candidate for the application in bone implants since its Young's modulus value of 42.93 ± 3.28 GPa was similar to the human cortical bone. Pröbstle. et. al. [42] used SLM to achieve improved creep strength of nickel-based super alloy compared to conventional cast and wrought material. Das [43] demonstrated the feasibility of fabricating components for defence applications by the selective laser sintering/hot isostatic pressing (SLS/HIP) technique; Hayashi et al. [44], Hollander et al. [45], Kanazawa et al. [46] and Wauthle et al. [47] employed SLS/SLM to process implants for medical purposes while Vasquez et al. [48] recently developed new SLS materials for snowboarding applications. Ardila et al. [49] and Seyda et al. [50] also highlighted that SLS/SLM allows an efficient use of the material, due to the possibility to recycle and reuse unmelted metal powder. They established that after recycling powders between 12 and 14 times, there were no significant changes in powder and test part properties. Therefore, SLM process costs less in manufacturing complicated parts compared with conventional process. For example, to fabricate some aerospace parts, only 2% metallic material, such as titanium or nickel, is used and the rest wasted as chips, which increases cost [32]. SLM also has advantages of manufacturing complicated parts, including FGMs, decreasing material waste, and fabricating metallic products as dense as those by conventional processes. However, SLM requires higher laser power, better beam quality and thinner layer thickness, causing a risk of instability of the melt pool [51]. Shrinkage may occur during the liquid-solid transformation

and stresses are accumulated in the parts. When cooling, the residual stresses increase, which is a key factor in the distortion and cracking of parts.

The EBM process, which uses a high powered electron beam, typically 4 kW to fuse the powder, is developed from the SLM technique. As shown in Figure 2.4, the process requires vacuum environment. An electron gun is on the top of powder bed as beam source, which is controlled by a lens system for movement. It carries out in a high temperature environment for electrical conduction of the powder bed. Each layer of powder is scanned twice with first scan to heat up the entire powder bed and second selectively scan to fuse powders for required geometry.

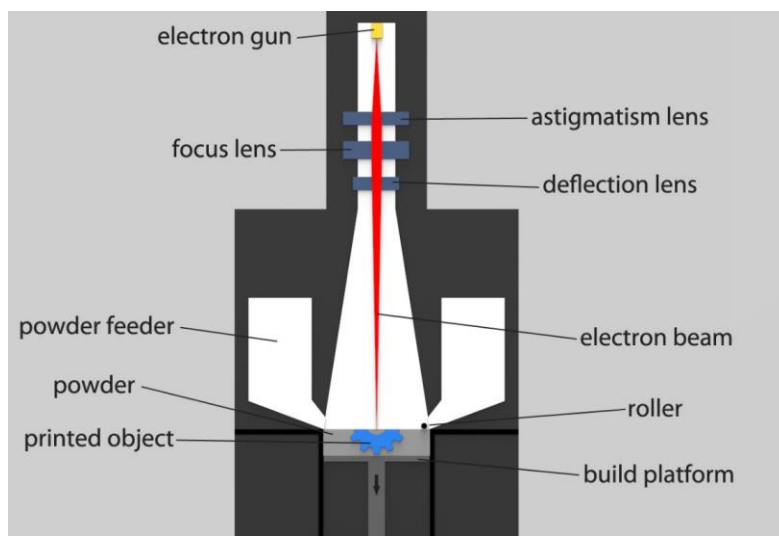


Figure 2.4. Schematic Drawing of the EBM Process [2]

EBM is most often used for fabrication of lattice titanium and titanium alloys, for instance, Ti-6Al-4V alloy. Figure 2.5 presents a Ti-6Al-4V lattice square structure manufactured by the EBM process [52]. Apart from titanium alloys, Co-Cr-based alloys have been built by EBM for biomedical implant applications [53]. Copper lattice parts are also fabricated for thermal and electrical management [54]. The EBM process, same as SLS and SLM, is able to manufacture products with more complex geometry, which is not achievable by conventional processes.

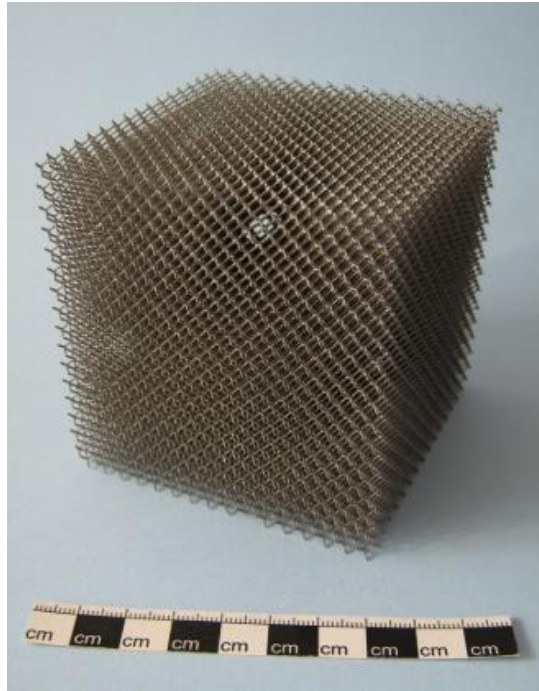


Figure 2.5. A Titanium Diamond Lattice Structure Manufactured by EBM [52]

2.1.3 Summary

AM technology is generally introduced in Section 2.1. Among all the AM techniques, DED and PBF are two commercially used processes for metallic products fabrication. Both techniques have been reviewed in this section. Metallic structures of titanium alloys, stainless steel, Inconel and so on have been successfully built by these two techniques. The high powered laser or electron beam makes their commercially wide use for manufacturing titanium parts since titanium and its alloys are with high melting temperature, which is difficult to process by conventional techniques. The traditional sintering methods to fabricate titanium alloys will be reviewed in Section 2.2. The advantages and disadvantages of these methods are indicated and compared to those of AM technique.

2.2 Titanium Foam and Manufacturing Methods

2.2.1 Titanium and its alloys

Titanium alloys have been increasingly used as biomaterials due to their superior biocompatibility, lower modulus and enhanced corrosion resistance compared to stainless steel and cobalt alloys. As given in Figure 2.6, titanium alloys exist in three structural forms: alpha (α) with hexagonal closely packed (hcp) crystallographic structure, beta (β) with body-centred cubic (bcc) form and alpha-beta. When pure titanium is mixed with other elements, the phases change. For example, aluminium is an alpha-phase stabilizer which increases the strength of the alloy, while vanadium is a beta-phase stabilizer. The transformation of pure titanium from α to β occurs at 882 °C [55], which can be changed by the addition of aluminium or vanadium. Depending on the composition and heat treatment, both α and β forms may coexist [56].

Ti-6Al-4V, the $\alpha+\beta$ combination alloy, is the most commonly used titanium alloy for dental implants. Heat treatment of the alloy generates fine precipitation and improves its strength, leading to enhanced mechanical and physical properties suitable for implants [57]. It is strong and highly resistant to fatigue and corrosion with a relatively low density. The elastic modulus is closer to bone than any other implant materials except pure titanium. [58]. Vanadium free $\alpha+\beta$ alloys, for instance, Ti-6Al-7Nb, have been developed due to toxicity concerns with vanadium. Moreover, some β phase titanium alloys composed of non-toxic elements, such as Nb, Ta and Zr, are under development because of their lower elastic modulus between 55 to 85 GPa, which is much lower than that of $\alpha+\beta$ alloys (113 GPa) and closer to human bones [59].

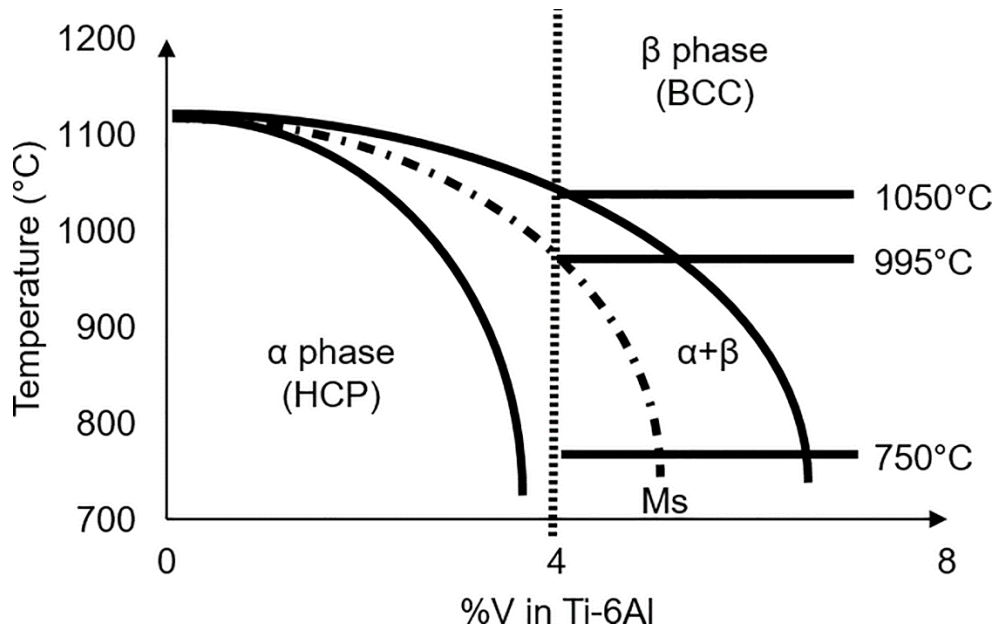


Figure 2.6. Ti-6Al-4V Phase Diagram Showing α , β and $\alpha+\beta$ Phase Change by Temperature and the Addition of Vanadium [60]

2.2.2 Cellular structures

Cellular materials are commonly found in nature in both regular and irregular (or stochastic) arrays [61]. The advantages of such structures, including high specific strength and weight, have been exploited in engineered analogues, such as honeycomb and foamed metal structures. For example, sandwich panels with foamed or honeycomb titanium cellular cores are used as structural materials for aerospace engineering, due to their low densities, high melting temperature and excellent mechanical properties [62]. They have also been developed as implant materials as they show good compressive properties and often exhibit excellent biocompatibility when appropriate alloys are used [57]. Furthermore, the compressive strength and modulus of titanium foams can be adjusted through the control of pore size, strut thickness and relative density [12].

There are several methods to fabricate titanium cellular structures. Traditional methods to

fabricate cellular Ti structures include reactive sintering [4], hollow sphere sintering [5], loose powder sintering [6] and ‘space holder’ techniques, which require a dissolution procedure [63]. In AM technology, laser beam deposition system, laser engineering net shaping and powder bed fusion process are able to manufacture titanium cellular structures. The following sections will introduce and compare advantages and disadvantages of these processes.

2.2.3 Reactive sintering

Reaction (chemical) sintering is developed because of a number of new materials which are not compacted according to classic mechanisms of solid-phase and liquid-phase sintering. The term "reaction sintering" indicates that compaction of the material takes place due to the occurrence of chemical reactions. In reactive sintering process, chemical reactions synthesize inter-metallic and generate heat of reaction. Combustion synthesis makes use of the produced heat. Figure 2.7 presents the schematic of the combustion process to form porous materials. In this figure, two powders, X and Y mixtures, are compacted together and part of the blend is heated to trigger a reaction between X and Y. Once the powders rapidly heat up and raise the neighbouring temperature, the reaction propagates and melts the powders. The gas bubbles, mostly hydrogen, contained in the liquid are entrapped during the procedure to create the pores when cooling rapidly. In Kanetake and Kobashi’s study [64], Nickel and Aluminium were used as X and Y element. As a result, nickel aluminide and porous titanium matrix composites were produced by the method shown in Figure 2.7.

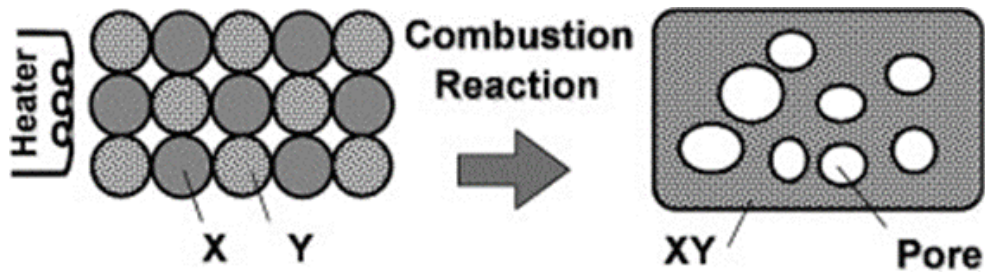


Figure 2.7. A Schematic of Combustion Reaction to Produce Foam Structure [64]

The porosity of the final product can be increased by the addition of materials such as carbon, which burns in the air to produce CO; or materials which react together with the powders to create higher reaction temperature and fine particles to stabilize the product. Kanetake and Kobashi [64] has reported the method to increase the porosity using Ti+B₄C foaming agent in the Na and Al blend. As given in Figure 2.8, The porosity was successfully increased from 30 to 90% with the addition of 5% Ti+B₄C. It can be seen that the shape of pores is irregular in shape and size.

No addition	0.5vol%	1.0vol%	2.0vol%
3.0vol%	4.0vol%	5.0vol%	
			10mm ↔

Figure 2.8. The Porosity is Increased with the Addition of Various Content of Ti+B₄C [64]

In another study, Ti-Al-Si alloys were successfully produced by reactive sintering process with Al content between 8-20 wt.% and Si content between 10-20 wt.% [4]. Although reactive sintering is a straightforward process to produce foams, the final shape and porosity of the foam cannot be accurately controlled. Also, the process is limited to materials which react

exothermically together. These limitations result in its low commercial use for foam products in the market.

2.2.4 Loose powder sintering and hollow sphere sintering

Loose powder sintering was the first method to fabricate porous metals and is now widely used to manufacture self-lubricating bearings and filters. The pores in the components are produced from the incomplete space filling of powders which are poured into and sintered in a die [3]. Basically, metallic powders are poured into a die and sintered. With this method, the densities are between 40-60%, but they are affected by particle shape and size [3]. A wide range of metal powders can use this method for producing foams due to the simplicity of the process. It has been commonly used for bronze powders to make bearings, but titanium, stainless steel and superalloys foams can also be fabricated using this technique. Owing to the need for sintering in a die, the size and structure of the part, and the productivity are quite limited.

Owing to the limitations and relatively low porosities achievable with the loose powder sintering process, another method, named hollow sphere sintering, has developed which is capable of much higher porosities foam. Using this process, both closed and open cell structures can be made, with sphere diameters between 1.5 to 10 mm and wall thickness from 20 to 500 μm . It has been reported that porosity of 80-97% can be achieved in this way [5]. An example in Figure 2.9 presents how the hollow spheres turn into an open cell foam after sintering.

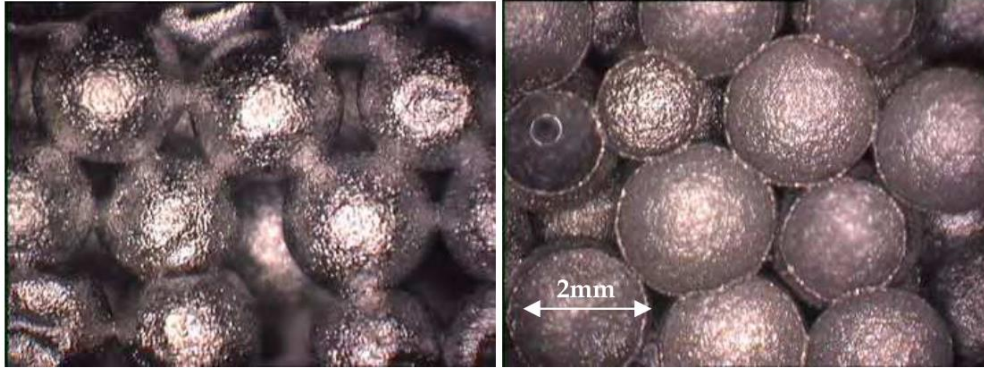


Figure 2.9. Hollow Spheres (left) Sintered to an Open-cell Foam (right) [5]

The advantage of foam structures prepared from sintered powders or hollow spheres is the good control of the size and geometry of the pores, leading to desired porosity and structure properties. The high porosity structures achieved with this process lead to their use in lightweight structural applications and energy absorption.

2.2.5 Space holder technique

The space holder compaction technique is another method to produce metal foam. Cellular structures are manufactured by mixing and compacting metal powders with space holder material, which is removable during sintering, or after the process by dissolving or thermal degrading to leave pores in structures. This method has the advantage that the size and morphology of pores can be determined by the characteristics of space holder materials. Furthermore, the porosity of final structures can be easily controlled by the ratio of metal powder and space holder.

Figure 2.10 presents the basic steps of this process to produce titanium porous structure. Titanium powders and NaCl particles were mixed together with organic binder. After compaction, removal of binder, sintering and removal of NaCl, a foam structure finally was produced. The cell size and shape in the foam was almost equal to the original NaCl particles.

The porosity and cell wall thickness varied by the ration of Ti: NaCl in the blend. The yield strength and Young’s modulus of the foams were 12-30 MPa and 8-15 GPa respectively, which was comparable with those of compact and cancellous bones [12]. NaCl is used as the space holder material in many cases because it can be removed effectively by water. Commercially pure titanium porous samples have been created using commercial pure (CP) Ti and NaCl powders with NaCl content between 40 and 70 vol.% [65]. The factors affecting dissolution rate of NaCl in the samples were investigated in this work, which included salt content, water temperature and immersion time per cycle. Water temperature between 50 and 60 °C and immersion time of 4 hours per cycle were found to be the optimum conditions for NaCl dissolution. NaCl space holder can be used in self-propagation of the chemical reaction process as well. For example, open-cellular TiAl was manufactured by a combustion reaction process between titanium and aluminum with a space holder powder of NaCl. [66].

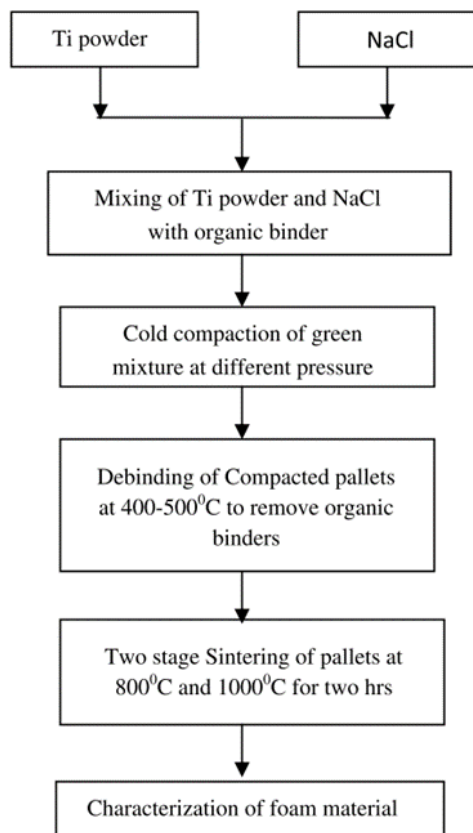


Figure 2.10. An Example of Flow Sheet for Making Open Cell Titanium Foam [12]

NaCl is not only used as space holder for titanium foams, but also for other metal foams, for example, aluminum alloys. An open cell A356 aluminum foam was successfully made by a gravity die casting process with the pore size and porosity controlled by the size and amount of NaCl [13]. Figure 2.11 presents the detailed process for producing aluminium foam by sintering metal and salt powders [3]. Graded FeAl intermetallic foams were fabricated using a NaCl space holder by powder metallurgy process with porosity from 40% to 60% [67]. An open cell porous Cu with adjustable pore size and shape and mechanical properties were successfully prepared using Cu and NaCl blend via sintering and dissolution process [68]. Precise fabrication of porous magnesium based scaffolds has been achieved using NaCl templates. The relationship between space holder particles, pore characteristics and mechanical properties has also been investigated [69].

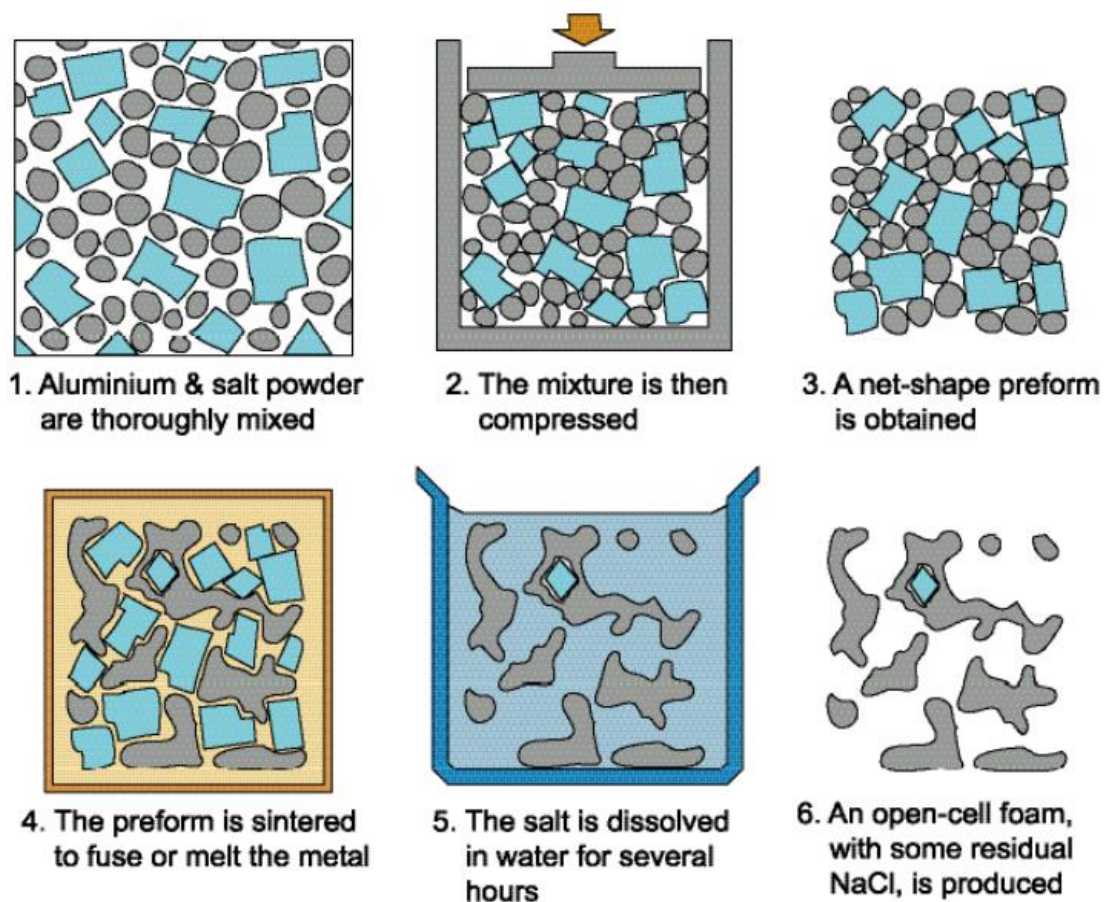


Figure 2.11. Production of an Open Cell Aluminium Foam by Sintering Metal and Salt Powders [3]

Apart from NaCl, other materials can also be used as space holders as long as they can be removed during or after the process. Carbamide of 710-1000 μm has been used as a space holder with polyvinylalcohol (PVA) as a binder [70]. Titanium and Cobalt powders were mixed with 1.5% PVA and compacted at 200 MPa into a cylindrical specimen, which was immersed in water so that the carbamide was leached out. After that, the specimen was sintered in a high purity argon gas atmosphere. Finally, Ti-Co alloy structure with 70% porosity and pore size between 400-550 μm was successfully manufactured by this method [70], as shown in Figure 2.12. The compression behavior of titanium and carbamide powder mixtures with various ratio of carbamide space holder was studied by Arifvianto et al. [10]. The results showed that the yield pressures decreased with increasing volume fraction of carbamide in the mixture. A model was built to predict the compression behavior using the ratio of titanium and carbamide powder mixtures.



Figure 2.12. Ti-Co Foam Manufactured by the Space Holder Sintering Process [70]

Magnesium has also been used as a space holder to process Ti-6Al-4V foams. In Asik and Bor's study [9], the magnesium powder was removed by heating Ti-Mg to 1200 °C in order to evaporate the Mg. Three sets of samples were prepared with 50%, 60% and 70% volume fraction of Mg. It was seen that the porosity increased and density decreased with Mg volume

fraction in the mixture. The Young's modulus and yield strengths of the samples were between 4-12 GPa and 69-167 MPa respectively, decreasing with increasing Mg content. The properties are in the range for implant applications [9].

Sugar is another space holder material for creating titanium foams. Graded porous titanium structures with various porosity and pore size have been manufactured by a powder metallurgy method, as shown in Figure 2.13 [71]. Two structures were designed for graded foam. In Figure 2.13 (a), there were three layers of various porosities and pore sizes. For instance, the top layer was in 30% porosity with pore size 0.3-0.425 mm, while the bottom layer was 50% porosity with pore size 0.425-0.5 mm. In Structure (b), the interior porosity was designed to be 50% while the outer porosity was 30%. It was found that the porosities and pore sizes were able to be controlled by the volume fraction and size of sugar pellet. The yield strength and Young's modulus were tested across the structure for the three-layer sample. The Young's modulus of the sample was 18.5, 16.4 and 12.1 GPa for 30%, 40% and 50% porosity, respectively, which is similar to that of natural bone. The yield strengths were 89.8, 176.5 and 202.3 MPa respectively, which is higher than that of natural bone [71].

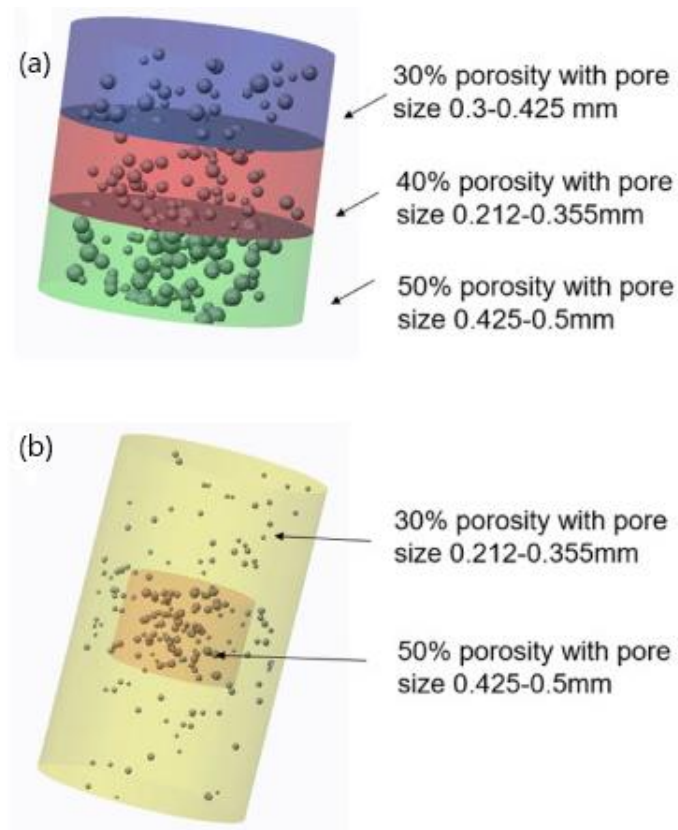


Figure 2.13. Schematic of Graded Structures with (a) Three Layers of Various Porosities and Cell Sizes, (b) Differing Interior Porosity and Cell Size [71]

However, a major drawback to the more general adoption of these materials is that current methods of Ti cellular structure manufacture present significant limitations, such as multiple process steps and the production of geometries which are limited by the mould tooling complexity. Furthermore, removal of the space-holder without surface residue and deleterious effects upon the near surface metallurgy are critical concerns when selecting materials for this purpose.

2.2.6 Additive manufacturing of titanium foam

With the advent of Additive Manufacturing processes, such as selective laser melting (SLM), and recent advances in lattice design, the creation of lattice structure without the limitation to complex internal structure has been achieved and used widely. For instance, In Figure 2.14, Ti-

6Al-4V lattices were built by the SLM process with porosity suitable for bone cell ingrowth and mechanical properties consistent with cancellous bone [72]. The following sub-section introduces a number of AM processes that can be used for fabricating Ti and Ti alloys.

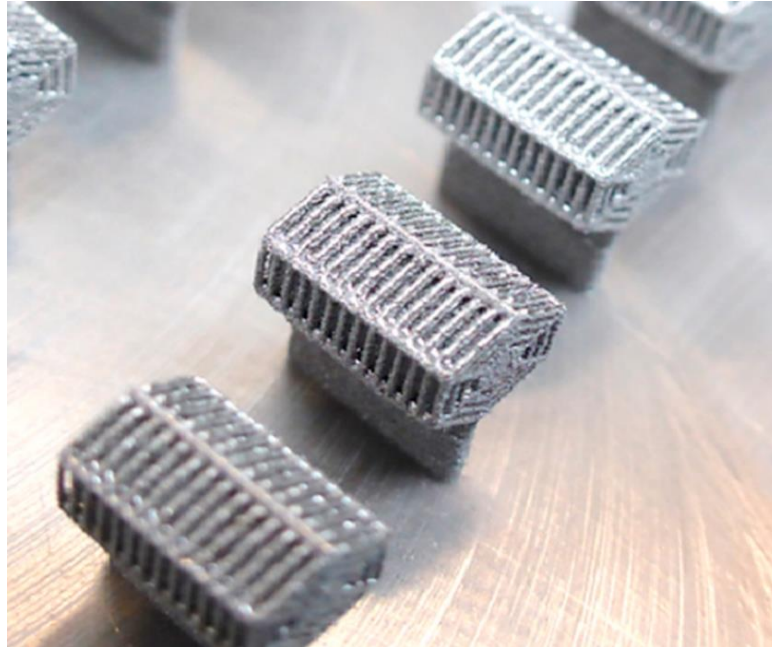


Figure 2.14. Ti-6Al-4V Lattice Structures Fabricated by SLM Process [72]

2.2.6.1 Directed energy deposition for titanium foam

The laser beam directed energy deposition system is made up of a head to deposit metals onto a substrate and was the first AM technique used for forming titanium alloys. The deposition system consists of optics for the laser beam, one or several nozzles to deliver materials in powder or wire form and the outlets for inert gases injection during the working process [21]. The substrate used in this system consists of a titanium platform for Ti alloys fabrication. LasformSM [73] is known as the first laser beam deposition process for Ti alloys and this system is shown in Figure 2.15.

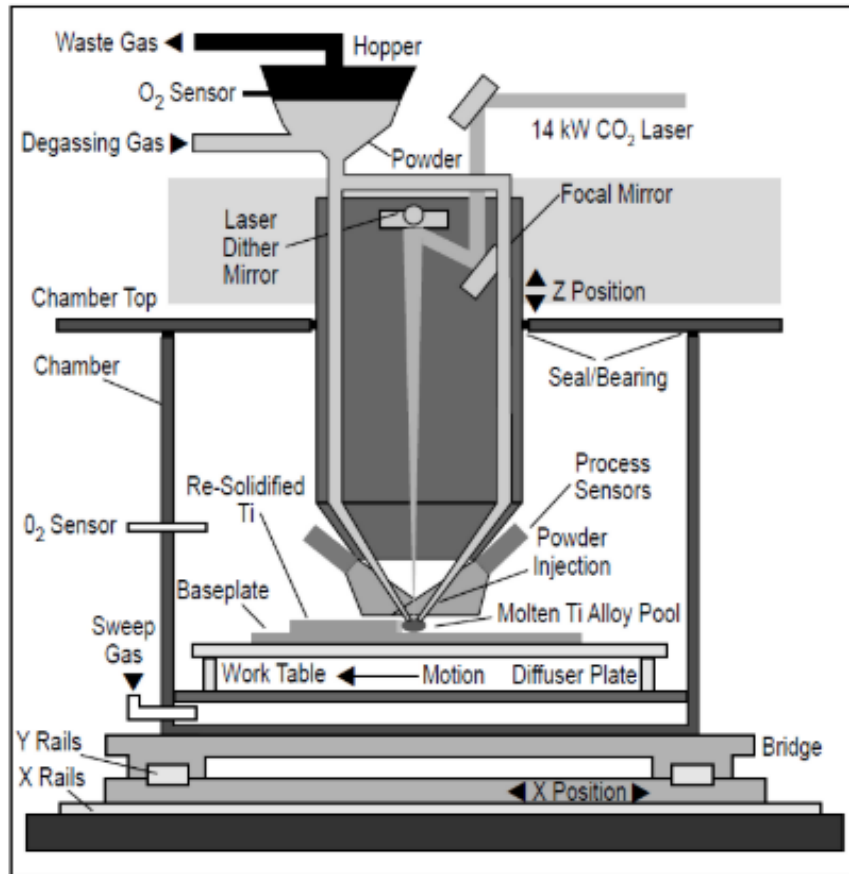


Figure 2.15. A Schematic of LasformSM System [74]

The deposition rate of this process is reported to be 0.9-4.5 kg/hour. It has shown its potential to manufacture large components with complex structures, which cannot be achieved by conventional processes. It has found application in Ti-6Al-4V aerospace components such as flanges, cones and door panels [73]

By adjusting the processing parameters, high density parts can be fabricated, therefore excellent mechanical properties are achieved. It has been reported that the tensile properties and fatigue resistance of Ti-6Al-4V samples from this process were comparable to those wrought and cast samples respectively. The microstructure of the Ti-6Al-4V parts created by LasformSM has been found to be significantly dissimilar to those from conventional processes. Columnar prior β grains and fine lamellar α were observed in Ti-6Al-4V parts by the LasformSM process [75].

Due to the success of LasformSM, researchers developed a more cost effective system called Laser Engineering Net Shaping (LENS). It simplifies the working process of Lasform, but shares similar working principles, which has been reviewed in Section 2.1.1. The LENS process has better accuracy than LasformSM system due to a smaller laser beam diameter [74]. It uses metal and its alloy powders for parts fabrication, such as titanium, aluminium and stainless steel. Griffith et al. [76] first reported a study on the microstructure of parts fabricated by LENS. They compared the tensile properties with wrought materials. It has been found that the yield strength is similar to that of wrought parts and it could be further optimized by adjusting processing parameters. Wu et al. [77] showed that laser power and laser scan speed have an effect on the morphology and size of columnar grains and lamellar microstructures.

The mechanical properties of as-built LENS Ti-6Al-4V parts are summarized in Table 2.2 [23]. It has been found that the Young's modulus is close to the wrought parts for both building orientation and small failure strains have been observed in LENS fabricated parts. The difference in yield strength and failure strain is caused by the presence of porosity in the as-fabricated material. Hot isostatic pressing (HIP) has been proved to be an effective way to improve ductility of LENS built Ti-6Al-4V products [74].

Table 2.2 Mechanical Properties of Ti-6Al-4V Fabricated by LENS Process [23]

Process	Orientation	Young's modulus, GPa	Yield strength, MPa	Failure strain
Wrought	Longitudinal	113	945	0.100
LENS	Horizontal	116	1066	0.053
LENS	Vertical	112	832	0.008

Titanium foams have been developed significantly due to their potential application in orthopaedic and dental area. For example, recently, porous titanium implants were successfully

produced by LENSTM technique [78]. As shown in Figure 2.16, cylindrical rods in 3.0 mm diameter were manufactured with 25% vol. in porosity and 200-300 μm in pore size. The surface porosity was achieved by partially fusing the materials with low laser power and optimize processing parameters such as layer thickness, hatch spacing and laser speed.

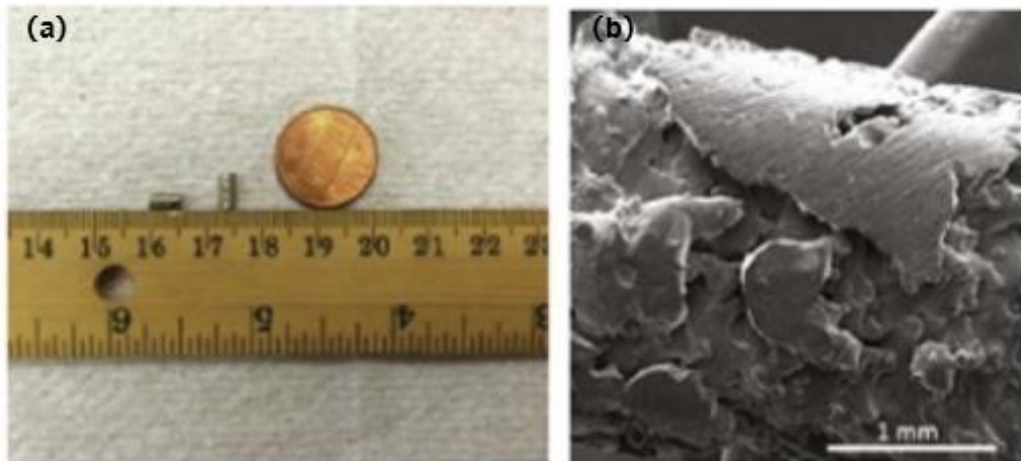


Figure 2.16. (a) LENSTM Processed Titanium Cylindrical Rods with Porosity of 25% vol. (b) SEM Image Showing the Porous Surface of the Produced Samples [78]

Recent research has found that laser beam deposition system with wire feedstock has higher deposition rate and reduces energy consumption and potential hazardous contamination compared with powder feedstock system. With these advantages, wire feedstock laser deposition system has been applied in areas such as aerospace components, components repair and functionally graded coatings [79]. It has been reported that the fatigue behaviour of Ti-6Al-4V built by wire feedstock laser system is similar or superior to cast Ti-6Al-4V [80]. The main disadvantage of wire laser beam is the poor resolution of as-built products and therefore, further machining is needed for better accuracy and surface finish [19].

2.2.6.2 Powder bed fusion for titanium foam

The powder bed fusion process differs from the laser beam deposition process in that the former uses a laser separated from the delivery system of the powder on the substrate [21]. This simplifies the delivery of the materials and enables the manufacture of complicated geometry with high resolution. Electron Beam Melting (EBM) and Selective Laser Melting (SLM) are the two energy source used with powder bed systems, which has been introduced in Section 2.1.2. SLM process was first developed in 1995 by MCP Tooling Technologies, and Ti alloys fabricated by SLM process started in late 2000s [21]. It has been focused on building cellular scaffolds and customised medical tools, for instance, teeth models, which were costly to make by conventional manufacturing processes [32]. Early studies of titanium and its alloys manufactured by the SLM did not meet the requirement for engineering applications because of the relatively high porosity compared with traditional processes [15]. For instance, in Figure 2.17, the SLM fabricated Ti-6Al-4V parts contain porosities due to trapped gas and insufficient heating.

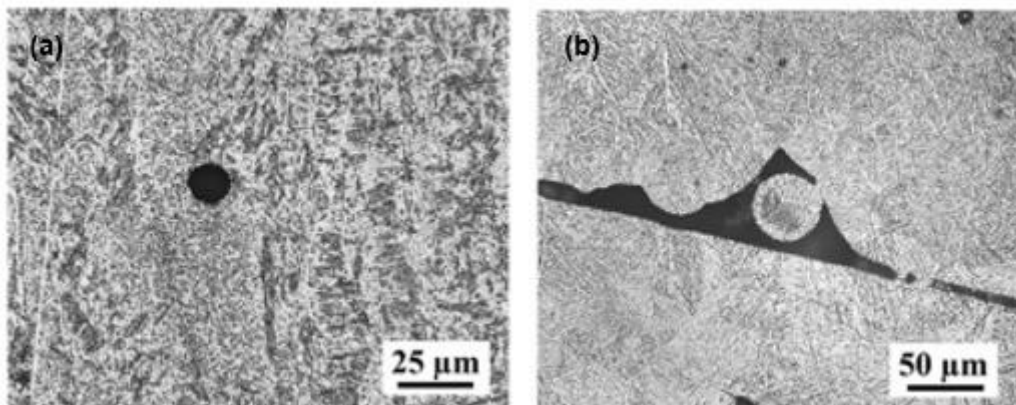


Figure 2.17. Microstructure of Fabricated Ti-6Al-4V Parts with (a) Pore due to Trapped Gas and (b) Pore due to Insufficient Heating [23]

With the development of knowledge on SLM, the relationship between processing parameters, titanium product microstructure and properties were investigated. The microstructures of SLM

parts are affected by temperature gradient and interface velocity, while both of them can be affected by processing parameters such as laser power, laser scan speed and layer thickness [23]. By adjusting processing parameters, high quality SLM manufactured Ti parts were obtained [81]. Thijs et al. [82] studied the relationship between scanning strategy and parameters on the microstructure of Ti parts. Song et.al [81] proved that processing parameters not only played a role in microstructure, but also in properties such as roughness, micro-hardness and densification for Ti-6Al-4V parts. Sun et al. [83] found that layer thickness had the most important effect on the density. By controlling the layer thickness, samples with high density above 95% were produced and α phase, β phase and α' acicular martensite were the main phases seen in the microstructure of SLM Ti-6Al-4V parts. Qiu et al. [84] studied the effect of layer thickness and scan speed and found that with the layer thickness fixed at 20 μm , when the scan speed was lower than 2700 mm/s, the products had relatively low porosity. Shi et al. [85] concluded that layer thickness had an influence on surface roughness but not on tensile properties for titanium SLM parts. It was found that with high layer thickness, although a coarse sample was obtained, the tensile properties including yield strength, ultimate tensile strength and tensile strain were not affected compared with those with low layer thickness. Li et al. [86] compared the influence of laser power, scan speed and hatch distance on relative density separately. As a result, scan speed was found to be the most significant factor on relative density. In conclusion, laser scan speed can be considered to be the most significant processing parameter for the SLM of Ti alloy because it directly effects both the laser energy density and the process time [87].

The mechanical properties of Ti-6Al-4V structures built by powder bed fusion technology are important for their applications in aerospace and medical implant. The tensile properties of Ti-6Al-4V fabricated by both EBM and SLM are presented in Table 2.3 [23]. It includes Young's modulus, yield strength and failure strain and these properties are compared with wrought Ti-

6Al-4V parts. In the table, horizontal is the in-plane direction and vertical is the direction of accumulation. As shown in Table 2.3, Young's modulus of SLM, EBM and wrought parts are similar. The yield strength of the SLM parts is better than that of the wrought material. As reported, this is because SLM uses fine powders as feedstock. The as-built parts are more brittle with less failure strains, while HIP process is able to increase the elongation, but decrease the yield strength.

Table 2.3. Tensile Properties of Ti-6Al-4V Parts Fabricated by Various Techniques [23]

Process	Condition	Orientation	Young's modulus, GPa	Yield Strength, MPa	Failure strain
Wrought	As fabricated	Longitudinal	113	945	0.100
SLM	As fabricated	Horizontal	105	1070	0.060
		Vertical	102	1050	0.080
	HIP	Horizontal	112	1000	0.125
		Vertical	110	920	0.160
EBM	As fabricated	Horizontal	104	844	0.088
		Vertical	101	782	0.099

SLM have been applied to manufacture titanium foams. A Ti-6Al-4V scaffold was successfully manufactured by the SLM process [88]. Figure 2.18 gives the top and bottom view of the product in Figure 2.18 (a) and (b) respectively. In Figure 2.18 (c), it shows that the sample was with regular pore size and distribution, and the pores were open which met its requirement in biomimetic material use. Surface quality has been effectively improved by chemical etching in a hydrofluoric acid for surface treatment as shown in Figure 2.18 (d). Another report shows that Ti-6Al-4V porous dental implant was fabricated using SLM. The final product was with rough surface for new bone ingrowth and thus strengthen the connection between the bone and implant [89].

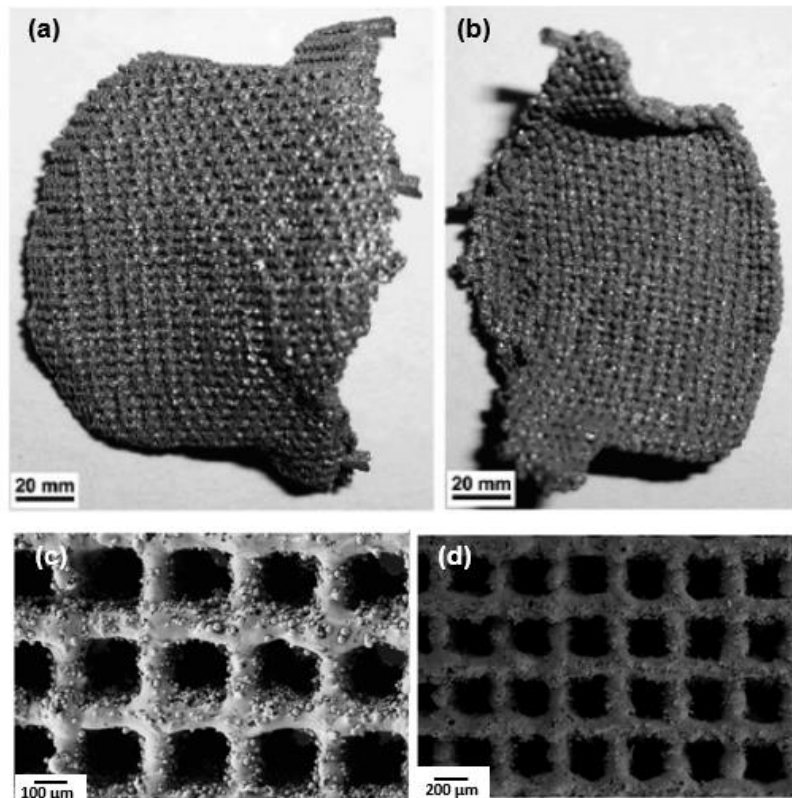


Figure 2.18. Ti-6Al-4V Scaffold Manufactured by SLM with (a) Top View; (b) Bottom View; (c) SEM Observation with 150× Magnification and (d) SEM Observation with 100×Magnification after Chemical Etching [88]

2.2.7 Summary

This section has reviewed the manufacturing processes to fabricated titanium foams. It includes conventional processes, such as reactive sintering, loose powder sintering and hollow sphere sintering and space holder technique, and AM technique such as DED, EBM and SLM. The relationship between processing parameters of SLM and microstructure and properties of final products has been reviewed, which will be further discussed in Chapter 5. Selective laser melting (SLM) have the advantages of directly building complex shaped metal parts into final porous products, therefore it has been widely used for Ti-6Al-4V cellular structures fabrication for the application of metal implants. However, connection problems between bone and implants with inhomogeneous porous structure need to be considered. It is also difficult to

satisfy the requirements for the stability of connection and strength of load bearing parts between bone and implants. Therefore, graded implant varying pore structure has attracted researchers' interest. In Section 2.3, it will focus on introducing graded structure and its manufacturing processes.

2.3 Functionally Graded Materials

The concept of Functionally Graded Materials (FGMs) was first proposed as thermal barrier materials for aerospace structures [45]. Functionally graded materials (FGMs) are materials in which the composition or the structure varies gradually over the volume, leading to an engineered, graded variation microstructure and properties in a single part [90]. These materials can meet the need of specific properties and applications. For example, structures working at high temperature can be designed with excellent thermo-mechanical properties. FGM has been applied in various areas, such as aerospace, bio-medical, electronics and automotive.

According to the grading type, FGMs can be classified into stepwise graded and continuous graded FGMs. Figure 2.19 shows the difference between the two types of FGMs. Figure 2.19 (a) shows clear interface between two materials while Figure 2.19 (b) gradually varies from one material to another.

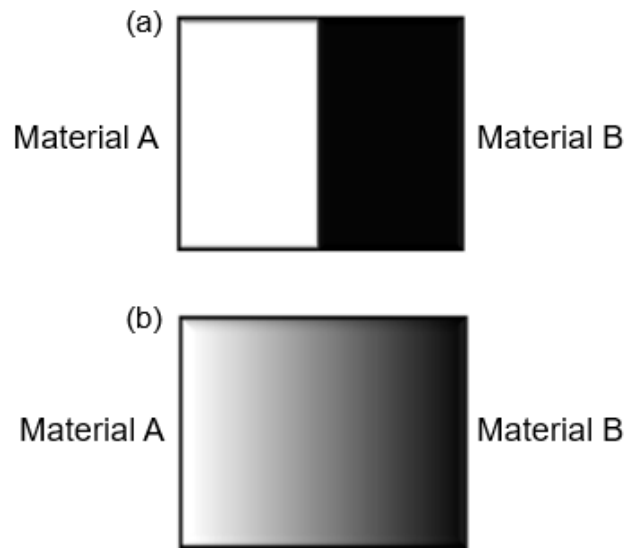


Figure 2.19. FGMs Made of Material A and B Showing (a) Stepwise Graded FGMs and (b) Continuous Graded FGMs

FGMs has found their application in a lot of areas such as aerospace, energy, sensors etc. Due to the high demand for FGMs for engineering application, many efforts have been made to develop and improve the fabrication process of FGMs. Thin and bulk FGMs are two broad groups for these materials. Thin FGMs refer to relatively small sections or surface coating. In contrast, bulk FGMs need more materials and processes. Thin FGMs can be produced by processes such as Plasma Spraying, Self-propagating High temperature Synthesis, Physical Vapour Deposition (PVD) and Chemical Vapour Deposition (CVD) etc [91]. Bulk FGMs can be produced by conventional methods including powder metallurgy and centrifugal casting method, or AM technique.

2.3.1 Conventional Methods for Functionally Graded Materials (FGMs)

Powder metallurgy (PM) technique is one of the most important processes used to fabricate FGMs. The flow chart in Figure 2.20 gives a typical example of a PM process to produce

functionally graded materials. The basic steps are as following process. Firstly, two powders, A and B, are weighed and mixed together. The blend is mixed in a ball mill. Next, the mixture is compacted and pressed in a prepared die. Finally, the two powders are sintered.

PM technique can create two types of gradients structure gradients and composition gradients. In structure gradients, grading is created with various pore size or porosity. For instance, in Figure 2.21, it indicates pore size grading from top to bottom. This is generally produced by using various particle size. Porosity grading can be achieved by various particle shape in powder mixtures. Composition gradients are created by variation in chemical compositions.

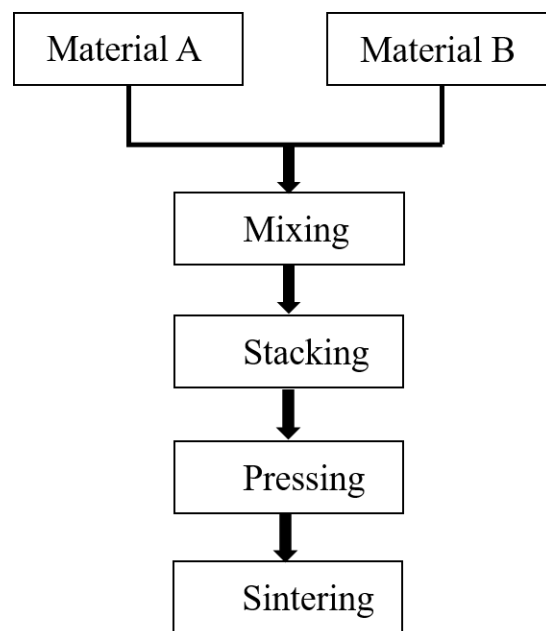


Figure 2.20. Flow Chart Diagram to Produce FGMs by PM Technique [3]

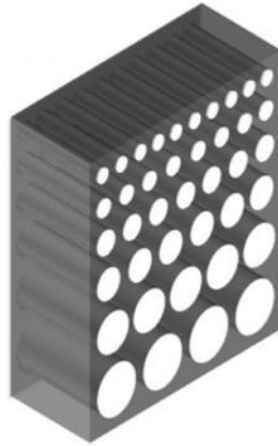


Figure 2.21. Shows Pore Size Grading in a Structure [92]

Although this process has its simplicity, it can only create stepwise graded structure. A continuous graded structure is difficult to achieve using this method. The FGMs with continuous gradients can be produced by centrifugal method [93].

The centrifugal cast method is a technique in which the particles of the reinforcement phase are poured into a melted metal liquid to create a uniform mixture. Through segregation of the particles and liquid by centrifugal forces, a chemical compositional gradient is created and maintained by controlling the solidification process [63]. This process has the limitation that only cylinders can be manufactured. Due to the density differences, there is also a limit to the type of gradient formed. Also, these methods comprise several steps, and are time and materials consuming. The thickness, chemical composition and microstructure cannot be precisely controlled and the geometry of the structure is limited to simple shapes, therefore, it is unable to meet the need of the complex net shapes for advanced applications. In order to solve this problem, another manufacturing method has been developed known as Additive Manufacturing.

2.3.2 Additive Manufacturing (AM) for Functionally Graded Materials (FGMs)

With the advent of Additive Manufacturing processes such as selective laser melting (SLM) and recent advances in lattice design, it is possible to create functionally graded lattice structure with spatially varying solid volume fraction [94], [95]. Additive Manufacturing for FGMs has a lot of advantages including high productivity, less energy consumption, material recycling, and ability to manufacture structure with less shape and size limitations. The basic steps for AM have been introduced in Section 2.1. There are several laser-based Additive Manufacturing processes able to create metal FGMs. Among these processes, selective laser melting enables the fabrication of fully dense parts. Maskery et al. [96] designed graded density Al-Si10-Mg lattice structures which were fabricated by the SLM process. In the study, the performance of uniform and graded density of Al-Si10-Mg lattices structures under quasistatic loading was examined. Figure 2.22 presents the two structures. In uniaxial compression tests, graded and uniform structures absorbed almost the same amount of energy prior to densification, 6.3 ± 0.2 MJ/m³ and 5.7 ± 0.2 MJ/m³ respectively. Choy et al. [97] investigated both honeycomb lattice structure and Ti-6Al-4V lattice with density gradient fabricated by the SLM. Grading was achieved by linearly changing the struts diameter. It has been observed that both structures display similar compressive phenomenon. It also gave the conclusion that lattice orientation had an effect on structure properties and FGMs with vertical struts behaved better at energy absorption.

Another typical example of graded lattice structure is varying gradually the strut distribution but with same strut diameter [98]. This type of Ti-6Al-4V density graded lattice structure was fabricated by the SLM using a rhombic dodecahedron unit cell. It exhibited excellent mechanical properties which were potentially promising for energy absorption applications. The samples were also tested by static loading with a strain rate of 0.001/s and dynamic loading of 1000/s. As a result, it showed the strain rate sensitivity in the bulk material [98].

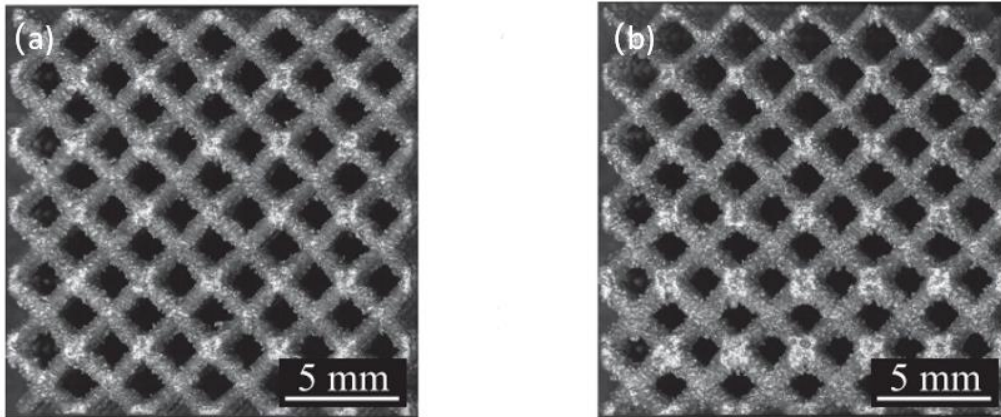


Figure 2.22. Optical Micrographs of (a) Uniform Lattice Structure and (b) Graded Lattice Structure [96]

2.3.3 Summary

Functionally graded materials have been generally introduced in this section including their classification and manufacturing processes. Although many processes can be applied to make FGMs, only powder metallurgy and centrifugal casting method enable to produce continuous graded structures. However, due to the limitation in shape and size of products manufactured by conventional techniques for FGMs, additive manufacturing technology including DED, EBM and SLM has been developed to build FGMs. Graded lattice metallic structures by the SLM process have been reviewed in Section 2.3.2.

2.4 Summary of Literature and Identified Gaps in the Literature

The AM technology classified by ASTM categorization has been summarized and introduced in Section 2.1. Powder bed fusion, for instance selective laser melting and directed energy deposition, for example direct metal deposition process, enable the fabrication of highly dense metal parts, with mechanical properties similar to those manufactured by conventional process [33]. Titanium and its alloys are the most common metal products fabricated by DMD and SLM [34]. However, the properties of these materials are controlled by processing parameters such as laser power, scan speed and the layer thickness. The complicated behaviour in the melt pool causes laser spatter and pore formation, therefore affecting the mechanical performance and leading to fatigue failure of the products [81].

Methods to fabricate titanium foams were discussed in Section 2.2. The traditional sintering processes, such as reactive sintering, loose powder sintering, hollow sphere sintering and space holder technique were introduced in Section 2.2.3-2.2.5. These processes, as discussed in Section 2.2, generally involve several steps including material mixing, compaction, debinding and sintering, which are complicated and instable in process. For instance, in the reactive sintering process, the final shape and porosity of the foam are unable to be controlled since the energy released in the procedure is unpredictable. Also, the process is limited to materials which can react exothermically together.

For all sintering processes, the size and shape of the final product is limited to those of the die. Complicated structures are unable to be achieved using these methods. Therefore, AM technology, for example, the SLM process, is an effective way to overcome the structure limitation. Lattice structures are achievable by SLM process. However, it requires the explicit design, analysis and optimisation of complex geometries.

Problems also exist in methods to fabricate functionally graded structures. Conventional processes comprise several steps. The properties, for example, density and porosity, cannot be achieved as desired due to the thickness, chemical composition and microstructure are unable to be precisely controlled. The geometry of the structure is difficult to meet the need of complex net shape for advanced application. With the SLM process, complex geometries can be achieved but it is challenging for design and optimisation work. Following the literature review of current research and outcomes these fields, the key gaps in the research are outlined below

1. The method to fabricate foam structures and functionally graded structures, which is straightforward without time and cost consuming design and optimisation, but with size and shape not limited to those of the die remains unexplored in the literatures.
2. The SLM process has been widely used for metal foam structure fabrication. The effect of processing parameters on the properties of the final product has been investigated for metals such as titanium, aluminium, stainless steel and Inconel. However, the effect of materials such as salt, remains largely unexplored and unknown. There is a lack of understanding at the process of how salt affecting the structure and how processing parameters in this case affecting the properties with respect to relative density and mechanical properties.

Chapter 3

Experimental Methods and Materials

As reviewed in Chapter 2, Ti-6Al-4V lattice and cellular structures can be manufactured by several methods including traditional sintering processes, the space holder technique and AM technology. This study accounts for the manufacturing of Ti-6Al-4V foam by adding space holder during AM process. Carbamide, magnesium, sugar and NaCl were used as space holder materials in literatures studied in Section 2.2.5. NaCl has been chosen as the space holder here due to its relatively high melting temperature compared with carbamide and sugar. Furthermore, NaCl is water soluble and is easy to remove after fabrication of samples. This chapter introduces experimental apparatus used in Section 3.1 and studies the powder morphology of experimental materials in Section 3.2, with the size and shape of two raw materials, Ti-6Al-4V and NaCl, presented in Section 3.2.1 and thermal properties obtained from the literature in Section 3.2.2. Section 3.2.3 describes the method to mix the two powders and lists the required weight of each powder with various NaCl volume fraction. Section 3.2.4 measures the flowability of powders, which is significant to deliver a uniform and compact powder layer. Section 3.3 presents all the types of samples which are fabricated in this study. NaCl particles need to be removed in the structure after fabrication, which is described in Section 3.4. After removal of NaCl, the properties are characterized in Section 3.5 and 3.6.

3.1 Experimental Apparatus

3.1.1 Realizer SLM 50

All of SLM processing work in this study was carried out using Realizer GmbH SLM-50, Germany, as shown in Figure 3.1, equipped with a CW Yttrium fibre laser with a powder bed spot size of 30 μm and maximum nominal power of 100 W. It has a wavelength of 1070 nm. All the samples were built on a Ti-6Al-4V substrates in an argon gas atmosphere. The SLM system was operated in its normal mode with the feedstock delivered from a standard hopper and conventional wiper arrangements were utilised.

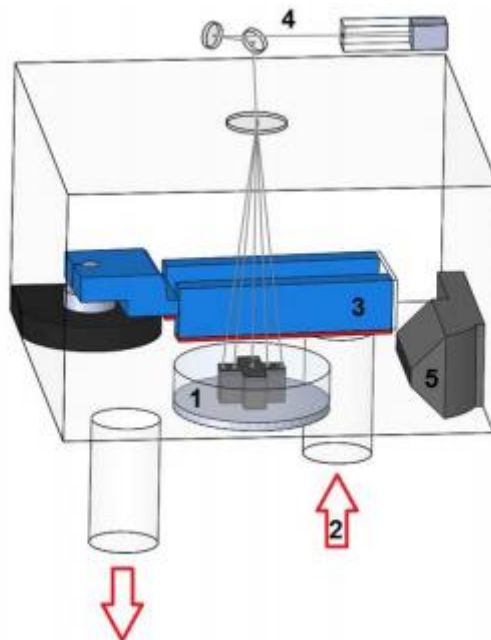


Figure 3.1. A Schematic Shows the ReaLizer SLM 50 with: 1, Building Platform; 2, Feed Container; 3, Deposition Unit; 4, Power Source; 5, Argon Flow Nozzle [99]

ReaLizer Control Software was used for setting build orientation and processing parameters. This software allows control of structure building by defining parameters including laser powder, hatch spacing, laser scan speed and laser scan strategy. Each layer can be scanned multiple times [74].

Table 3.1. Technical Specifications of the ReaLizer SLM50 in This Study

ReaLizer SLM50	
External Dimensions, mm	800×700×500
Weight, kg	80
Build Envelop, mm	70×40
Power Supply	230 V, 16 A
Layer Thickness, μm	20-100

A double scan strategy, or called 90° alternating scanning strategy, as presented in Figure 3.2, in which each layer was scanned in both x and y directions was employed in this study. After the first scan, the second turns the building orientation by 90°. It has been reported for SLM Ti-6Al-4V parts, double scan strategy gives the lowest residual stress among all tested strategies [100]. A layer thickness of 45 μm and hatch spacing of 60 μm were used based on the material size given in Section 3.2 and previous studies for the processing of titanium powders [74].

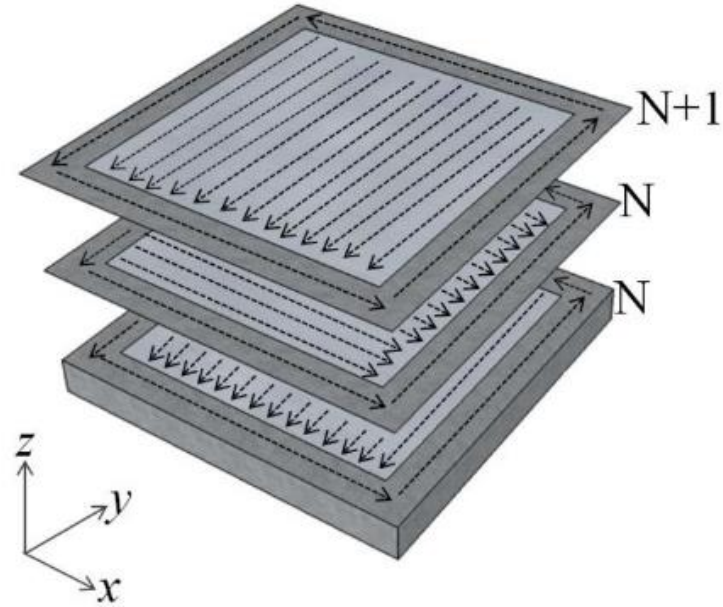


Figure 3.2. Schematic of the Double Scan Strategy Showing That Each Layer N is Scanned both in x and y Direction

The effects of laser power and scan speed were investigated, with power ranging from 10W to 100W and scan speeds from 100 mm/s to 500 mm/s. The build platform was held at 200°C throughout fabrication. Laser energy density (E) is considered to be a crucial factor affecting the properties of fabricated parts in the SLM process. It is defined in Equation 3.1, where P is laser power (W), v is scan speed (mm/s), h is hatch spacing (mm) and t is layer thickness (mm).

$$E = \frac{P}{v \times h \times t} \quad (3.1)$$

3.1.2 Techniques for characterisation of meso and microstructure

The particle size distribution was determined using a Malvern UK Mastersizer 3000, which uses laser diffraction to measure the size of particles through measuring the intensity of light scattered as a laser beam passes through a dispersed particulate sample. The morphology of Ti-6Al-4V was characterised using a Hitachi TM3030 scanning electron microscope (SEM), and

the NaCl powder was observed with a Nikon Eclipse LV100ND optical microscope. The weight of the cubes were measured using an ABT100-5M (Kern & Sohn GmbH, Germany) analytical balance.

In order to characterize the cellular structures created by the SLM of the combined metal-salt feed material, test samples were prepared for analysis by sectioning, mounting, grinding and polishing. The microstructure was studied using both optical microscopy and scanning electron microscopy (SEM). Composition of the samples was assessed using energy dispersive spectroscopy (EDX) in the SEM. The meso-structure of the samples, here defined as the structure on the scale of the individual lattice cells, was characterized by micro-focus X-ray computed tomography (micro-XCT). XCT data processing was performed using the public domain image processing software ImageJ. Each XCT measurement provided a stack of images, each representing a cross-section in the xy plane with a layer thickness of 7.16 μm . A sample of 100 images, equally spaced throughout the vertical direction of the specimen, was taken to expedite the analysis procedure. The densities of each cube were calculated from the measured weight and volume of each sample. The volume was determined from physical dimensions measured by Vernier Caliper. Therefore, the density of the sample was calculated by Equation 3.2.

$$\rho = \frac{M}{V} \quad (3.2)$$

3.2 Experimental Materials

3.2.1 Materials morphology in the research

Plasma-atomized, spherical Ti-6Al-4V powder (ASTM B348, LPW Technology Ltd., Cheshire, UK) with a mean particle size of $\sim 35 \mu\text{m}$ and sodium chloride (NaCl-98% purity) powder with

a mean size of $\sim 150 \mu\text{m}$ were used as the lattice material and space holder respectively. The composition of the Ti-6Al-4V powder is shown in Table 3.2.

Table 3.2. Composition of the Ti-6Al-4V as Supplied by LPW

	Ti (wt. %)	Al (wt. %)	V (wt. %)	Fe (wt. %)	O (wt. %)
Nominal	Balance	5.5-6.5	3.5-4.5	<0.25	<0.13

The morphology and size distribution of the two materials is shown in Figure 3.3. It can be seen in the figure that the NaCl particles are cubic in shape, compared to the much smaller, spheroidal Ti-6Al-4V powder. This increases the probability that the finer Ti-6Al-4V powders will surround the coarser NaCl powders when they are mixed to form a continuous lattice structure, as desired.

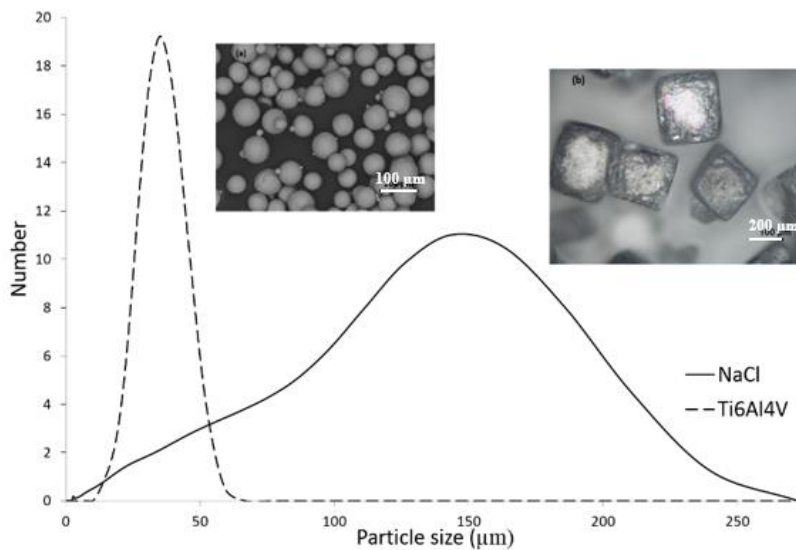


Figure 3.3. Morphology and Particle Size of (a). Ti-6Al-4V Particles; (b). NaCl Powders

3.2.2 Thermal properties of materials

The thermal properties including melting temperature, evaporation temperature and thermal

conductivity of both materials are shown in Table 3.3. It is notable that the boiling temperature of the salt is lower than the melting temperature of the metal, indicating that at least some vaporisation of the salt may be expected during processing if the metal is melted. Furthermore, the thermal conductivity of the salt is lower than that of the metal at typical processing temperatures, hence, localised heat would be expected to flow through the metal in preference to through the salt.

Table 3.3. Thermal Properties of Ti-6Al-4V and NaCl after Nagasaka et al. [17] and Boiveneau et al. [18]

Material	Melting temperature, °C	Boiling temperature, °C	Thermal conductivity, W/(m·°C)
Ti-6Al-4V	1604-1660		15 at 1200°C 20 at 1400°C
NaCl	801	1413	0.5 at 1170°C 0.45 at 1400°C

3.2.3 Powder mixing

In order to produce samples with a range of relative densities in the final structure, feedstock of various volume ratios of NaCl: Ti6Al4V were prepared. In the first step, 300g of Ti-6Al-4V powder was hand-mixed with NaCl for 2-3 minutes, with NaCl proportions varying from 10% to 60 vol. %. The weights of the two powders for the feedstock are presented in Table 3.4.

Table 3.4. Weights of Two Powders in Various NaCl Volume Fraction

NaCl Volume Fraction, vol. %	Weight of Ti-6Al-4V, g	Weight of NaCl, g
10	300	16.3
15	300	25.8
20	300	36.6
25	300	48.8
30	300	62.7
35	300	78.8
40	300	97.5
45	300	119.7
50	300	146.3
55	300	178.8
60	300	219.4

Following this, the blends were mixed in a gyroscopic mixer. The powder mixes were dried in an oven before use. Figure 3.4 shows a 50 vol. % NaCl mixture. The NaCl and smaller, more spherical Ti-6Al-4V particles can be clearly differentiated. Some of the NaCl particles appeared to cleave during mixing and as a result smaller NaCl crystals are observed in the mixture. It may be expected that the range of salt crystal sizes would result in a corresponding range in lattice cell sizes in the processed material. This is not investigated explicitly in this work but clearly the potential to control the stochasticity of the cellular structure through control of the space holder (in this case NaCl) size distribution exists.

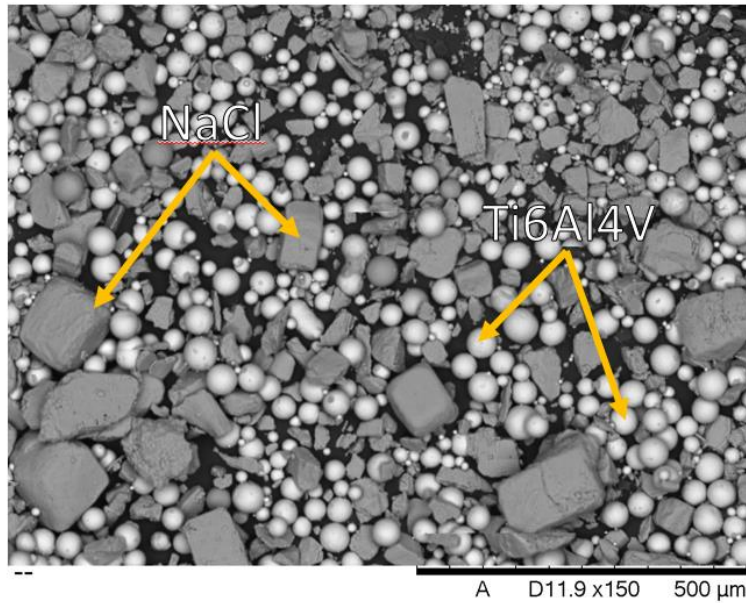


Figure 3.4. Exemplar Blend of 50% Mixture by Volume. Salt and Metal Constituents Can Be Clearly Observed

3.2.4 Flowability test

An important consideration in using such a mixed feedstock is that the resulting powder mix retains sufficient flowability to enable the feed and spreading mechanisms in the particular SLM machine used to deliver a uniform and compact powder layer. The flowabilities of the mixed feedstock were evaluated using a hall flow test according to ASTM B213. Figure 3.5 shows the equipment used to measure the time needed for 50g mixtures of powder to flow through the orifice. It tested the feedstock blend with NaCl volume fraction from 10% to 60%. Each feedstock was measured three times to get an average value.

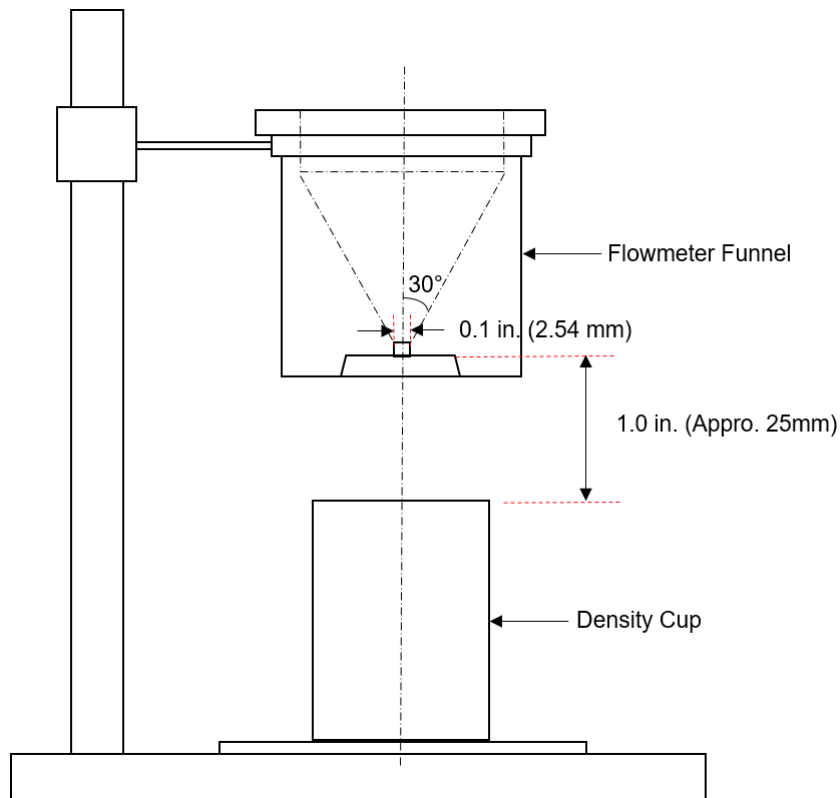


Figure 3.5. Schematic of the Hall Flow Test Measuring the Time Needed for 50g Mixtures of Powders to Flow Through

3.3 Types of Samples

3.3.1 SLM samples with various NaCl content

The investigation of processing parameters allows successful fabrication of samples of feedstock blend with various NaCl volume fraction from 10 vol.% to 60 vol.%. 5 mm cubes were built using laser power from 10W to 100W and laser scan speed from 100 mm/s to 500 mm/s. Apart from laser power and laser scan speed, other processing parameters were set as Table 3.5.

Table 3.5. Processing Parameters Set-up for SLM Samples with Various NaCl

Processing parameter	Set-up
<i>Scan strategy</i>	Double scan strategy
<i>Layer thickness, μm</i>	45
<i>Hatch spacing, μm</i>	60

3.3.2 An investigation of relationship between densities of SLM samples and processing parameters

In this study, the effect of laser power and laser scan speed on the structure of the samples was investigated by the blend with 50 vol. % NaCl. Based on the optimum processing parameters in Section 4.3, the samples were built with laser power from 30 W to 50 W, and scan speed from 100 mm/s to 400 mm/s.

3.3.3 SLM vertical graded samples

It has been found in Section 5.1 that with the same blend, the processing parameters have an effect on the final relative density of the structure. Therefore, various processing parameters were set in one structure. For example, in Figure 3.6, a 6 × 6 × 9 mm sample was built with three processing parameters: 30 W, 200 mm/s in Section 1; 40 W, 200 mm/s in Section 2; 50 W, 200 mm/s in Section 3.

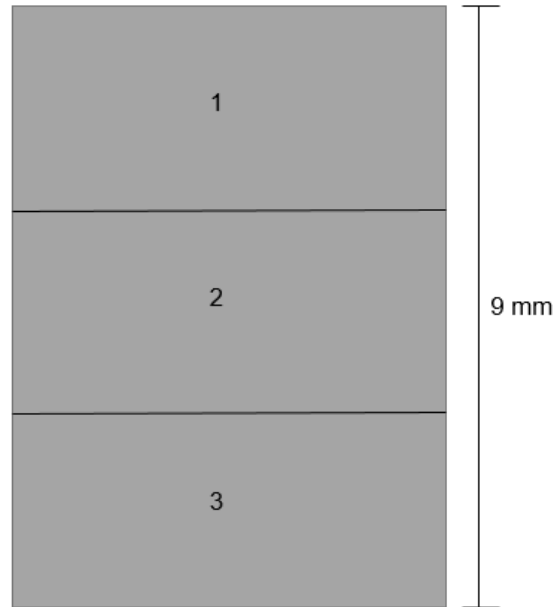


Figure 3.6. A 9 mm Sample in Three Process Parameters with Each One of 3 mm

3.3.4 SLM horizontal graded samples

Density graduation in horizontal direction (x-y plane) was achieved in this section. Figure 3.7 presents the two parts of the structure. Volume 1 is a cube with removal of a cylinder in the centre, where Volume 2 is fit. Table 3.6 presents the specific processing parameters used to create the nested structure. The two volumes used the same scan speed but with different laser power, and finally lead to density difference.

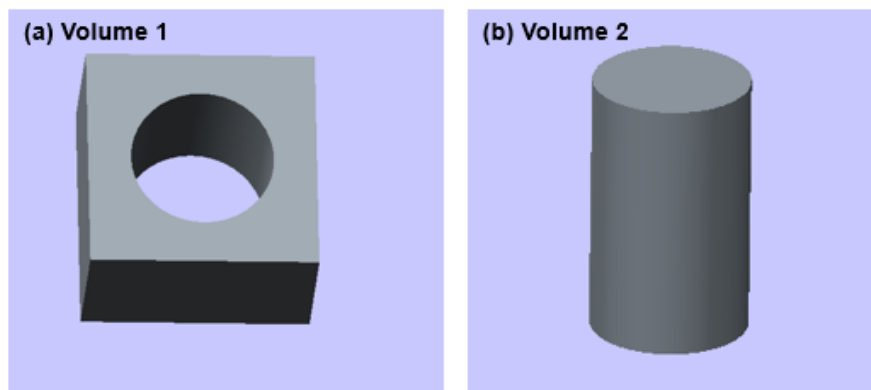


Figure 3.7. Simple Assembly of Structures and Assignment of Localised 'Build' Parameters (see Table 3.6) Allows Location Specific Density to be Created

Table 3.6. Volume Specific Parameters Used to Create the Nested Cylinder

Volume	Laser power, W	Scan speed, mm/s	Energy density, J/mm³
1	40	300	49.38
2	25	300	30.86

In Table 3.6, energy density is calculated from Equation 3.1. For example, with laser power 40 W, scan speed 300 mm/s, layer thickness 45 μm and hatch spacing 60 μm,

$$E = \frac{40}{300 \times 45 \times 60} \times 10^6 = 49.38 \text{ J/mm}^3$$

3.3.5 Graded overhang structure

Using the same processing parameters for Volume 1 and 2 as stated in Table 3.6, density graduation in vertical direction was achieved in this section. Figure 3.8 displays an encased Letter ‘A’ in a dissimilar porosity matrix, where the salt will be removed by water, indicating the effect of processing parameters on the porosity.

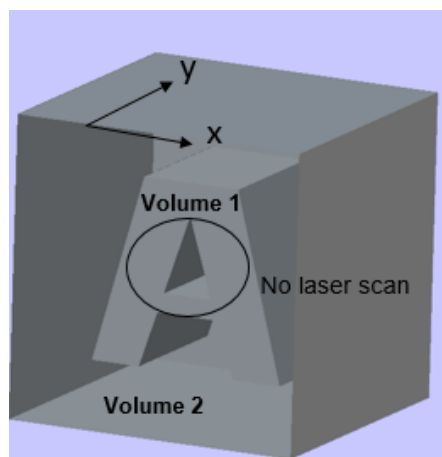


Figure 3.8. Letter ‘A’ is Fully Encased in a Dissimilar Porosity Matrix Demonstrating the Effect of Distinct Process Parameters on Resulting Porosity

3.4 Salt Dissolution

Fabricated cubes were placed in water at room temperature in order to leach out the NaCl. In initial trials the cubes were removed from the water, dried and weighed periodically until the weight of the cubes was stable, at which point it was assumed that all unbound NaCl had been removed from the cube. The cubes were weighed before putting in water. It also weighed after 1, 3, 5, 10, 15 minutes after placing in water. The final weight of cubes after removal of the NaCl was used to determine the density of the lattice structure using Equation 3.2.

3.5 Mechanical Testing

Compression testing to evaluate yield strength and modulus was carried out using samples of approximately $5 \times 5 \times 5 \text{ mm}^3$. Samples were tested using an Instron 5969 universal testing machine at room temperature with a strain rate of 10^{-3} s^{-1} . For each specimen type, five repeat tests were carried out. In the calculation of stresses, the sample cross section was used rather than the actual material cross section, which varied with relative density of the cellular structure. Hence lattice, rather, than bulk properties were generated.

The data from compression test included displacement and compressive stress. To obtain stress-strain curve, strain should be calculated from Equation 3.3, where ϵ was the compressive strain. The original length was 5 mm theoretically. Compressive Young's modulus was obtained from Equation 3.4, where E^* was compressive Young's modulus and σ was compressive stress.

$$\epsilon = \frac{\text{displacement}}{\text{original length}} \quad (3.3)$$

$$E^* = \frac{\sigma}{\epsilon} \quad (3.4)$$

3.6 Heat Treatment

To reduce the residual stresses in the SLM samples, samples fabricated by 50 vol.% NaCl in various processing parameters, with laser power from 30W to 50W, scan speed from 200 mm/s to 400 mm/s, were heat treated at 730 °C in argon gas atmosphere for 2 hours. After this, the samples were cooled to the room temperature at a cooling rate of 10 °C/min. The samples then were prepared for analysis by sectioning, mounting, grinding and polishing.

Chapter 4

Composition Modulation for Ti-6Al-4V Cellular Structures by Varying

NaCl Content

A new method to fabricate cellular structure has been demonstrated in this chapter. To investigate the effect of NaCl on the structure, the study started with selective laser melting (SLM) process by adding NaCl particles into Ti-6Al-4V metal powders.

Blends with various NaCl content from 10% to 60% were used as initial materials for sample fabrication. The flowability of blend with various NaCl content was tested in Section 4.1. The investigation started with building thin wall using the mixed powders in Section 4.2, where the effect of salt has been obviously presented. The salt can be clearly seen in the slice and the EDX results revealed the existence of NaCl. After removal of NaCl, pores were presented; Therefore, cubes were then fabricated for processing parameters selection in Section 4.3. A processing map was produced in this section. The fabricated samples were then placed in water for NaCl removal (Section 4.4) and characterized by meso- and microstructure and mechanical property (Section 4.5, 4.6, 4.7, and 4.8). Mechanical testing reveals that the strength and stiffness of the cellular structures can be tuned through control of feedstock composition, and hence, relative density.

4.1 Flowability Test

Figure 4.1 shows the relationship between NaCl content and the time needed for 50g mixtures of powder to flow through the orifice. It can be seen that time increased, i.e. flowability decreased, linearly with increasing NaCl content. Poor flowability is known to lead to an uneven distribution of powder, which can result in build defects. However, flow conditions are

well known to be different within powder bed feed mechanisms where temperature and hopper conditions are important factors. Mellin et al. [101] have reported on the evaluation of flowability for powder bed processes and have related simple techniques to powder bed formation

In this case, even though flowability decreased with increasing salt content, the powder distribution system was able to deliver a visually compact and even powder bed within the salt content range of interest. Even so, it should be borne in mind that with the proposed technique, this is a factor that requires careful consideration when selecting the size and shape distributions of the matrix and space holder powders.

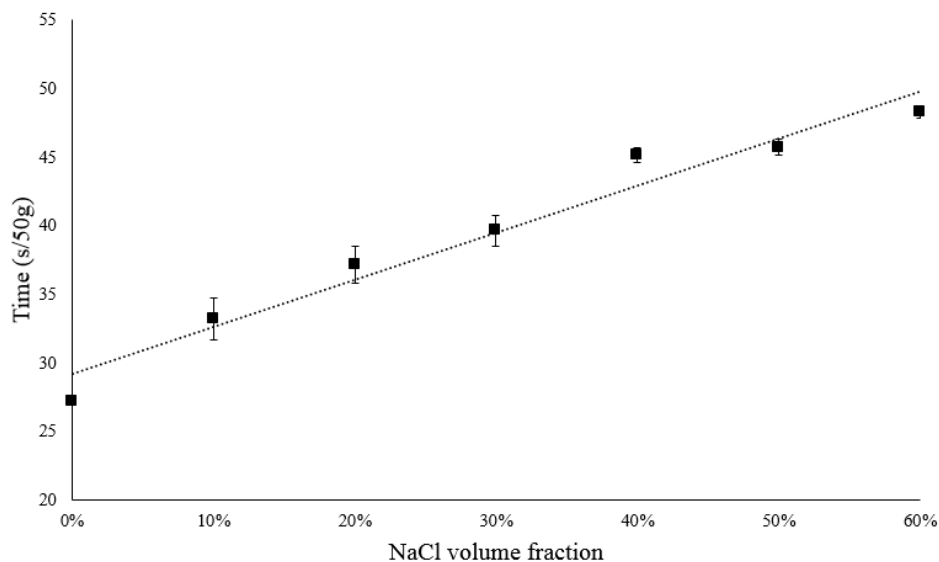


Figure 4.1. Hall Flow Test Results as a Function of Salt Content in the Mixed Powder Feedstock

4.2 Thin Walls Built by SLM Process with Ti-6Al-4V and Salt Mixture

To start with investigation, single walls were built with various salt content using various processing parameters as shown in Figure 4.2. Scan speed increases from 100mm/s to 400mm/s

and laser power increases from 20W to 50W in the figure using 40 vol.% NaCl. The detailed effect of processing parameter will be discussed in Section 4.3.

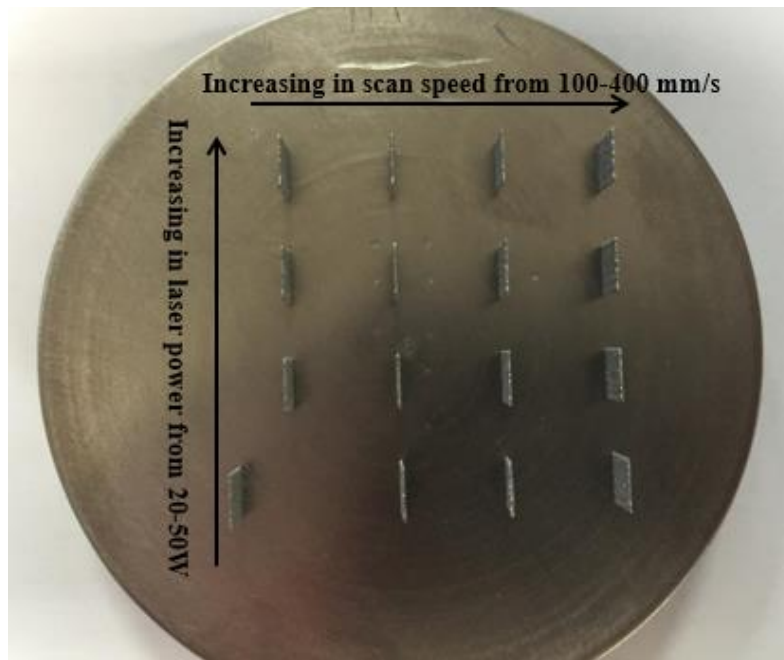


Figure 4.2. Single Wall built with Various Processing Parameters Using Ti-6Al-4V and NaCl Mixture with 40 vol.% Salt

Single walls of pure Ti-6Al-4V powders without NaCl were built with various energy densities as well for comparison with the above samples. Figure 4.3 presents the resultant morphology of the slice with energy density from 92.6 J/mm^3 to 25.9 J/mm^3 . Low energy density, as in Figure 4.3 (c), was not sufficient to melt metal powders so that the structure was in poor density. Energy density about and above 49 J/mm^3 shown in (a) and (b) successfully fabricated slices in comparably higher density, which is consistent with the results in the literature [74] showing the relationship between energy density and density. Therefore, energy density around 49.3 J/mm^3 was considered as the starting parameter.

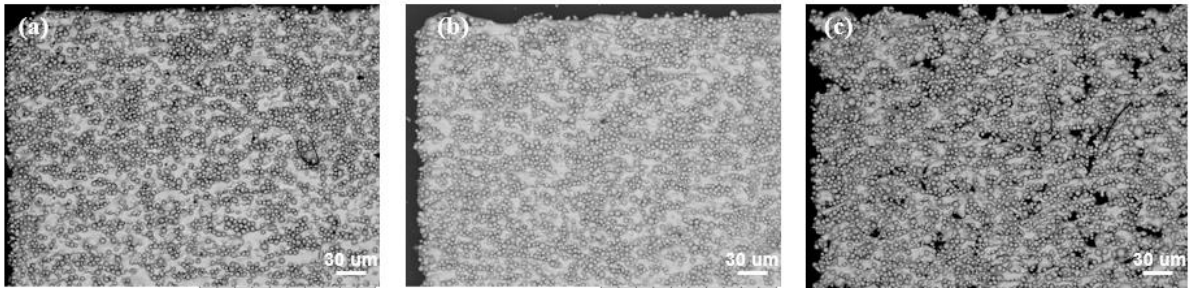


Figure 4.3. Single Slice Built without NaCl by Energy Density of (a) 92.6 J/mm^3 ; (b) 49.3 J/mm^3 and (c) 25.9 J/mm^3

Element mapping by scanning electron microscope (SEM) of the as-built slice was made to verify the composition in the sample with the presence of NaCl. In Figure 4.4 (a), un-melted Ti-6Al-4V powders can be clearly seen, surrounded by cracked NaCl particles as presented in mapping (c) and (d). The NaCl particles were not in the original cubic shape, indicating that most of them were melted and re-solidified during the working process, however higher energy density was required to completely melt Ti-6Al-4V powders.

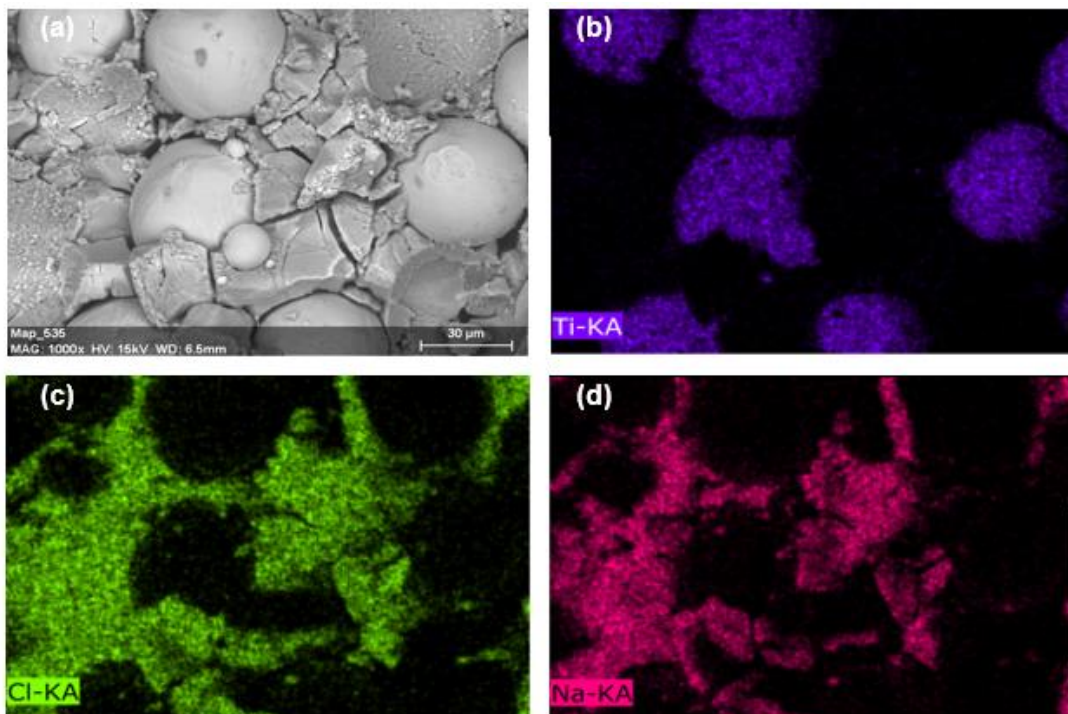


Figure 4.4. Element Mapping by SEM of the Single Slice with (a): As-built Slice with Un-melted Metal Powders and Cracked NaCl Powders; and Mapping of Element (b) Ti, (c) Cl and (d) Na

The single slice was then placed in water at room temperature for removal of NaCl. Due to poor connectivity, Figure 4.5 (a) was a part of the as-built single slice, which was covered by un-melted Ti-6Al-4V powders and NaCl particles as indicated in Figure 4.4. After dissolving in water, NaCl was successfully removed, leaving pores in the structure as a result shown in Figure 4.5 (b). This process indicated that NaCl has an effect on the thin walls, making them as porous structure. However, some processing parameters cannot build a completed slice since higher energy density may lead to completed evaporation of NaCl so that the slice cannot be formed without connectivity between metal and space holder materials.

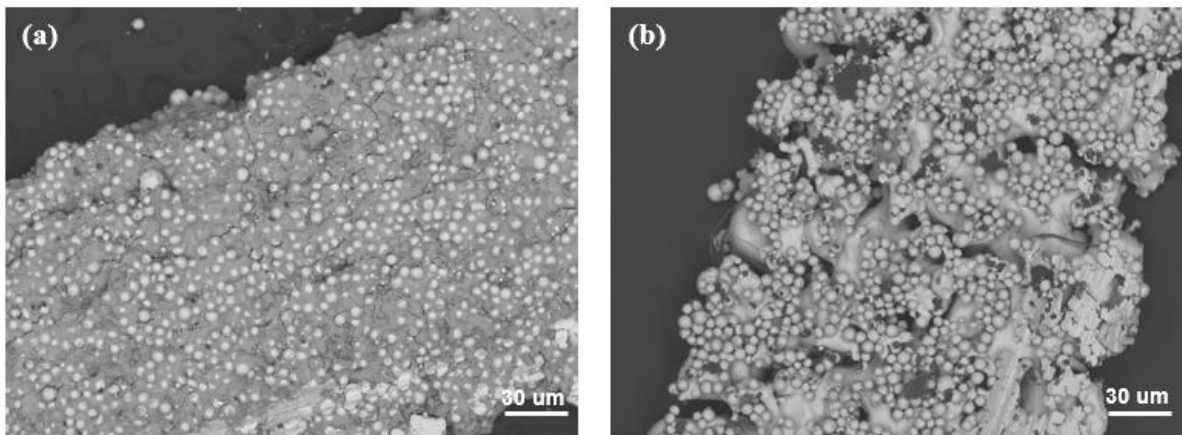


Figure 4.5. SEM of (a) As-built Slice and (b) after Dissolving in Water for NaCl Removal

Figure 4.6 shows a schematic of the process used to create the cellular structures, in which leaching of the space holder material succeeds the SLM stage. In Figure 4.6 (a), the blend of Ti-6Al-4V and NaCl powders was distributed on the powder bed. Following Figure 4.6 (b), laser consolidation metal flows around the salt inclusion, therefore embedded salt was trapped in the structure. Finally, in Figure 4.6 (c), the sample will be placed in water for removal of NaCl and leaving a porous structure.

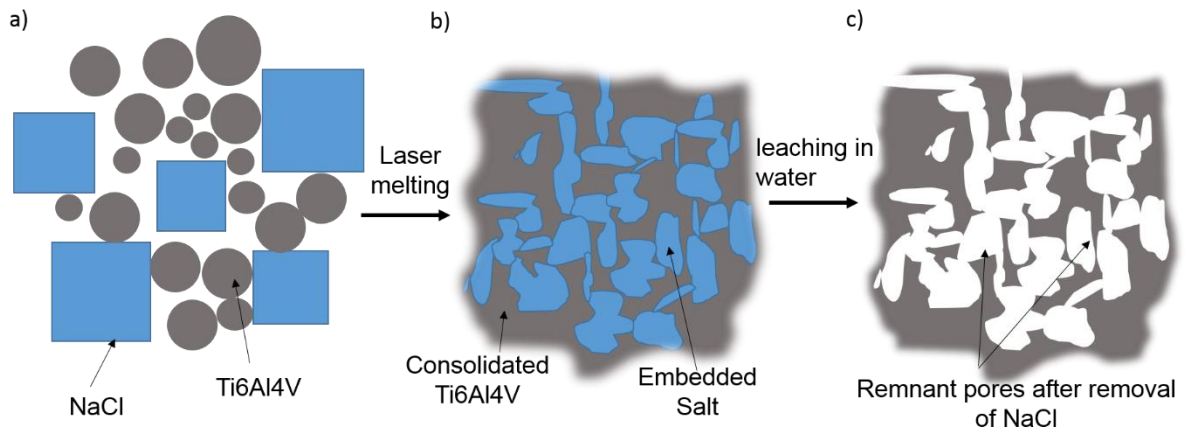


Figure 4.6. Schematic of the Process Creating Cellular Structures.

4.3 Optimisation of Processing Parameters

The energy density for each SLM parameter set was calculated from Equation 3.1. The resulting processing map is shown in Figure 4.7. Energy density is shown to have a marked effect on the properties of as-built parts. The optimum energy density at each NaCl volume fraction varies with salt content. With 10 to 30 vol. % NaCl, the majority of the parameter sets investigated were able to successfully build parts. However, with 60 vol. %, a limited range of parameters with low energy density was successful. In subsequent experiments processing parameters used to fabricate cubes were selected from the process map shown in Figure 4.7.

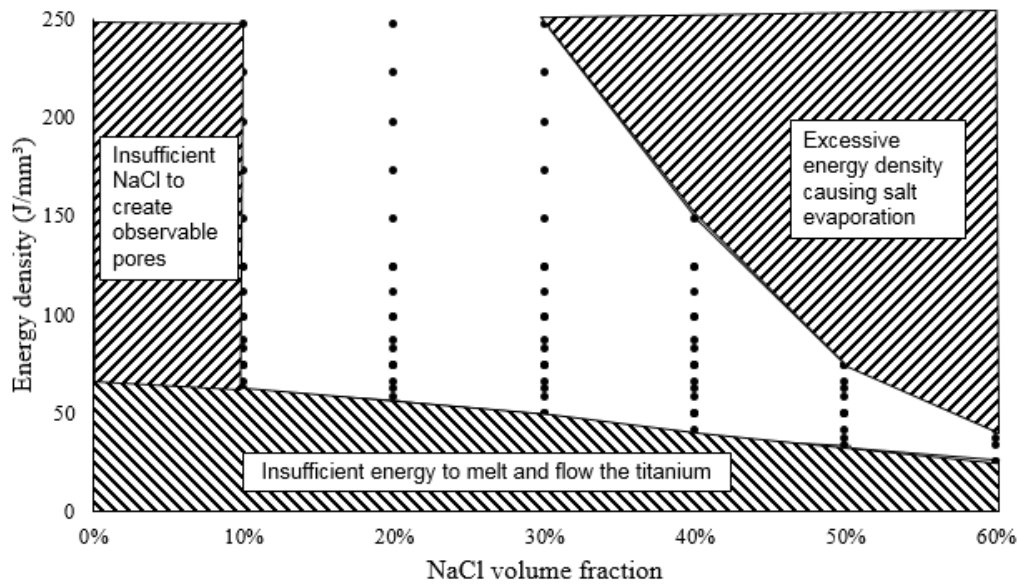


Figure 4.7. Processing Map of Mixtures with Various NaCl Content

According to this processing map less energy is needed with higher NaCl content in the mixture since there is a lower volume of localised Ti-6Al-4V which must be melted in order to consolidate the part. For example, in Figure 4.7, when lower than 50 J/mm³, there is insufficient heat to melt and flow titanium powders at 10 and 20 vol. % NaCl. By increasing NaCl content, less energy is needed for sample fabrication due to the lower localised melting mass. At the other extreme, if the input energy is excessive, for example, when energy density exceeds 100 J/mm³ for 50 and 60 vol. % NaCl, excessive evaporation leads to the failure of fabrication.

4.4 Salt Dissolution

Figure 4.8 presents the salt dissolution rate of each cube with varying NaCl content. The weight of NaCl removed was calculated from the weight measured as the method in Section 3.4. For example, for the sample with 10 vol.% NaCl, Table 4.1 gives the weight of 5 mm cube after placing in water.

Table 4.1. Weight Change with Time of Cube with 10 vol.% NaCl after Placing in Water

Time, min	Weight, g
0	0.5970
1	0.5810
4	0.5731
9	0.5718
19	0.5705
34	0.5705

The initial weight of as-built 5 mm cube was 0.5970 g and the final weight was 0.5705 g after removal of NaCl, therefore the weight of removed NaCl was 0.0265 g. The actual size of the sample was 5.17×5.15×5.25 mm. The density of the cube was calculated from Equation 3.2:

$$\rho = \frac{0.5705}{5.17 \times 5.15 \times 5.25} \times 10^6 = 4081 \text{ kg/m}^3$$

As the volume fraction of NaCl in the initial powder state increases, the as-fabricated weight of the cubes decreases from ~0.60 g (at 10 vol. % NaCl) to ~0.37 g (at 60 vol. % NaCl). After dissolving in water for 10 minutes, the weight remains constant for all cubes. As would be expected, it can be seen that the initial rate of NaCl removal, as well as total amount removed, increased with the percentage of salt crystals in the feedstock.

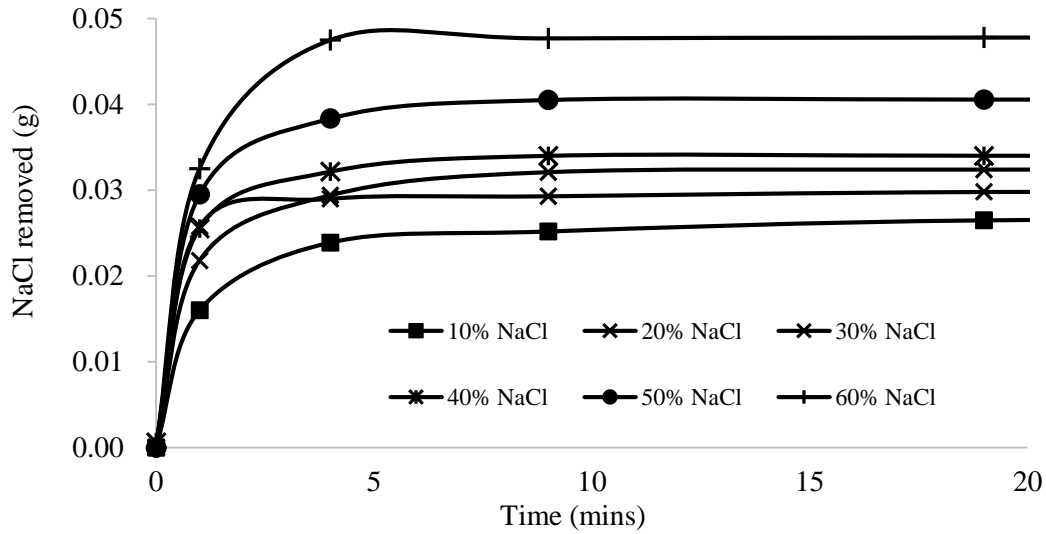


Figure 4.8. Salt Dissolution as Measure by the Change in Specimen Mass with Time

It should be noted that the amount of salt removed from the built part was less than that calculated based on the initial volume fraction of the feedstock. This is because some of the salt is evaporated during processing, as indicated by Table 3.3. It was also seen that at low volume fractions of salt, residual NaCl could be seen to be trapped in the built sample, as discussed further in the next section.

4.5 Characterisation of the Cellular Structure

Sections of the 5 mm cubes with NaCl volume fraction from 10% to 60% are presented in Figure 4.9. It is observed that with increasing NaCl volume fraction in the feedstock, the volume fraction of voids in the built structure increased, or in other words, the relative density of the lattice structure decreased. The structure developed from a closed-cell at low volume fractions of NaCl in the feedstock to a more inter-connected, and finally to an open-cell foam-like structure, as salt content in the feedstock increased. The pores in this process are irregular in shape and size compared with traditional space holder sintering techniques. Analysis of pore

volume indicated that at low salt content, pores tended to be smaller than the salt particles in the initial feedstock but at high volume fractions of salt, pore size tended to be larger than the salt particles. The observed structures can be attributed to a number of influences. The sintering of Ti alloys can occur at a lower temperature, 720 °C for instance [65], than the melting temperature of NaCl, 801 °C, however, full melting of Ti-6Al-4V occurs above the boiling point of the NaCl. From this we may deduce that during processing some salt evaporates, resulting in there being less salt (and hence) pores in the built structures than in the feedstock and also accounting for the pores being smaller than the salt particles at low salt volumes. It is also notable that the thermal conduction of the Ti-6Al-4V is an order of magnitude greater than that of the salt at typical processing temperatures, hence, heat will tend to flow preferentially through the consolidated metal, resulting in some of the salt either remaining solid or melting and solidifying, the latter accounting for the change in morphology of the pores. Furthermore, it is proposed that the pores that are greater in size are formed by agglomerations of salt particles, either from the powder bed distribution or from salt melt-solidification during processing.

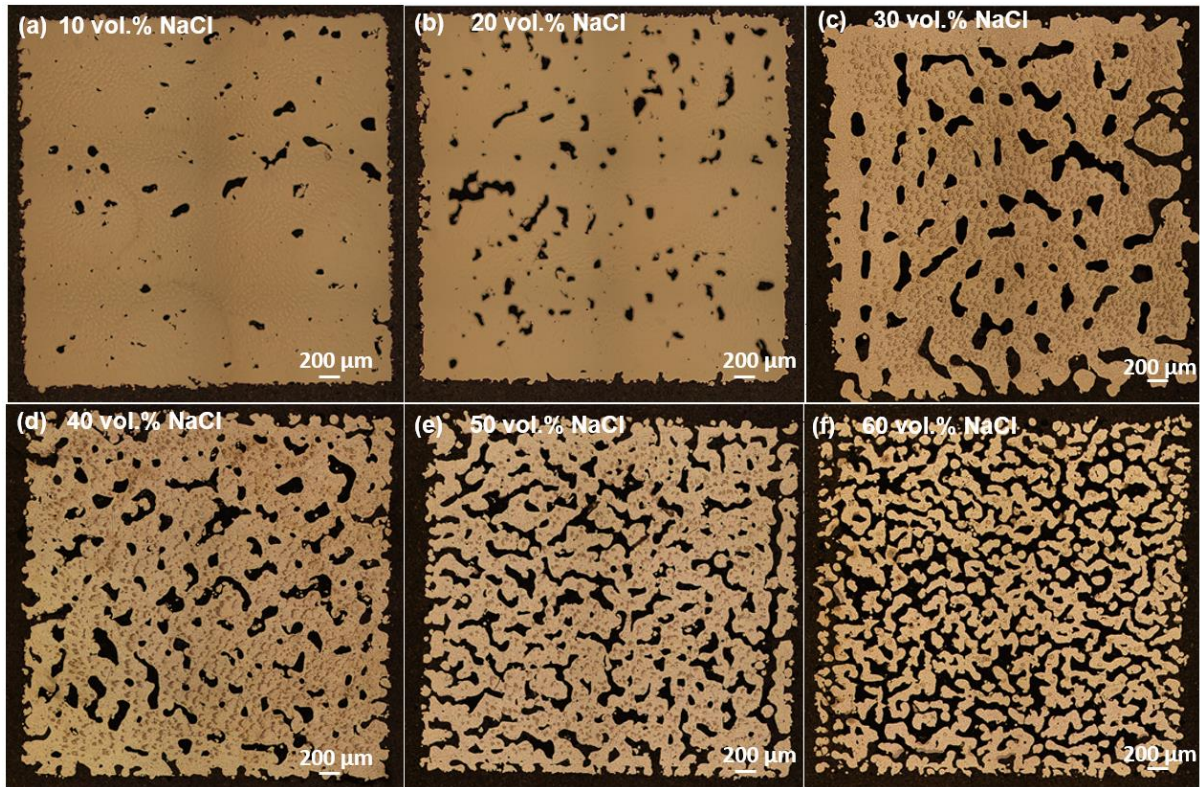


Figure 4.9. Optical Micrograph Sections in the x - y Plane Showing the Pore Distribution within Cubes with Varying Volume Fraction of NaCl at (a) 10%; (b) 20%; (c) 30%; (d) 40%; (e) 50%; (f) 60%.

4.6 Characterisation of Microstructure

Figure 4.10 shows a comparison between a typical pure Ti-6Al-4V microstructure and a region around a pore in a 30 vol. % NaCl specimen. Ti-6Al-4V transforms fully into the β phase field above the β transfer temperature ($\sim 950^\circ\text{C}$) and into an $\alpha+\beta$ phase mixture below this critical temperature. The amount of β phase retained at room temperature is governed by the cooling rate experienced from the β phase field. During SLM, each layer cools rapidly thus the microstructure is dominated by the martensitic (α') phase. In Figure 4.10 (a), a complete martensitic structure can be observed. In Figure 4.10 (b), complete α' phase is still clearly seen in the metal in close proximity to the pore. It can, therefore, be concluded that there is no significant metallurgical effect due to the proximity of NaCl during processing of the mixed feedstock.

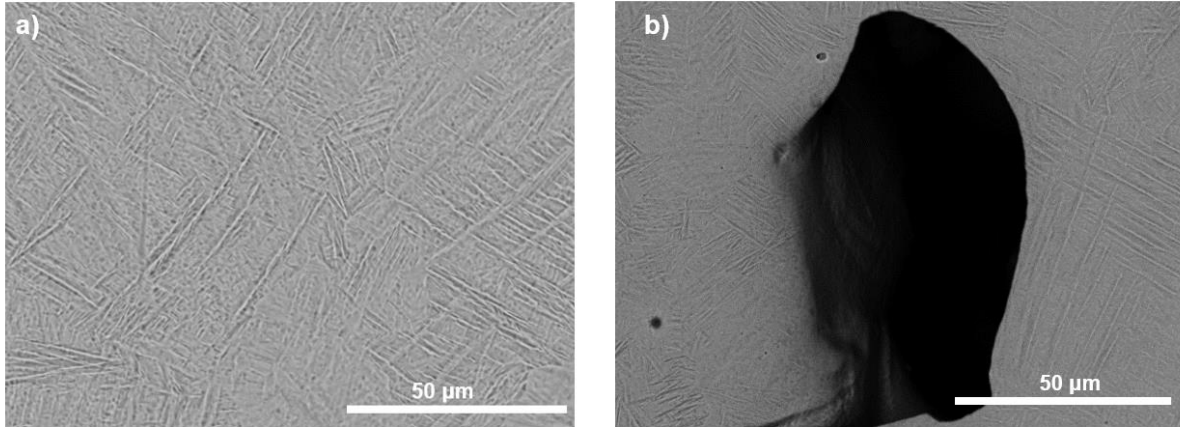


Figure 4.10. Metallurgy Comparison between (a) Cube without NaCl and (b) Cube with 30 vol. % NaCl

In order to determine the degree of diffusion of NaCl into the bulk of the porous structure EDX was carried out. Two regions were investigated which were evaluated using elemental mapping techniques. This can be observed in Figure 4.11. The contribution to the bulk metallurgy of the resulting material is shown to be minimal.

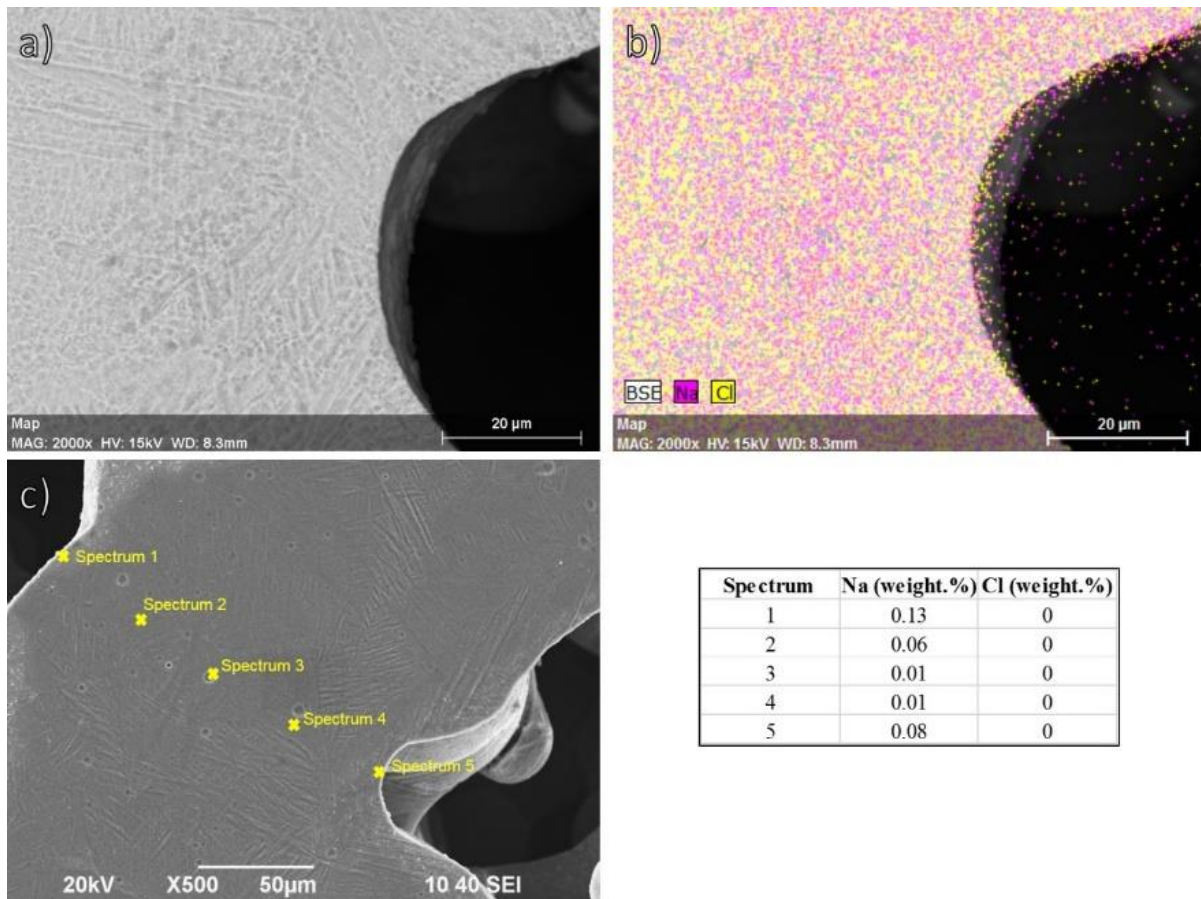


Figure 4.11. The Contribution of Na and Cl to the Elemental Composition of the Porous Structure is Minimal. b) Shows an Elemental EDX Map of the Micrograph Shown in a). c) and the Inset Table Show the Distribution of Na within the Solid as Minimal. Cl was not Detected here.

The Concentration of Na and Cl is not observed to be markedly higher at the near surface but point analysis (Figure 4.11 c) shows that Cl was not detected under the evaluation conditions detailed here. It is clear that the selection of space holder material can have a critical role in the morphology of the resultant material but in this case a minimal effect on metallurgy is observed.

4.7 Relationship between Feedstock Composition and Relative Density

The relative density (ρ_r) of a lattice (or cellular) structure is defined as the ratio of the density

of the lattice structure (ρ^*) and the density of the solid material (ρ_s), as defined in Equation 4.1. Figure 4.12 illustrates the relationship between NaCl volume fraction and the relative density of the cellular structures created from the mixed feedstock method.

$$\rho_r = \frac{\rho^*}{\rho_s} \quad (4.1)$$

Take the sample with 10 vol.% NaCl for example, it has been known that the density of the cube was 4081 kg/m³ and the density of as-built fully dense Ti-6Al-4V cubes was 4430 kg/m³, therefore, relative density can be calculated from Equation 4.1:

$$\rho_r = \frac{4081}{4430} = 0.92$$

Increasing NaCl content in the feedstock is shown, as expected, to cause a systematic increase in porosity and corresponding decrease in relative density. Assuming zero evaporation or dissolution of the NaCl, the porosity volume would equate to the NaCl volume fraction. In practice the relative density is higher than would be predicted with this assumption, indicating NaCl evaporation takes place. In addition, where NaCl is entirely encapsulated it will not be removed by leaching. It can be seen that the relationship between NaCl volume fraction and relative density is quite linear over a significant range but deviates at high relative density to meet the boundary condition of relative density equal to 1 at 0% NaCl. The equation displayed in Figure 4.12 gives the relationship between NaCl volume fraction and actual relative density in the linear region, which also corresponds to the range in which useful cellular structures are seen, as will be demonstrated in Chapter 4.8. This can be used to predict the experimental porosity and relative density of fabricated samples taking the above caveats into consideration.

The traditional furnace-based sintering and space holder technique presents significant limitations when compared to this approach. Furthermore, functionally graded structures may be achievable by controlling the NaCl content in one part, using the equation for prediction of

densities at each subsection without any explicit design, analysis and optimisation, reducing the computational design and analysis overhead compared with deterministic lattice structures produced by SLM process.

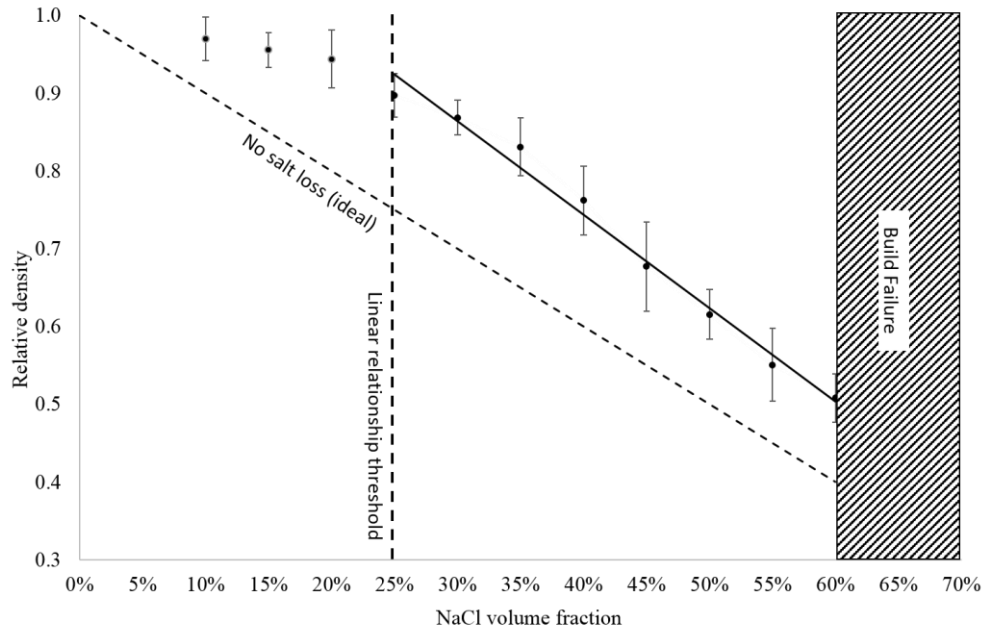


Figure 4.12. The Experimentally Obtained Relative Density Showing the Uniform Error across Salt Content within the Feedstock. Equation for the Linear Region is Given by $\rho_r = -1.2016X + 1.2245$ Where X is the NaCl Volume Fraction. XCT was Used to Calculate the Relative Density Here

4.8 Mechanical Testing

Figure 4.13 presents the stress-strain compression curves of the 5 mm cubes with various NaCl volume fractions. As expected, compressive yield strength and modulus of the lattices were observed to decrease with increasing NaCl content. Figure 4.14 shows images of two cubes with 30 vol. % NaCl and 60 vol. % NaCl respectively during compression testing. All specimens show an initial region in which full contact is made followed by a linear elastic region. As load is increased beyond this region, plastic deformation occurs, followed by cracking.

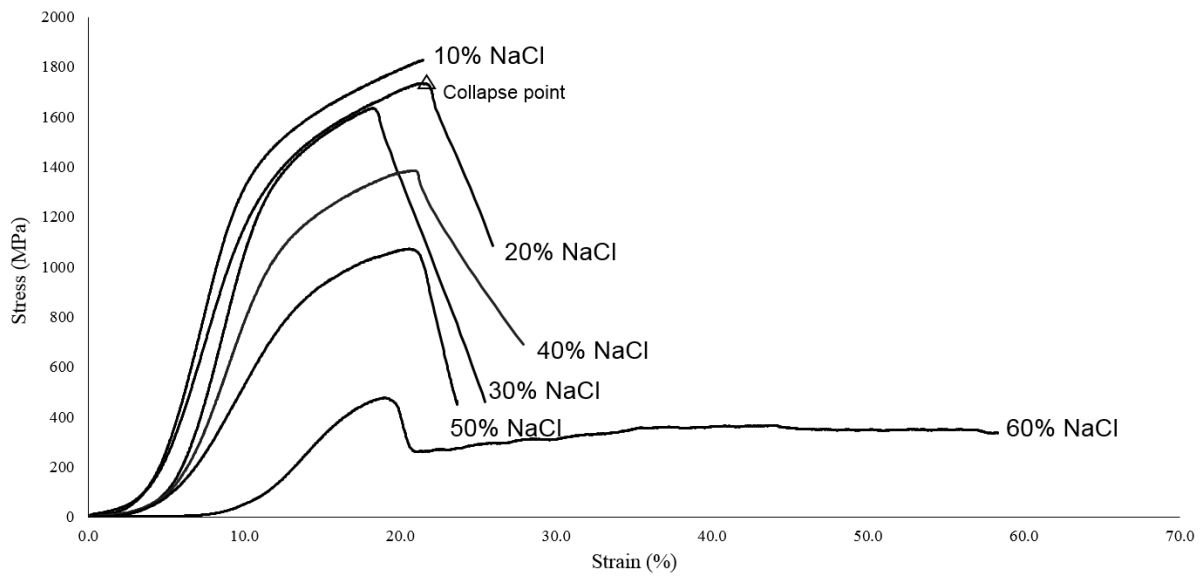


Figure 4.13. Effect of Salt Content on Mechanical Properties in Compression Demonstrated by the Characteristic Stress-strain Relationships

The stress-strain curve in Figure 4.13 is indicative of the brittle nature of the as-built material, as it may be expected with a ductile material that rather than cracking, the behaviour under high loads would feature an increasing load as plastic deformation leads to contact and compaction of the lattice. The brittle behaviour observed here is typical of the as built condition of high strength metals manufactured by the SLM, however, ductility can often be recovered in these materials by a suitable heat treatment.

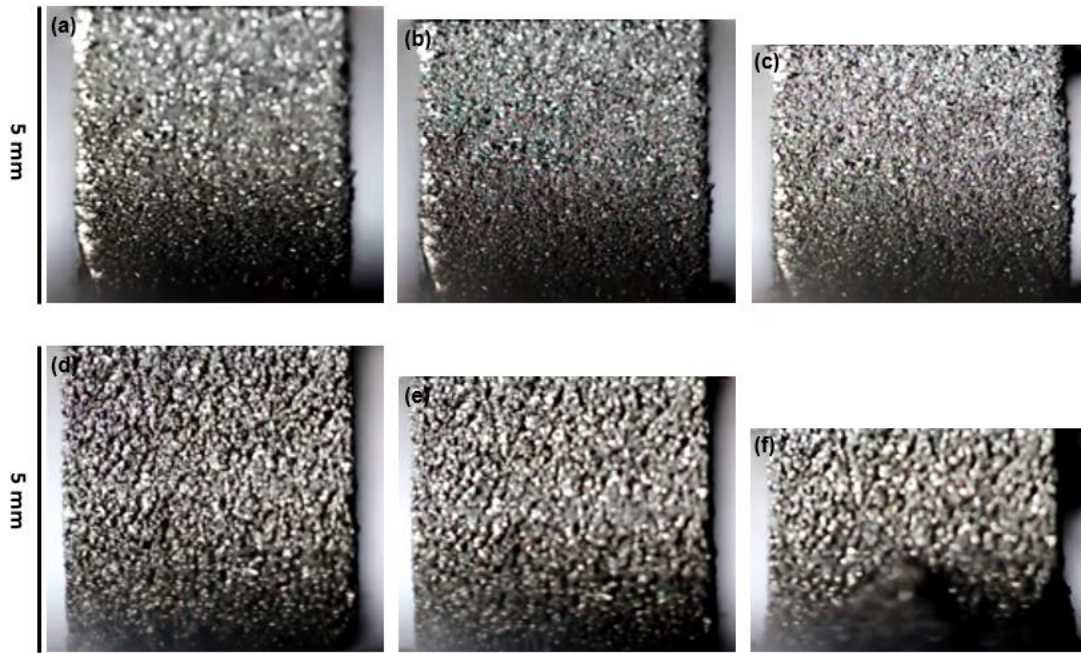


Figure 4.14. Specimens Failed under Loading: (a), (b), (c) Failed with 30 vol.% NaCl and (d), (e), (f) Failed with 60 vol.% NaCl

In Figure 4.15, Region 1 indicates an open cellular structure type response and Region 2 denotes semi-solid structures with a population of isolated pores. It is Region 1 that is of interest in terms of useful lattice structures and it is instructive to compare the mechanical response in this region to Equations 4.2 and 4.3 proposed by Gibson and Ashby [61]. The coefficients C_1 and C_2 were determined by Gibson and Ashby to be approximately 0.3 and 1.0 respectively from a study of metal foam data [61].

$$\frac{\sigma^*}{\sigma_s} = C_1 \left(\frac{\rho^*}{\rho_s} \right)^{3/2} \quad (4.2)$$

$$\frac{E^*}{E_s} = C_2 \left(\frac{\rho^*}{\rho_s} \right)^2 \quad (4.3)$$

Relative compressive strength and relative compressive modulus were evaluated in this study. Since processing parameters were optimised for salt integration and not the fabrication of solid builds comparison with wrought (114 GPa) [102] or even optimised compressive moduli

through SLM was not appropriate. In this case a specimen was produced with zero salt addition at the laser parameters used for the 10 vol. % NaCl composition. This was found to be 25.9 GPa and was thus considered to be the modulus of a solid specimen which was used to normalise compressive moduli data. In Figure 4.15, it can be seen that in Region 1 both the compressive strength and modulus decrease with decreasing relative density. The experimental data indicates a slightly non-linear relationship between relative density and relative compressive properties in Region 1. Fitting equations of the form of Equation 4.2 and 4.3 results in a proportionality and exponent constants of 1.13 ± 0.06 and 1.58 ± 0.15 , respectively, for the yield strength, and 0.06 ± 0.01 and 2.41 ± 0.33 , respectively, for the compressive modulus. In Region 2, with relative density above approximately 0.8, the relative compressive yield strength and modulus fluctuate around 0.97 and 0.9 respectively.

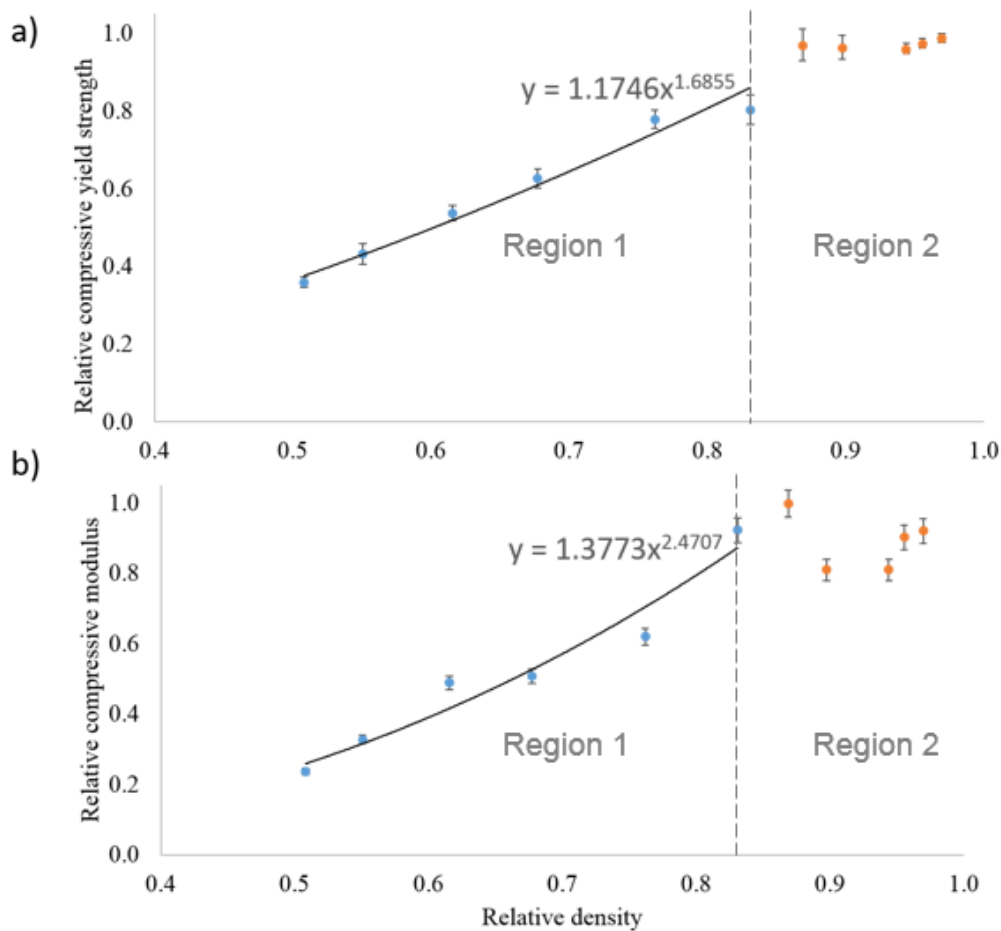


Figure 4.15. Relationship between Cube Relative Density and Compressive Properties. Error Bars Result from the Standard Deviation of 5 Compression Test and Three Density Measurements per Specimen. a) Shows Specimen Relative Compressive Yield Strength and b) Shows Relative Compressive Modulus Normalised by Compressive Modulus of 100% Ti6Al4V Built Using Parameters Optimised for Salt Inclusion (See Section 4.3)

In Figure 4.15, the theoretically calculated values of the exponent constants in Equation 4.2 and (4.3) are based on the mechanics of open cell foams as represented by a regular cubic array of square sectioned members. Whilst this model has been shown to be generally applicable to equiaxed open cell foams, this is far from the case with the cells produced here, which may account for the difference in the values of the constants from those proposed by Gibson and Ashby. However, the forms of Equation 4.2 and 4.3 fit the data well in Region 1 and the experimentally determined constants can be used to predict properties based on salt content of

the feedstock to a fair degree of accuracy. In Region 2, it is best to consider the structure as that of a solid with a population of isolated pores.

4.9 Summary

SLM process has been investigated to fabricate cellular structures using Ti-6Al-4V and NaCl mixed powders. The single layers built by SLM process were found to be with NaCl particles before removal of salt and after leaching out NaCl, the layer was cellular structure as a result. Therefore, it is essential to further investigate the effect of NaCl on the structure.

With various NaCl contents in the blend, processing parameters used for each blend were correspondingly varied. A processing map was created to present the energy density range for NaCl volume fraction from 0 to 60% in Section 4.3. With the aid of the processing map, Ti-6Al-4V cubes with relative density between 0.97 and 0.51 were successfully fabricated. Increasing the volume fraction of NaCl in the feedstock resulted in increased relative density of the manufactured cubes. More inter-connected pores were observed in the cubes resulting in the likely removal of all NaCl and formation of an open-cellular structure. The relationship between relative density and compressive properties of the cubes was evaluated by Gibson and Ashby's scaling equations, which provide a method to predict the relative density and compressive properties with as-known NaCl content.

Chapter 5

Modulation for Functionally Graded Structures

This chapter is further work of Chapter 4, where the same type of feedstock material of Ti-6Al-4V and NaCl mixture by SLM process has been used to fabricate functionally graded cellular structures. The effect of laser power on the relative density has been investigated in Section 5.1, with the same feedstock material for all the samples but with laser power from 30W to 50W. Following this section, compression tests have been done to compare the compressive properties of these samples in Section 5.2. To effectively improve the compressive properties, the samples have been heat treated at 730 °C for stress relief in SLM process in Section 5.3.

It can be seen in Section 5.1 that the relative density is affected by laser power, therefore graded structures have been further built in Section 5.4, 5.5 and 5.6 by adjusting laser power. Following SLM processing, the salt is dissolved to leave a graded metallic, cellular structure. Mechanical testing in Section 5.2, 5.3 and 5.4.1 reveals that the strength and stiffness of the cellular structures can be tuned through control of processing parameters, and hence, relative density.

5.1 Effect of Laser Processing Parameters on Relative Density

In Chapter 4, it has been found that properties including relative density and compressive properties can be affected by NaCl content in the blend. In this section, the effect of processing parameters, laser power in this case will be further studied. According to the processing map in Section 4.3, with 50% volume fraction NaCl, the laser power was varied from 30W to 50W with the same scan speed of 200 mm/s.

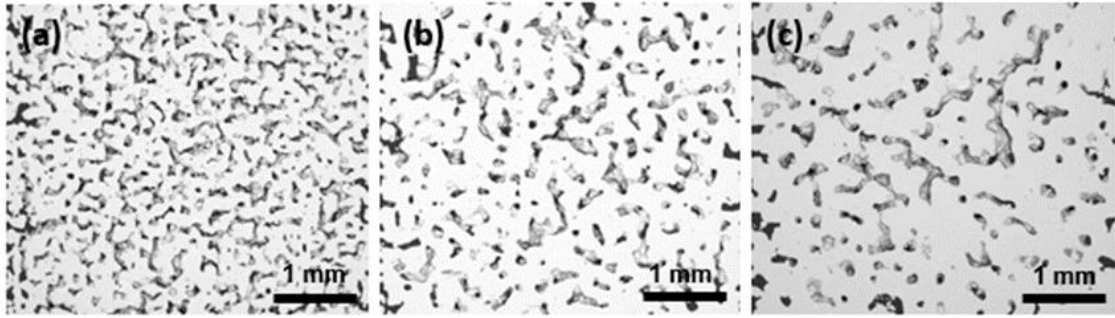


Figure 5.1. Sections in the x-y Plane Showing the Pore Distribution within Cubes with 50 vol.% NaCl Varying Processing Parameters at (a) 30W, 200mm/s; (b) 40W, 200 mm/s; (3) 50W, 200 mm/s

Sections of the 5 mm cubes with various laser power from 30W to 50W are presented in Figure 5.1. It is observed that with increasing laser power during the process, the volume fraction of voids in the structure decreased, which means the relative density of the cellular structure increased, as given in Figure 5.2, the relative density increased from 0.72 to 0.85. The structure developed from an inter-connected to finally a closed-cell foam structure, as laser power increased. The pores in this process are irregular in shape and size. Although same blend was used, change of laser power led to various relative density of the structure. The observed structures can be attributed to the energy, and hence working temperature. The sintering of Ti alloys occurs at a lower temperature, 720 °C for instance [65], than the melting temperature of NaCl, 801 °C, however, full melting of Ti-6Al-4V occurs above the boiling point of the NaCl. From this it may be deduced that with higher energy, more salt evaporates, which means it is no longer available as a space holder in the manufactured sample, and hence less porosity in the built structures when the salt is removed.

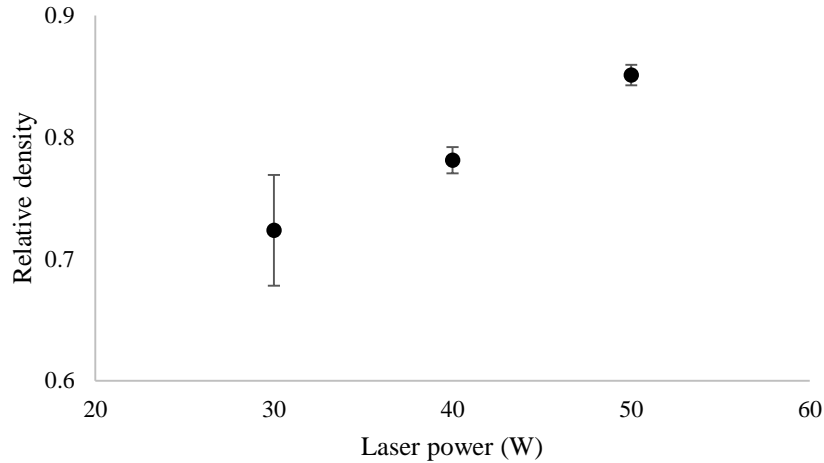


Figure 5.2. Laser Power against Structure Relative Density Which Shows That the Relative Density Increases with Laser Power

5.2 Compressive Properties of the Structure

Figure 5.3 presents the stress-strain compression curves of the 5 mm cubes with various laser power. As expected, compressive yield strength and modulus of the lattice were observed to increase with increasing laser power due to increasing relative density. All the specimens with three laser powers have displayed macro elastic behaviour in the initial stages of the test. As load increased, cracking occurs due to stress concentration upon loading in cell walls. The behaviour after collapse was significantly affected by the laser power. With 30W, the after collapse, the compressed cube experienced a further plateau region due to the cell wall of this ductile structure squeezed and collapsed repeatedly. With the laser power of 40W and 50W, both specimens displayed a shear fracture with loading increased to a maximum stress, and then following on a plateau region with cell wall squeezing and collapsing, finally further fracture was shown after the plateau region. From 30W to 50W, the compressive strength increased from ~400 to ~1000 MPa and the modulus increased from 3.70 to 15.53 GPa.

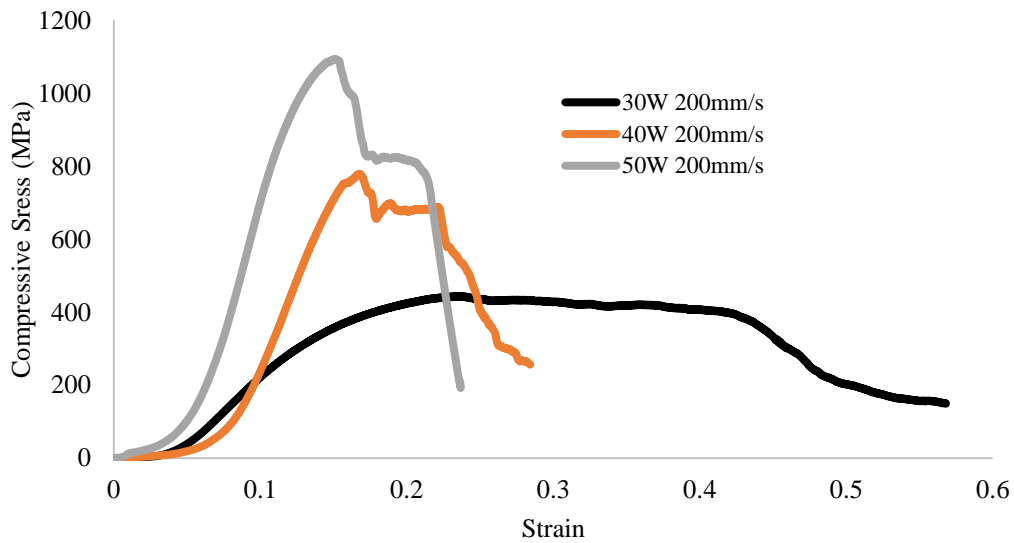


Figure 5.3. Effect of Laser Power on Mechanical Properties in Compression

5.3 Compressive Properties for Heat Treated Samples

5.3.1 Compressive properties for treated samples without NaCl

Compression test has been done for 5 mm pure Ti-6Al-4V cubes in order to compare with those with NaCl. Figure 5.4 shows the compressive properties for as-built and heat treated samples. It can be clearly seen that heat treatment has an effect on the properties. The yield strength of as-built cubes are higher than those after heat treatment. It reduces from 970 ± 23 MPa to 800 ± 15 MPa.

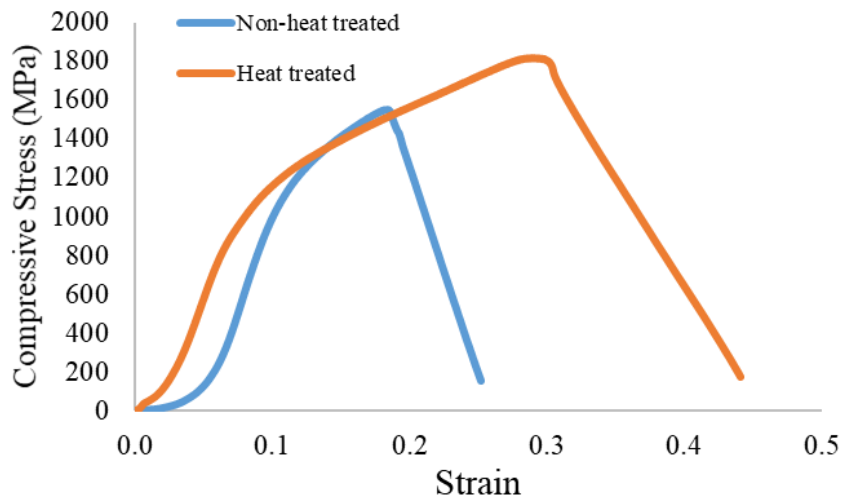


Figure 5.4. Compressive Properties of As-built and Heat Treated Pure Ti-6Al-4V Cubes

This result may be probably due to the slow cooling rate after heat treatment and the α' to α transformation as shown in Figure 5.5 [103]. The as-built Ti-6Al-4V cubes show in general a poor elongation at failure, approximately 0.2. The heat treated samples, on the other hand, shows increased elongation because of the existence of β phase, which contributes to good ductility.

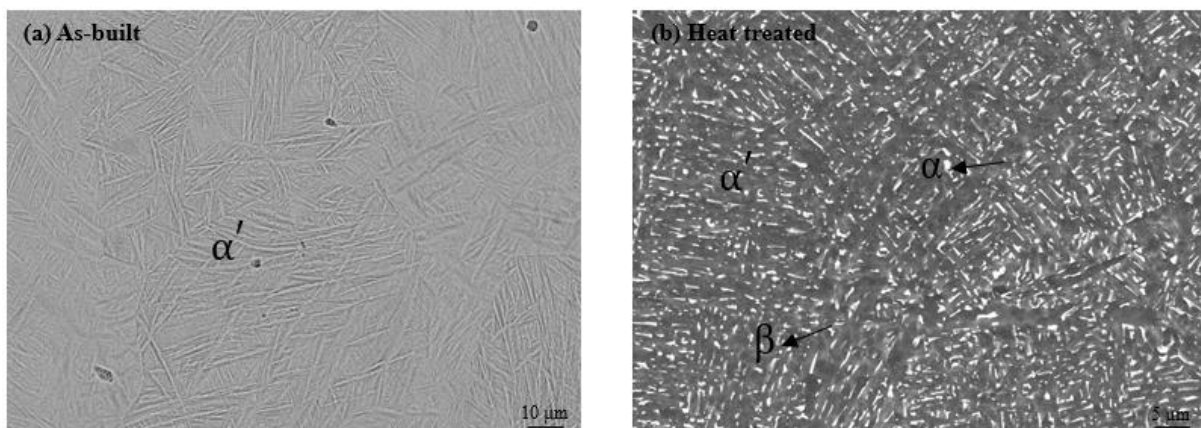


Figure 5.5. Microstructure and Phase Distribution in Pure Ti-6Al-4V Cubes with (a) as-built Samples and (b) Heat Treated Samples

5.3.2 Compressive properties for treated samples with 50% NaCl by various parameters

Compression test has been done for 5 mm cubes with 50% NaCl in blend. Three processing parameters have been investigated, with laser power of 30W, and scan speed from 200 mm/s to 400 mm/s. As shown in Figure 5.6, samples with different scan speed displays a distinction in compressive properties. In Figure 5.6 (c), the yield strength of as-built cube is 320 ± 10 MPa, obviously lower than that in (a) and (b), which are 510 ± 20 MPa and 560 ± 10 MPa respectively. For as-built specimens, all show an initial region in which full contact is made followed by a linear elastic region. As load is increased beyond this region, plastic deformation occurs, followed by cracking. This sequence is indicative of the brittle nature of the as-built material, which is typical of the as built condition of high strength metals manufactured by the SLM, however, ductility can often be recovered in these materials by a suitable heat treatment.

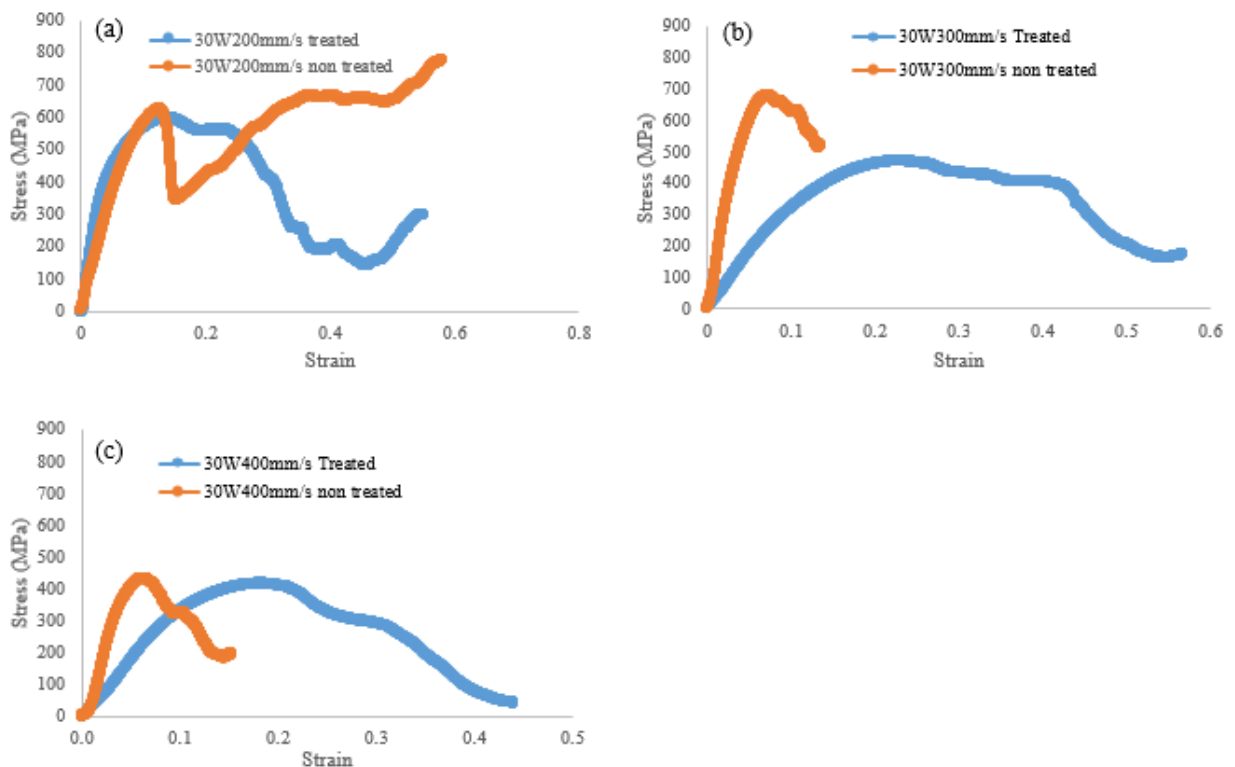


Figure 5.6. Compressive Properties of Heat Treated Cubes in Several Processing Parameters: (a) 30W, 200 mm/s; (b) 30W, 300 mm/s; (c) 30W, 400 mm/s

After heat treatment at the stress relieving temperature, both yield strength and elongation has changed. For all samples, yield strength decreases and elongation increases. In Figure 5.6 (a), yield strength decreases from 495 ± 9 MPa to 375 ± 15 MPa and elongation of the first failure increases from 0.1 to 0.18 approximately, which indicates that the specimens are more ductile after treatment. In (b) and (c), both treated specimens presents better ductility and lower yield strength.

5.4 Graded Structure in Vertical Direction

5.4.1 Relative density of the structure

Due to the variation in relative density as stated in Section 5.1, more complicated structures were developed in the study. Figure 5.7 shows the cross section in y-z plane of the $6\times 6\times 9$ mm sample using the same blend in Section 5.1. The structure has been divided into three regions. Region I was built by the processing parameters of laser power 30W, scan speed 200 mm/s; Region II and III were with the same scan speed, but with the laser power of 40W and 50W respectively. Each region was 3 mm in height.

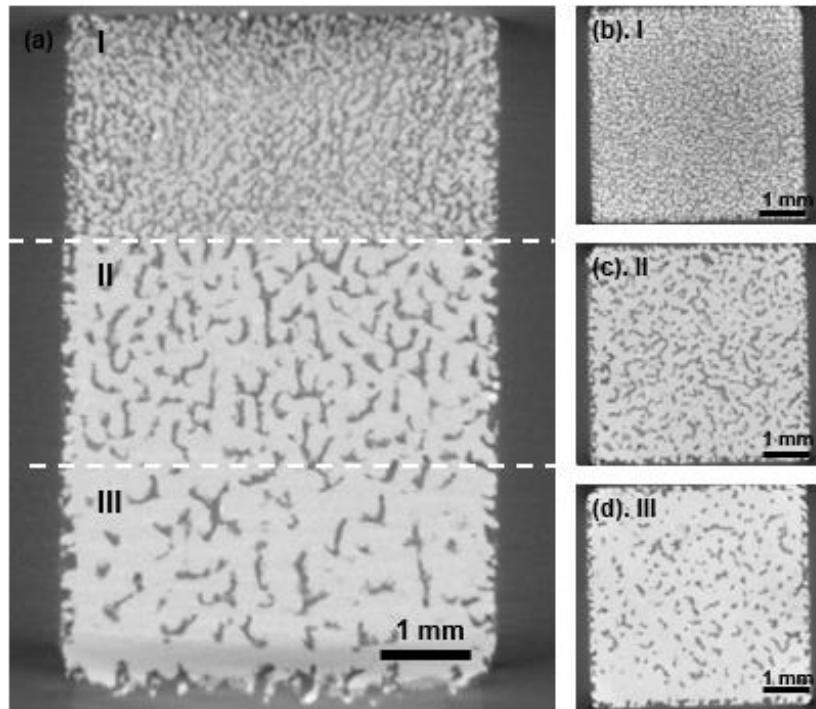


Figure 5.7. Graduation in Density Can Also be Achieved through Modulation of Layer-wise Build Parameters Resulting in This Case in Three Distinct Regions. Sections of the Graduation (b), (c) and (d) Confirm the Apparent Variation.

It can be seen that the density of the three regions was not same, resulting in a graded structure in three densities. Table 5.1 gives the density properties of each region. From Region I to III, the laser power increased from 30W to 50W, resulting in increasing of relative density from 0.69 to 0.84.

Table 5.1. The Density of Regions Demonstrating Functionally Graduation in the z-axis

Region	Average porosity, %	Relative density
I	30.6	0.69
II	21.4	0.79
III	16.4	0.84

This experiment clearly shows that a controlled variation in porosity can be achieved by changing the process parameters for a given feedstock material. This is consistent with the results in Section 5.1. There is a clear step change in the structure from one set of processing parameters to another as shown in Figure 5.7. It was also seen that connectivity between the pores allowed efficient salt dissolution from the structure. As can be seen in Figure 5.8, only a thin layer (below 10 μm) of residual NaCl remained on the internal periphery of the pore; this was confirmed using Energy Dispersive Spectroscopy (EDS).

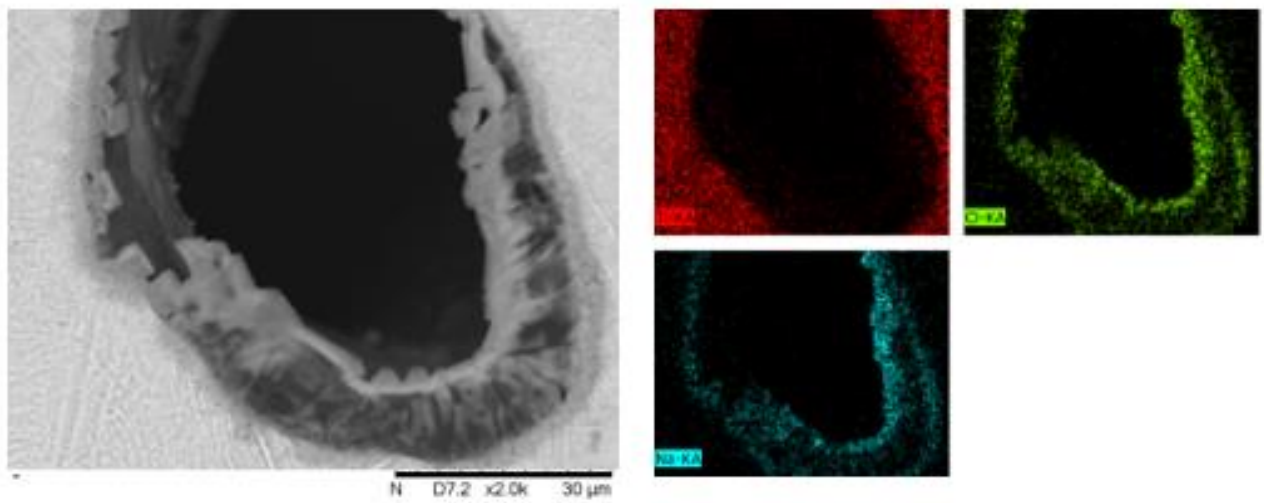


Figure 5.8. EDS Maps at a Pore Showing NaCl on the Pore Boundary

5.4.2 Compressive properties of the structure

Figure 5.9 presents the stress-strain compression curves of the 6×6×9 mm specimen with graded density. It has been observed in Section 5.2, as the porosity increases, the mechanical properties deteriorate. This can also be related to the graded structure in this section. The sample failed region by region sequentially, identified in Figure 5.7 as Region I, Region II and Region III. The failure started with Region I, with the highest porosity, which was the weakest part of the sample and the region built by the lowest energy density. It failed at nearly 600 MPa. Region III failed at approximately 700 MPa, which was the region with lowest porosity and

fabricated by the highest energy density. The compressive strength of Region II was about 590 MPa. Compressive strength in all three regions was lower than that shown in Figure 5.3. The porosity in each region was comparable to that of uniform samples which were built by the same processing parameters, but the compressive strength not. The connectivity between the boundaries of two regions may cause less discrepancy in compressive properties. The compressive strain, however, increased by graduating the porosity. Processing parameters modulation enables control of porosity and hence material's properties and functionality. It provides an opportunity for engineers to design an object's response to an impact event.

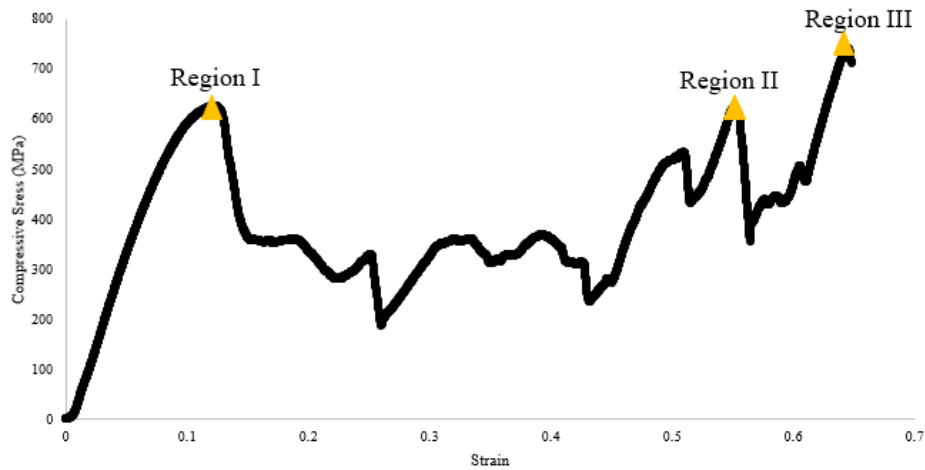


Figure 5.9. Graded Specimen Shows the Compression Behaviour of Several Stages at (I) First Collapse; (II) Second Collapse; (III): Third Collapse

5.5 Graded Structure in Horizontal Direction

A nested structure, grading within an individual layer has been fabricated here. It had discrete volumes with different shapes in one structure, as shown in Figure 5.10. It was made up of a cylinder encased within a cuboid. The structure was grading in each individual layer in horizontal. Figure 5.10 (b) presents the X-Ray computed Tomography of the nested structures which clearly shows an interface between the two volumes indicating the two processing parameters. It is observed that the two regions have shown different densities. Volume 1 was

with the relative density of 0.80 and Volume 2 was 0.68. It gives this approach another advantage of controlling density variations with a layer (X-Y plane) by processing parameters.

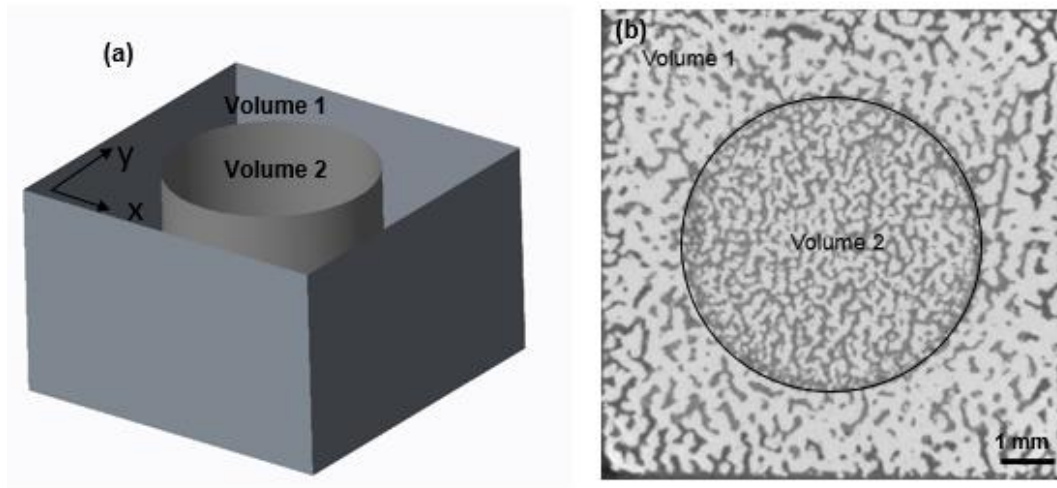


Figure 5.10. Simple Assembly of Structures and Assignment of Localised 'Build' Parameters (See Table 3.6) Allows Location Specific Density to be Created, Where (a) is the CAD Design Model and (b) is the Cross Section Scanned by XCT

5.6 Graded Structure in Vertical Direction

Using the same processing parameters for Volume 1 and 2 as stated in Table 3.6, density gradation in vertical direction was achieved in this section. Figure 5.11 displays an encased Letter 'A' in a dissimilar porosity matrix, where the salt has been removed by water, indicating the effect of processing parameters on the porosity. It has been observed that the Letter A was in lower relative density than Volume 2. Volume 1 was with the relative density of 0.80 and Volume 2 was 0.68. There was a triangular region without any laser scan during the manufacturing process. The region was filled by metal particles which were sintered together and able to be removed. In this case, it is an indicative that overhanging structures are able to successfully build by modulating processing parameters across three axes X, Y and Z.

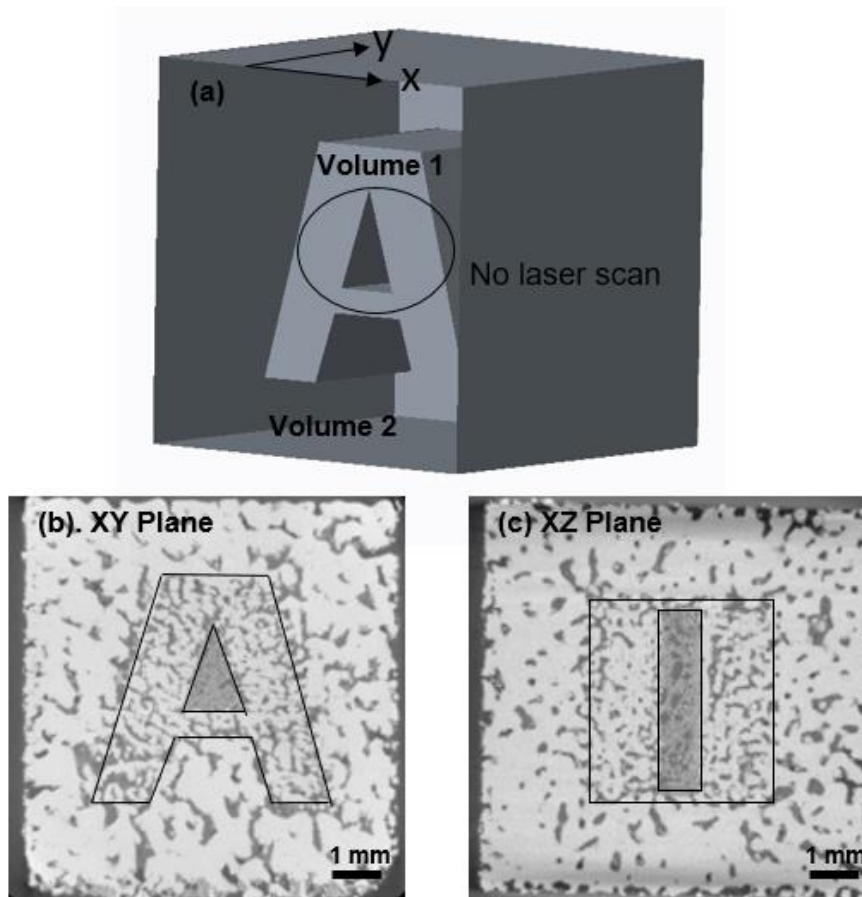


Figure 5.11. Letter 'A' is Fully Encased in a Dissimilar Porosity Matrix Demonstrating the Effect of Distinct Process Parameters on Resulting Porosity, Where (a) is the CAD Model; (b) and (c) Shows XCT Scanning Result of XY and XZ Plane Respectively

Although in Chapter 4, it has been proved that samples in various porosity can be successfully fabricated by varying the volume fraction of NaCl in the powder, graded structures are not achievable with current class powder-bed fusion, which only accommodates on feedstock material. This chapter has proposed a novel method for density grading in the build direction by modulation of energy density.

5.7 Summary

Further investigations on Ti-6Al-4V and NaCl blend to manufacture functionally graded cellular structures with SLM have been demonstrated. The technique is shown to be repeatable and will permit new opportunities in design for a number of potential material systems. Ti-6Al-4V cubes in relative density from 0.85 to 0.72 were successfully fabricated by controlling the laser power from 30W to 50W. Increasing the laser power of the process resulted in increasing relative density and compressive properties including compressive yield strength and young's modulus of the manufactured cubes. Density graded structures were successfully fabricated by modulation of processing parameters, hence energy density in regions. The density gradient can be along building direction, within X-Y plane and hence across all three axes (X, Y and Z). The conditions for successfully build graded cellular structures using this feedstock are first demonstrated, followed by an investigation into how the processing parameters can be used to control the relative density of the cellular material. This presents a significant enhancement to the state-of-the-art for manufacturing processes of FGMs, since for the first time, graded cellular structures can be fast created by parameters set-up without explicitly defining or analysing the unit cell geometry. Further studies are currently investigated for the correlation between the process parameters and the meso and microstructures in fabricated parts. it shows strong potential to fabricate more complex structures with finer details.

Chapter 6

Discussion

Titanium foams can be manufactured by traditional sintering process and AM technology. The traditional sintering processes, for example, reactive sintering, are generally complicated and involve several steps including material mixing, compaction, debinding and sintering. The size and shape of products are limited to those of die. With the development of AM technology, it provides an effective way to fabricate complicated structures, for instance, lattice structures. However, it requires the explicit design, analysis and optimisation of complex geometries, which is extremely challenging, in terms of computational methods and computer resources.

In the literatures, several methods to fabricate foam structures and functionally graded structures have been investigated, but it remains unexplored of products not limited to the die. With the aid of the SLM process, metallic lattice structures have been successfully manufactured with finer details. The effect of processing parameters on the properties of the final product has been investigated for a wide range of metals such as titanium, aluminium, stainless steel and Inconel. However, the effect of materials such as salt, remains largely unexplored and unknown. There is a lack of understanding at the process of how salt affecting the structure and how processing parameters in this case affecting the properties with respect to relative density and mechanical properties. Other areas such as the response of the structure depending on the content of salt in the mixture, and the microstructure and chemical composition in the structure are unknown so far. Therefore, a novel method using a blend of Ti-6Al-4V and NaCl with the SLM has been demonstrated so that foam structures are fabricated directly without an explicit lattice design.

The technique relies upon the fabricated parts being placed in water to enable removal of the remaining NaCl after processing through the open porosity generated, leaving the structure as

a metallic part with a cellular, or lattice, structure. To achieve such a structure requires a sufficient level of connectivity between the space holding material to allow removal by leaching. In order to investigate the relationship between processing parameters and NaCl volume ratio in the blends, a range of processing parameters were explored in order to accommodate a wide range of Ti-6Al-4V: NaCl feedstocks, Relative density of the cellular structures can be adjusted by controlling volume fraction of NaCl in blend, and can be predicted based on the composition of the feedstock. This presents a useful design guide in order to modulate porosity uniformly without the need for complex fabrication strategies to be defined.

Processing parameters have an effect on relative density of the final structures, therefore FGMs can be achieved by controlling the parameters in a specific volume. In this study, it has been investigated to vary in density both in vertical and horizontal directions for graded structures. Specimens were successfully built by controlling the laser power in two or three regions to enable density graded in these regions.

In this study, functionally graded cellular structures have been achievable by controlling the processing parameters in one part without any explicit design, analysis and optimisation, reducing the computational and time overhead compared with traditional lattice or functionally graded structure by the SLM process. It is thought that there is strong potential to translate more complex structures with finer details and variations down to the single layer level, where there is potential for an almost continuous structural grading.

The technique used in this thesis provides an alternative method, which is proposed in the first time, to manufacture cellular structure through Additive Manufacturing technology. The traditional furnace-based sintering and space holder technique presents significant limitations when compared to this approach. For instance, the size and shape of traditional sintering structures is limited to those of the die [17], [21], [23]. It also shows great potential to create

graded lattice structure with NaCl and various metal powders, such as aluminium, copper and stainless steel, which can be manufactured by the SLM process. Other additive manufacturing process, such as direct metal deposition and electron beam melting process, will be expected to be compatible with this approach. However, there are some limitations keeping unexplored in this study.

- Compared with the traditional sintering process and SLM fabricated lattices, the pore size, shape and distribution from this process is stochastic, therefore the mechanical properties, for example, the compressive modulus and yield strength do not closely fit to Gibson and Ashby's equation of foam structures.
- All samples, for instance, in Section 4.4, were weighed before and after removal of salt. However, it is believed that some salt particles are trapped and not removed in the structure due to their closed-cell foam structure. How much salt not leached out remains unknown so far. Due to salt evaporation during the SLM process, how much NaCl evaporated is unknown.
- Microstructure of Ti-6Al-4V only performed between samples without NaCl and with 30 vol.% NaCl in Section 4.6. Microstructure of those with other amounts of NaCl, or fabricated by various processing parameters is not investigated.
- The relationship between laser power and density has been investigated but only with laser power of 30 W, 40 W and 50 W. It keeps unknown that the change of density with laser power beyond this range. The relationship between other processing parameters, such as laser scan speed, layer thickness, hatch spacing and density are not explored in this study.

Chapter 7

Conclusions and Future Work

7.1 Conclusions

A novel technique using Ti-6Al-4V and NaCl blend to manufacture cellular structures with SLM has been demonstrated in this research. Both feedstock and laser build parameters were subject to experimentation. The technique for porous structure creation is shown to be repeatable and will permit new opportunities in designing for a number of potential material systems. Analysis of the process and fabricated structures demonstrated the below conclusions.

- Ti-6Al-4V cubes with relative density between 0.97 and 0.51 were successfully fabricated using NaCl content from 10% to 60% in the blend. Increasing the volume fraction of NaCl in the feedstock resulted in increased relative density of the manufactured cubes.
- An SLM process window was defined for the range of feedstock prepared for this study which is bounded by material response to process which results in failed builds.
- When the relative density reached 0.8, the cubes exhibited a solid-like behaviour, with some isolated pores. With increasing NaCl, more inter-connected pores were observed in the cubes resulting in the likely removal of all NaCl and formation of an open-cellular structure. The relationship between relative density and compressive properties of the cubes was evaluated by Gibson and Ashby's scaling equations and it was shown that whilst constants differed from those reported for regular metal foams, this form of equation, with experimentally determined constants could be used to predict mechanical performance based on relative density (and hence salt ration in the feedstock) with a prescribed range.

- Further investigations on Ti-6Al-4V and NaCl blend to manufacture functionally graded cellular structures with SLM have been demonstrated. The technique is shown to be repeatable and will permit new opportunities in design for a number of potential material systems.
- Ti-6Al-4V cubes in relative density from 0.72 to 0.85 were successfully fabricated by controlling the laser power from 30W to 50W. Increasing the laser power of the process resulted in increasing relative density and compressive properties including compressive yield strength and young's modulus of the manufactured cubes. From 30W to 50W, the compressive strength increased from ~400 to ~1000 MPa and the modulus increased from 3.70 to 15.53 GPa.
- Compressive properties of as-built samples and heat treated samples have been compared. After heat treatment at the stress relieving temperature, both yield strength and elongation has changed. For all samples, yield strength decreases and elongation increases.
- Density graded structures were successfully fabricated by varying laser power in volumes. The density gradient can be both in horizontal and vertical direction based on the design of the structure.

7.2 Future Work

Apart from the investigation done in this study, further work presented below in future could be achieved.

- It is necessary to further investigate the relationship between raw material, processing parameters and properties in future work so that fabricated parts can better fit the Gibson and Ashby's equation of foam structure and meet the requirements for

application.

- In future, the salt trapped in the sample could be achieved by modelling with the aid of XCT and then obtain an equation about NaCl in the blend and trapped in the final structure. Therefore, the amount of NaCl evaporated during the working process can be obtained.
- In the future work, to achieve the overall aim proposed, more work should be done by studying the microstructure of all samples to obtain the relationship in material, parameters, microstructure and properties.
- The functionally graded structures have been successfully fabricated in Section 5.4, 5.5 and 5.6. Applying this method to more complex structure with internal geometry is a challenge. Further work is needed to fast fabricate complex lattice structures in this method in future.
- Further investigation is required for explore the relationship between density and processing parameters. In this study, very limited work has been done for investigation between laser power and relative density. In the future, more work should be done for the relationship between relative density and laser power beyond the range of 30 W to 50 W. It also needs investigation of laser scan speed, layer thickness and hatch spacing for better achieve the aim in this study.
- This process shows significant potential to create cellular structures with NaCl. Other metals, such as aluminium, copper and stainless steel, which may be potentially processed by the SLM process, will be compatible with this approach as well. In the future work, more metal powders can be investigated by this method to fabricate cellular structures.
- Other Additive Manufacturing process, such as selective laser sintering, direct metal deposition and electron beam melting process may also allow the incorporation of salt

blended feedstock to produce porous structures. Further investigation work should be done for these processes, therefore more materials and processes will be related to this study and the final structures will find their application in some areas.

References

- [1] K. V. Wong and A. Hernandez, "A Review of Additive Manufacturing," *ISRN Mech. Eng.*, vol. 2012, pp. 1–10, 2012.
- [2] K. S. Prakash, T. Nancharaih, and V. V. S. Rao, "Additive Manufacturing Techniques in Manufacturing -An Overview," *Mater. Today Proc.*, vol. 5, no. 2, pp. 3873–3882, 2018.
- [3] A. Kennedy, "Porous Metals and Metal Foams Made from Powders," *Powder Metall.*, 2012.
- [4] P. Novák, F. Průša, J. Šerák, D. Vojtěch, and A. Michalcová, "High-temperature behaviour of Ti-Al-Si alloys produced by reactive sintering," *J. Alloys Compd.*, vol. 504, no. 2, pp. 320–324, 2010.
- [5] C. Augustin and W. Hungerbach, "Production of hollow spheres (HS) and hollow sphere structures (HSS)," *Mater. Lett.*, vol. 63, no. 13–14, pp. 1109–1112, 2009.
- [6] Y. Torres, S. Lascano, J. Bris, J. Pav??n, and J. A. Rodriguez, "Development of porous titanium for biomedical applications: A comparison between loose sintering and space-holder techniques," *Mater. Sci. Eng. C*, vol. 37, no. 1, pp. 148–155, 2014.
- [7] A. Laptev and M. Bram, "Manufacturing hollow titanium parts by powder metallurgy route and space holder technique," *Mater. Lett.*, vol. 160, pp. 101–103, 2015.
- [8] H. Bafti and A. Habibolahzadeh, "Production of aluminum foam by spherical carbamide space holder technique-processing parameters," *Mater. Des.*, vol. 31, no. 9, pp. 4122–4129, 2010.
- [9] E. E. Asik and S. Bor, "Fatigue behavior of Ti-6Al-4V foams processed by magnesium space holder technique," *Mater. Sci. Eng. A*, vol. 621, pp. 157–165, 2015.
- [10] B. Arifvianto, M. A. Leeflang, and J. Zhou, "The compression behaviors of titanium/carbamide powder mixtures in the preparation of biomedical titanium scaffolds with the space holder method," *Powder Technol.*, vol. 284, pp. 112–121, 2015.
- [11] J. Wu, H. Z. Cui, L. L. Cao, and Z. Z. Gu, "Open-celled porous NiAl intermetallics prepared by replication of carbamide space-holders," *Trans. Nonferrous Met. Soc. China (English Ed.)*, vol. 21, no. 8, pp. 1750–1754, 2011.
- [12] N. Jha, D. P. Mondal, J. Dutta Majumdar, A. Badkul, a. K. Jha, and a. K. Khare, "Highly porous open cell Ti-foam using NaCl as temporary space holder through powder metallurgy route," *Mater. Des.*, vol. 47, pp. 810–819, 2013.
- [13] S. F. Aida, M. N. Hijrah, A. H. Amirah, H. Zuhailawati, and A. S. Anasyida, "Effect of NaCl as a Space Holder in Producing Open Cell A356 Aluminium Foam by Gravity Die Casting Process," *Procedia Chem.*, vol. 19, pp. 234–240, 2016.
- [14] D. P. Mondal, M. Patel, H. Jain, A. K. Jha, S. Das, and R. Dasgupta, "The effect of the particle shape and strain rate on microstructure and compressive deformation response of pure Ti-foam made using acrowax as space holder," *Mater. Sci. Eng. A*, vol. 625, pp. 331–342, 2015.
- [15] M. Simonelli, Y. Y. Tse, and C. Tuck, "Microstructure of Ti-6Al-4V produced by selective laser melting," *J. Phys. Conf. Ser.*, vol. 371, 2012.
- [16] D. Sun *et al.*, "Selective laser melting of titanium parts: Influence of laser process parameters on macro- and microstructures and tensile property," *Powder Technol.*, vol. 342, pp. 371–379, 2018.

- [17] C. C. Seepersad, "Challenges and Opportunities in Design for Additive Manufacturing," vol. 1, no. 1, pp. 10–13, 2014.
- [18] C. W. Hull, Arcadia, and Calif, "United States Patent (19)," no. 19, p. 16, 1984.
- [19] T. D. Ngo, A. Kashani, G. Imbalzano, K. T. Q. Nguyen, and D. Hui, "Additive manufacturing (3D printing): A review of materials, methods, applications and challenges," *Compos. Part B Eng.*, vol. 143, no. February, pp. 172–196, 2018.
- [20] ASTM International, "F2792-12a - Standard Terminology for Additive Manufacturing Technologies," *Am. Soc. Test. Mater.*, pp. 10–12, 2013.
- [21] I. Gibson, D. W. Rosen, and B. Stucker, *Additive Manufacturing Technologies*. Springer, New York, NY, 2010.
- [22] W. Gao *et al.*, "The status, challenges, and future of additive manufacturing in engineering," *Comput. Des.*, 2015.
- [23] Y. Zhang *et al.*, "Additive Manufacturing of Metallic Materials: A Review," *J. Mater. Eng. Perform.*, vol. 27, no. 1, pp. 1–13, 2018.
- [24] B. Dutta, V. Singh, H. Natu, J. Choi, and J. Mazumder, "Direct Metal Deposition," *Adv. Mater. Process*, vol. 167, no. 3, pp. 33–36, 2009.
- [25] K. Shah, A. Khan, S. Ali, M. Khan, and A. J. Pinkerton, "Parametric study of development of Inconel-steel functionally graded materials by laser direct metal deposition," *Mater. Des.*, vol. 54, pp. 531–538, 2014.
- [26] T. E. Abioye, J. Folkes, and a. T. Clare, "A parametric study of Inconel 625 wire laser deposition," *J. Mater. Process. Technol.*, vol. 213, no. 12, pp. 2145–2151, 2013.
- [27] A. Mengel, "Mengel , Aaron Finite Element Modeling of LENS Deposition Using SYSWELD," 2002.
- [28] M. N. Mokgalaka, S. L. Pityana, P. Abimbola, I. Popoola, and T. Mathebula, "NiTi Intermetallic Surface Coatings by Laser Metal Deposition for Improving Wear Properties of Ti-6Al-4V Substrates," vol. 2014, 2014.
- [29] H. K. Lee, "Effects of the cladding parameters on the deposition efficiency in pulsed Nd:YAG laser cladding," *J. Mater. Process. Technol.*, vol. 202, no. 1–3, pp. 321–327, 2008.
- [30] J. Yu, M. Rombouts, G. Maes, and F. Motmans, "Material Properties of Ti6Al4V Parts Produced by Laser Metal Deposition," *Phys. Procedia*, vol. 39, pp. 416–424, 2012.
- [31] P. Bertrand, F. Bayle, C. Combe, P. Goeuriot, and I. Smurov, "Ceramic components manufacturing by selective laser sintering," *Appl. Surf. Sci.*, vol. 254, no. 4, pp. 989–992, 2007.
- [32] S. Kumar, *Selective Laser Sintering/Melting*, vol. 10. Elsevier, 2014.
- [33] D. D. Gu, W. Meiners, K. Wissenbach, and R. Poprawe, "Laser additive manufacturing of metallic components: materials, processes and mechanisms," *Int. Mater. Rev.*, vol. 57, no. 3, pp. 133–164, 2012.
- [34] A. J. Pinkerton, "Lasers in additive manufacturing," *Opt. Laser Technol.*, vol. 78, pp. 25–32, 2015.
- [35] Z. Sun, X. Tan, S. B. Tor, and W. Y. Yeong, "Selective laser melting of stainless steel 316L with low porosity and high build rates," *Mater. Des.*, vol. 104, pp. 197–204, 2016.

- [36] E. O. Olakanmi, R. F. Cochrane, and K. W. Dalgarno, "A review on selective laser sintering/melting (SLS/SLM) of aluminium alloy powders: Processing, microstructure, and properties," *Prog. Mater. Sci.*, vol. 74, pp. 401–477, 2015.
- [37] N. Taniguchi *et al.*, "Effect of pore size on bone ingrowth into porous titanium implants fabricated by additive manufacturing: An in vivo experiment," *Mater. Sci. Eng. C*, vol. 59, pp. 690–701, 2015.
- [38] Q. Chen and G. A. Thouas, "Metallic implant biomaterials," *Mater. Sci. Eng. R Reports*, vol. 87, pp. 1–57, 2015.
- [39] Q. Wei *et al.*, "Selective laser melting of stainless-steel/nano-hydroxyapatite composites for medical applications: Microstructure, element distribution, crack and mechanical properties," *J. Mater. Process. Technol.*, vol. 222, pp. 444–453, 2015.
- [40] Q. Jia and D. Gu, "Selective laser melting additive manufacturing of Inconel 718 superalloy parts: Densification, microstructure and properties," *J. Alloys Compd.*, vol. 585, pp. 713–721, 2014.
- [41] L. Yan, Y. Yuan, L. Ouyang, H. Li, A. Mirzasadeghi, and L. Li, "Improved mechanical properties of the new Ti-15Ta-xZr alloys fabricated by selective laser melting for biomedical application," *J. Alloys Compd.*, vol. 688, pp. 156–162, 2016.
- [42] M. Pr??bstle *et al.*, "Superior creep strength of a nickel-based superalloy produced by selective laser melting," *Mater. Sci. Eng. A*, vol. 674, pp. 299–307, 2016.
- [43] S. Das, "Producing metal parts with selective laser sintering/hot isostatic pressing," *Jom*, vol. 51, no. 4, pp. 2–2, 1999.
- [44] T. Hayashi, K. Maekawa, M. Tamura, and K. Hanyu, "Selective Laser Sintering Method Using Titanium Powder Sheet Toward Fabrication of Porous Bone Substitutes," *JSME Int. J. Ser. A*, vol. 48, no. 4, pp. 369–375, 2005.
- [45] D. A. Hollander *et al.*, "Structural, mechanical and in vitro characterization of individually structured Ti-6Al-4V produced by direct laser forming," *Biomaterials*, vol. 27, no. 7, pp. 955–963, 2006.
- [46] M. Kanazawa, M. Iwaki, S. Minakuchi, and N. Nomura, "Fabrication of titanium alloy frameworks for complete dentures by selective laser melting," *J. Prosthet. Dent.*, vol. 112, no. 6, pp. 1441–1447, 2014.
- [47] R. Wauthle *et al.*, "Additively manufactured porous tantalum implants," *Acta Biomater.*, vol. 14, pp. 217–225, 2015.
- [48] M. Vasquez, J. Cross, N. Hopkinson, and B. Haworth, "Developing new laser sintering materials for snowboarding applications," *Procedia Eng.*, vol. 34, pp. 325–330, 2012.
- [49] L. C. Ardila *et al.*, "Effect of IN718 recycled powder reuse on properties of parts manufactured by means of Selective Laser Melting," *Phys. Procedia*, vol. 56, no. C, pp. 99–107, 2014.
- [50] V. Seyda, N. Kaufmann, and C. Emmelmann, "Investigation of Aging Processes of Ti-6Al-4 V Powder Material in Laser Melting," *Phys. Procedia*, vol. 39, no. January, pp. 425–431, 2012.
- [51] E. C. Santos, M. Shiomi, K. Osakada, and T. Laoui, "Rapid manufacturing of metal components by laser forming," *Int. J. Mach. Tools Manuf.*, vol. 46, no. 12–13, pp. 1459–1468, 2006.
- [52] R. Goodall and A. Mortensen, *Porous Metals*, Fifth Edit., vol. 1, no. Bâtiment MX. Elsevier B.V., 2014.

- [53] L. E. Murr *et al.*, “Microstructure and mechanical properties of open-cellular biomaterials prototypes for total knee replacement implants fabricated by electron beam melting,” *J. Mech. Behav. Biomed. Mater.*, vol. 4, no. 7, pp. 1396–1411, 2011.
- [54] D. A. Ramirez *et al.*, “Open-cellular copper structures fabricated by additive manufacturing using electron beam melting,” *Mater. Sci. Eng. A*, vol. 528, no. 16–17, pp. 5379–5386, 2011.
- [55] F. A. Shah, M. Trobos, P. Thomsen, and A. Palmquist, “Commercially pure titanium (cp-Ti) versus titanium alloy (Ti6Al4V) materials as bone anchored implants — Is one truly better than the other?,” *Mater. Sci. Eng. C*, 2016.
- [56] K. A. Nazari, A. Nouri, and T. Hilditch, “Mechanical properties and microstructure of powder metallurgy Ti-xNb-yMo alloys for implant materials,” *Mater. Des.*, vol. 88, pp. 1164–1174, 2015.
- [57] R. Osman and M. Swain, “A Critical Review of Dental Implant Materials with an Emphasis on Titanium versus Zirconia,” *Materials (Basel)*, vol. 8, no. 3, pp. 932–958, 2015.
- [58] N. Sykaras, a M. Iacopino, V. a Marker, R. G. Triplett, and R. D. Woody, “Implant materials, designs, and surface topographies: their effect on osseointegration. A literature review.,” *Int. J. Oral Maxillofac. Implants*, vol. 15, no. 5, pp. 675–690, 2000.
- [59] D. P. de Andrade *et al.*, “Titanium-35Niobium alloy as a potential material for biomedical implants: In vitro study,” *Mater. Sci. Eng. C*, vol. 56, pp. 538–544, 2015.
- [60] A. Ducato, L. Fratini, M. La Cascia, and G. Mazzola, “An automated visual inspection system for the classification of the phases of Ti-6Al-4V titanium alloy,” *Lect. Notes Comput. Sci. (including Subser. Lect. Notes Artif. Intell. Lect. Notes Bioinformatics)*, vol. 8048 LNCS, no. PART 2, pp. 362–369, 2013.
- [61] L. J. Gibson and M. F. Ashby, *Cellular Solids: Structure and properties*, 2nd Editio. Cambridge, UK: Cambridge University Press, 1999.
- [62] F. García-Moreno, “Commercial applications of metal foams: Their properties and production,” *Materials (Basel)*, vol. 9, no. 2, pp. 20–24, 2016.
- [63] S. Muñoz, J. Pavón, J. A. Rodríguez-Ortiz, A. Civantos, J. P. Allain, and Y. Torres, “On the influence of space holder in the development of porous titanium implants: Mechanical, computational and biological evaluation,” *Mater. Charact.*, vol. 108, pp. 68–78, 2015.
- [64] N. Kanetake and M. Kobashi, “Innovative processing of porous and cellular materials by chemical reaction,” *Scr. Mater.*, vol. 54, no. 4 SPEC. ISS., pp. 521–525, 2006.
- [65] Y. Torres, J. J. Pavón, and J. A. Rodríguez, “Processing and characterization of porous titanium for implants by using NaCl as space holder,” *J. Mater. Process. Technol.*, vol. 212, no. 5, pp. 1061–1069, 2012.
- [66] M. Kobashi, S. Miyake, and N. Kanetake, “Hierarchical open cellular porous TiAl manufactured by space holder process,” *Intermetallics*, vol. 42, pp. 32–34, 2013.
- [67] M. Łazińska, T. Durejko, S. Lipiński, W. Polkowski, T. Czujko, and R. A. Varin, “Porous graded FeAl intermetallic foams fabricated by sintering process using NaCl space holders,” *Mater. Sci. Eng. A*, vol. 636, pp. 407–414, 2015.
- [68] Q. Z. Wang, C. X. Cui, S. J. Liu, and L. C. Zhao, “Open-celled porous Cu prepared by replication of NaCl space-holders,” *Mater. Sci. Eng. A*, pp. 1275–1278, 2010.
- [69] G. Jia, Y. Hou, C. Chen, J. Niu, H. Zhang, and G. Yuan, “Precise fabrication of open porous Mg

- scaffolds using NaCl templates: Relationship between space holder particles, pore characteristics and mechanical behavior," *Mater. Des.*, vol. 140, pp. 106–113, 2018.
- [70] I. MUTLU, "Synthesis and characterization of Ti–Co alloy foam for biomedical applications," *Trans. Nonferrous Met. Soc. China*, vol. 26, no. 1, pp. 126–137, 2016.
- [71] Y. Chen *et al.*, "Manufacturing of graded titanium scaffolds using a novel space holder technique," *Bioact. Mater.*, vol. 2, no. 4, pp. 248–252, 2017.
- [72] Z. J. Wally, A. M. Haque, A. Feteira, and G. C. Reilly, "Selective laser melting processed Ti6Al4V lattices with graded porosities for dental applications," *J. Mech. Behav. Biomed. Mater.*, vol. 90, pp. 20–29, 2019.
- [73] F. G. Arcella and F. H. Froes, "Producing titanium aerospace components from powder using laser forming," *J. Miner. Met. Mater. Soc.*, vol. 52, no. 5, pp. 28–30.
- [74] M. Simonelli, "' Microstructure Evolution and Mechanical Properties of Selective Laser Melted Ti-6Al-4V ", " 2014.
- [75] F. G. Arcella and F. H. Froes, "Components from Powder Using Laser Forming," *Jom*, vol. 52, no. 5, pp. 28–30, 2000.
- [76] M. L. Griffith *et al.*, "Free Form Fabrication of Metallic Components Using Laser Engineered Net Shaping (LENS)," *Proc. 7th Solid Free. Fabr. Symp.*, pp. 125–132, 1996.
- [77] X. Wu, J. Liang, J. Mei, C. Mitchell, P. S. Goodwin, and W. Voice, "Microstructures of laser-deposited Ti–6Al–4V," *Mater. Des.*, vol. 25, no. 2, pp. 137–144, 2004.
- [78] J. D. Avila, S. Bose, and A. Bandyopadhyay, "3.7 - Additive manufacturing of titanium and titanium alloys for biomedical applications," in *Titanium in Medical and Dental Applications*, 2018, pp. 35–343.
- [79] R. P. Mudge and N. R. Wald, "Laser engineered net shaping advances additive manufacturing and repair," *Weld. J. (Miami, Fla)*, vol. 86, no. 1, pp. 44–48, 2007.
- [80] B. Baufeld, E. Brandl, and O. van der Biesst, "Wire based additive layer manufacturing: Comparison of microstructure and mechanical properties of Ti–6Al–4V components fabricated by laser-beam deposition and shaped metal deposition," *J. Mater. Process. Technol.*, vol. 211, no. 6, pp. 1146–1158, 2011.
- [81] B. Song, S. Dong, B. Zhang, H. Liao, and C. Coddet, "Effects of processing parameters on microstructure and mechanical property of selective laser melted Ti6Al4V," *Mater. Des.*, vol. 35, pp. 120–125, 2012.
- [82] L. Thijs, F. Verhaeghe, T. Craeghs, J. Van Humbeeck, and J.-P. Kruth, "A study of the microstructural evolution during selective laser melting of Ti–6Al–4V," *Acta Mater.*, vol. 58, no. 9, pp. 3303–3312, 2010.
- [83] J. Sun, Y. Yang, and D. Wang, "Parametric optimization of selective laser melting for forming Ti6Al4V samples by Taguchi method," *Opt. Laser Technol.*, vol. 49, pp. 118–124, 2013.
- [84] C. Qiu, C. Panwisawas, M. Ward, H. C. Basoalto, J. W. Brooks, and M. M. Attallah, "On the role of melt flow into the surface structure and porosity development during selective laser melting," *Acta Mater.*, vol. 96, pp. 72–79, 2015.
- [85] X. Shi *et al.*, "Performance of high layer thickness in selective laser melting of Ti6Al4V," *Materials (Basel)*, vol. 9, no. 12, pp. 1–15, 2016.

- [86] J. Li and Z. Wei, "Process Optimization and Microstructure Characterization of Ti6Al4V Manufactured by Selective Laser Melting," *IOP Conf. Ser. Mater. Sci. Eng.*, vol. 269, no. 1, 2017.
- [87] J.-P. Choi, G.-H. Shin, S. Yang, D.-Y. Yang, J.-S. Lee, and J.-H. Yu, "Densification and microstructural investigation of Inconel 718 parts fabricated by selective laser melting," *Powder Technol.*, vol. 310, pp. 60–66, 2017.
- [88] L. A. Dobrzański, A. D. Dobrzańska-Danikiewicz, P. Malara, T. G. Gaweł, L. B. Dobrzański, and A. Achteлик-Franczak, "Fabrication of scaffolds from Ti6Al4V powders using the computer aided laser method," *Arch. Metall. Mater.*, vol. 60, no. 2A, pp. 1065–1070, 2015.
- [89] Y. Bo, Z. Linxi, Y. Quanzhan, Z. Guirong, Z. Fangxin, and S. Gang, "Additive manufacturing technologies of porous metal implants," *China Foundry*, vol. 11, no. 4, 2014.
- [90] Y. Miyamoto, W. A. Kaysser, B. H. Rabin, A. Kawasaki, and R. G. (Eds. . Ford, *Functionally Graded Materials: Design, Processing and Applications*. 1999.
- [91] M. Naebe and K. Shirvanimoghaddam, "Functionally graded materials: A review of fabrication and properties," *Appl. Mater. Today*, vol. 5, pp. 223–245, 2016.
- [92] B. Zhang, P. Jaiswal, R. Rai, and S. Nelaturi, "Additive Manufacturing of Functionally Graded Material Objects: A Review," *J. Comput. Inf. Sci. Eng.*, vol. 18, no. 4, pp. 1215–1231, 2018.
- [93] T. P. D. Rajan, R. M. Pillai, and B. C. Pai, "Characterization of centrifugal cast functionally graded aluminum-silicon carbide metal matrix composites," *Mater. Charact.*, vol. 61, no. 10, pp. 923–928, 2010.
- [94] C. Han *et al.*, "Continuous functionally graded porous titanium scaffolds manufactured by selective laser melting for bone implants," *J. Mech. Behav. Biomed. Mater.*, 2018.
- [95] S. Y. Choy, C. N. Sun, K. F. Leong, and J. Wei, "Compressive properties of functionally graded lattice structures manufactured by selective laser melting," *Mater. Des.*, vol. 131, no. June, pp. 112–120, 2017.
- [96] I. Maskery *et al.*, "A mechanical property evaluation of graded density Al-Si10-Mg lattice structures manufactured by selective laser melting," *Mater. Sci. Eng. A*, vol. 670, pp. 264–274, 2016.
- [97] S. Y. Choy, C. N. Sun, K. F. Leong, and J. Wei, "Compressive properties of Ti-6Al-4V lattice structures fabricated by selective laser melting: Design, orientation and density," *Addit. Manuf.*, vol. 16, pp. 213–224, 2017.
- [98] L. Xiao and W. Song, "Additively-manufactured functionally graded Ti-6Al-4V lattice structures with high strength under static and dynamic loading: Experiments," *Int. J. Impact Eng.*, vol. 111, pp. 255–272, 2018.
- [99] B. Wysocki, P. Maj, R. Sitek, J. Buhagiar, K. J. Kurzydłowski, and W. Świeszkowski, "Laser and electron beam additive manufacturing methods of fabricating titanium bone implants," *Appl. Sci.*, vol. 7, no. 7, pp. 1–20, 2017.
- [100] H. Ali, H. Ghadbeigi, and K. Mumtaz, "Effect of scanning strategies on residual stress and mechanical properties of Selective Laser Melted Ti6Al4V," *Mater. Sci. Eng. A*, vol. 712, no. November 2017, pp. 175–187, 2018.
- [101] P. Mellin, O. Lyckfeldt, P. Harlin, H. Brodin, H. Blom, and A. Strondl, "Evaluating flowability of additive manufacturing powders, using the Gustavsson flow meter," *Met. Powder Rep.*, vol. 72, no. 5, pp. 322–326, 2017.

- [102] Y. N. Loginov, A. I. Golodnov, S. I. Stepanov, and E. Y. Kovalev, "Determining the Young's modulus of a cellular titanium implant by FEM simulation," *AIP Conf. Proc.*, vol. 1915, 2017.
- [103] M. Simonelli, Y. Y. Tse, and C. Tuck, "Effect of the build orientation on the mechanical properties and fracture modes of SLM Ti-6Al-4V," *Mater. Sci. Eng. A*, vol. 616, pp. 1–11, 2014.